

Hot Dry Rocks Pty Ltd

Geothermal Energy Consultants

HEAD OFFICE

PO Box 251

South Yarra, Vic 3141

Australia

T +61 4 0733 7069

E info@hotdryrocks.com

W www.hotdryrocks.com

ABN: 12 114 617 622

SERVICES

Exploration

Rock Property Measurements

Project Development

Portfolio Management

Grant Applications

‘Reduced Surface Heat Flow’ at the Los Azufres Geothermal Region, Mexico

February 2018

Graeme Beardsmore

This document is formatted for two-sided printing

Executive summary

This document reports the world's first measurements of 'reduced surface heat flow', for six sites in the Los Azufres geothermal region to the east of Morelia, Michoacán, Mexico (Figure A). It demonstrates the detection and quantification of the subterranean component of conductive heat flow from within the dominant solar and meteorological near-surface thermal 'noise' to a precision of $\pm 0.05 \text{ Wm}^{-2}$ (50 mWm^{-2}).

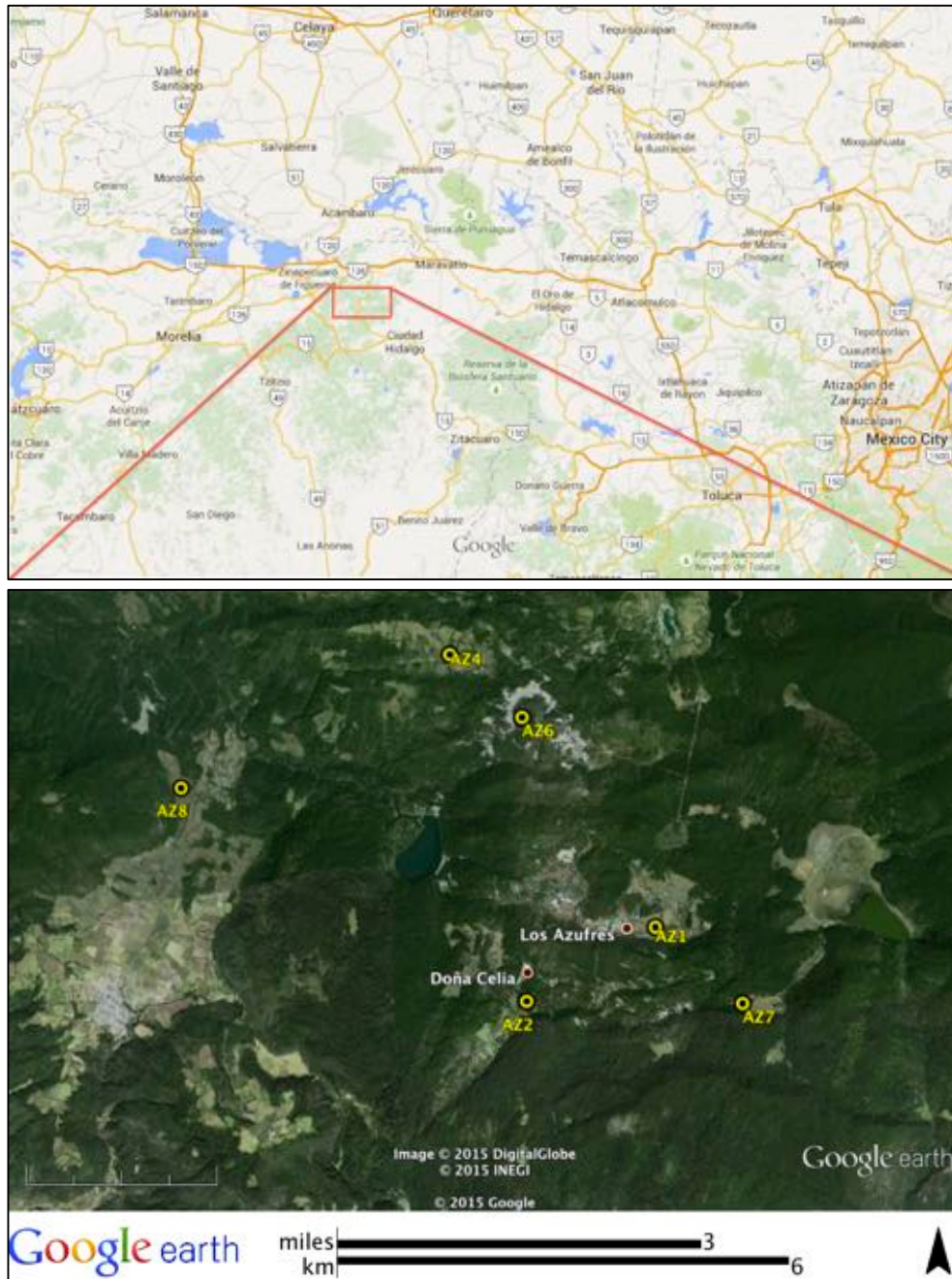


Figure A: Locations of survey sites

The report describes a new algorithm to accurately predict and remove the thermal effect of historical surface temperature variations in the top meter of the ground, to reveal the static ‘reduced surface heat flow’ due to buried heat sources. The algorithm combines ground temperature records, thermal conductivity measurements and historical satellite land surface temperature data in the public domain. This report draws on ground temperature data produced over a six-month period during a project run under the auspices of the Mexican Center for Geothermal Energy Innovation (CEMIE-Geo) in 2014–2015. The results demonstrate that three months of data would provide the same outcome.

The algorithm can be summarized as follows:

1. Precisely determine the thermal diffusivity of the ground between 30 cm and 110 cm using a Fourier spectral method
2. Estimate historical ground temperature variations at 30 cm depth from correlations with satellite land surface temperature data
3. Calculate the diffusion of the historical ground temperature signal to 50 cm, 70 cm, 90 cm and 110 cm depth
4. Subtract the calculated diffusion signal from the observed ground temperatures at 50 cm, 70 cm, 90 cm and 110 cm
5. Combine the ‘reduced ground temperature’ signals with thermal conductivity measured over the same depth interval to produce ‘reduced surface heat flow’

‘Reduced surface heat flow’ is the relatively static component of the observed surface heat flow signal. It can be attributed to buried heat sources.

Figure B shows the ‘reduced surface heat flow’ calculated daily for each of the six sites, revealing changes in heat flow at some sites over the six-month measurement period. Heat flow was elevated (relative to ‘background’ site AZ8) at AZ1, AZ2, AZ4 and AZ6. Heat flow at site AZ1 was relatively constant at $1.63 \pm 0.01 \text{ Wm}^{-2}$. Heat flow at site AZ2 was relatively constant at $2.15 \pm 0.05 \text{ Wm}^{-2}$ over a three-month period before a gradual decline of 25% followed by a rapid recovery to initial levels. This could indicate a transient, shallow heat sink beneath the top meter of soil at that location, perhaps related to water movement into or out of the sediments from a proximal stream. Heat flow at AZ4 was relatively constant at $1.90 \pm 0.05 \text{ Wm}^{-2}$. Heat

flow values at AZ6 and AZ8 were stable at $3.05 \pm 0.05 \text{ Wm}^{-2}$ and $0.30 \pm 0.02 \text{ Wm}^{-2}$, respectively. Reduced surface heat flow at AZ7 was relatively stable at $0.10 \pm 0.05 \text{ Wm}^{-2}$. This is much lower than expected for a site adjacent to a geothermal production well, suggesting a cooling effect possibly by infiltration of meteoric water into the shallow subsurface.

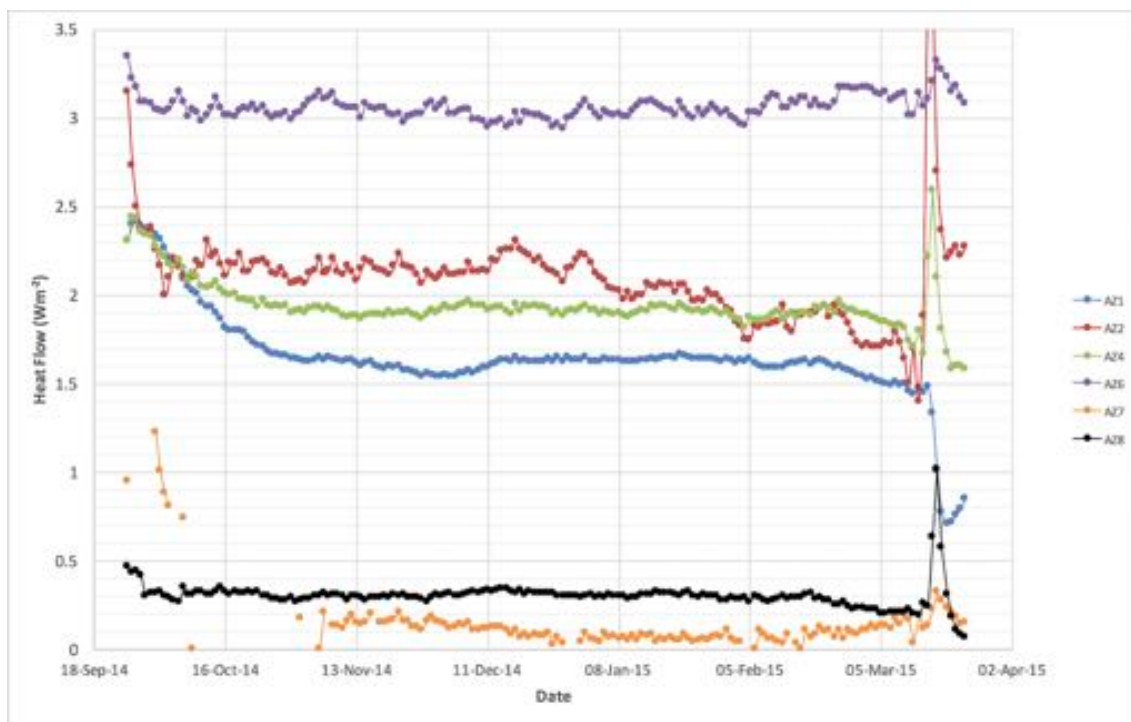


Figure B: Calculated 'reduced surface heat flow' (Wm^{-2}) for each day at each survey site

The results for AZ2 and AZ7 indicated that surveys designed to detect and delineate deep geothermal reservoirs should avoid sites above suspected pathways of shallow groundwater flow, where meteoric water can percolate and homogenize ground temperature or 'flush' heat away before it reaches the surface.

'Reduced surface heat flow' was relatively static at all sites in December 2014, three months after the survey commenced. Figure C shows the static heat flow values for each site on a Google Earth background, as well as two published values of conductive heat flow based on borehole measurements. The high 'reduced surface heat flow' at site AZ6 (relative to 'MEX00063' measured deeper in the section) very likely reflects the presence of a shallow conduit of hot fluid feeding the nearby thermal manifestations.

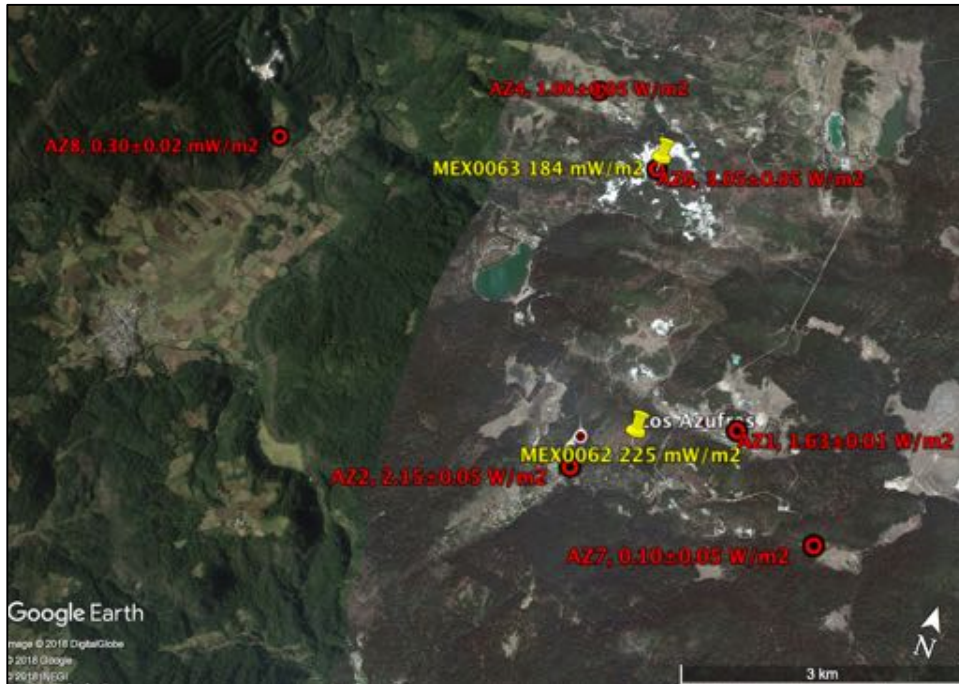


Figure C: Static ‘reduced surface heat flow’ at each survey site (red) in late 2014. Published heat flow from borehole measurements (yellow).

A robust, relatively cheap tool now exists to map the distribution of sub-surface heat sources and sinks to a precision of $\pm 0.05 \text{ Wm}^{-2}$, greatly surpassing that required for preliminary geothermal energy investigations. A ‘reduced surface heat flow’ survey with 1 km^{-1} site spacing could potentially delineate the full extent and magnitude of a geothermal system; a powerful new tool for pre-drill risk mitigation. Future surveys could generate ‘heat maps’ to look like Figure D.

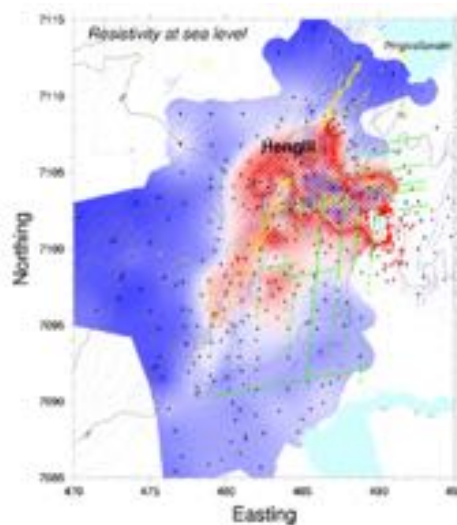


Figure D: An analog for a future ‘heat map’ⁱ

ⁱ Figure from: Árnason, K., Eysteinnsson, H. and Hersir, G.P. (2010), “Joint 1D inversion of TEM and MT data and 3D inversion of MT data in the Hengillarea, SW Iceland,” *Geothermics*, **39**, 13-34.

Table of Contents

- 1.0 INTRODUCTION5**
- 2.0 SURVEY SITES.....11**
 - 2.1 SITE AZ1: RESIDENCIA DE AGUA FRÍA14
 - 2.1.1 Location.....14
 - 2.1.2 Temperature records.....15
 - 2.1.3 Thermal diffusivity.....16
 - 2.1.4 Temperature history and ‘reduced ground temperature’16
 - 2.1.5 Thermal conductivity and thermal resistance19
 - 2.1.6 Reduced surface heat flow through time20
 - 2.1.7 Summary.....21
 - 2.2 SITE AZ2: BALNEARIO RANCHO VIEJO.....22
 - 2.2.1 Location.....22
 - 2.2.2 Temperature records.....23
 - 2.2.3 Thermal diffusivity.....24
 - 2.2.4 Temperature history and ‘reduced ground temperature’24
 - 2.2.5 Thermal conductivity and thermal resistance27
 - 2.2.6 Reduced surface heat flow through time28
 - 2.2.7 Summary.....29
 - 2.3 SITE AZ4: BALNEARIO LA CUMBRE30
 - 2.3.1 Location.....30
 - 2.3.2 Temperature records31
 - 2.3.3 Thermal diffusivity.....32
 - 2.3.4. Temperature history and ‘reduced ground temperature’32
 - 2.3.5 Thermal conductivity and thermal resistance35
 - 2.3.6 Reduced surface heat flow through time36
 - 2.3.7 Summary.....37
 - 2.4 SITE AZ6: DRILLING PAD FOR WELL AZ-4138
 - 2.4.1 Location.....38
 - 2.4.2 Temperature records.....39
 - 2.4.3 Thermal diffusivity.....40
 - 2.4.4. Temperature history and ‘reduced ground temperature’40
 - 2.4.5 Thermal conductivity and thermal resistance43
 - 2.4.6 Reduced surface heat flow through time44
 - 2.4.7 Summary.....45
 - 2.5 SITE AZ7: DRILLING PAD FOR WELL AZ-2646
 - 2.5.1 Location.....46
 - 2.5.2 Temperature records.....47
 - 2.5.3 Thermal diffusivity.....48
 - 2.5.4. Temperature history and ‘reduced ground temperature’49
 - 2.5.5 Thermal conductivity and thermal resistance50
 - 2.5.6 Reduced surface heat flow through time53
 - 2.5.7 Summary.....54
 - 2.6 SITE AZ8: POBLADO LA YERBABUENA55
 - 2.6.1 Location.....55
 - 2.6.2 Temperature records.....55
 - 2.6.3 Thermal diffusivity.....55
 - 2.6.4. Temperature history and ‘reduced ground temperature’57
 - 2.6.5 Thermal conductivity and thermal resistance60
 - 2.6.6 Reduced surface heat flow through time61
 - 2.6.7 Summary.....62
- 3.0 CONCLUSIONS63**
 - 3.1 REDUCED SURFACE HEAT FLOW63
 - 3.2 IMPLICATIONS OF RESULTS64

List of Figures

Figure 1. Mean daily temperatures at 30 cm depth measured by a Heat Needle (green dots and line), and Terra and Aqua night time temperatures (blue and orange dots, respectively). Correlation between the Heat Needle data and the 7-point moving average of the satellite data (red line) indicating a mean offset of about 6°C. _____	7
Figure 2. More than 10 years of mean daily temperatures at 30 cm depth (blue dots) at a Heat Needle survey location estimated through correlation with satellite-measured night time temperatures. Actual temperatures measured by the Heat Needle are at the end of the record (orange dots). _____	7
Figure 3. Temperatures observed by a Heat Needle at 30 cm depth (black dots and line). Temperatures predicted for 50 cm (blue), 70 cm (red), 90 cm (green) and 110 cm (purple) for the diffusion of the historical temperature signal from 30 cm to those depths. _____	8
Figure 4. Detecting constant offsets between observed (dots) and predicted (lines) temperatures at 50 cm (blue) and 110 cm (purple) for a Heat Needle site. _____	9
Figure 5. Reduced ground temperature signals at 50 cm (blue), 70 cm (red), 90 cm (green) and 110 cm (purple) for a Heat Needle site. The ground at 110 cm at this site is constantly $3.1 \pm 0.1^\circ\text{C}$ warmer than can be explained by the diffusion of surface temperature fluctuations. _____	9
Figure 6. Reduced surface heat flow through time deduced from a Heat Needle survey. The values in the first weeks of the survey are influenced by random errors in the surface temperature history, but equilibrate to a constant $2.9 \pm 0.1 \text{ Wm}^{-2}$. No significant temporal changes in 'reduced surface heat flow' are seen in this case. _____	10
Figure 7. Locations of Heat Needle survey sites (yellow circles) east of Morelia, Michoacán, Mexico. _____	11
Figure 8. Location in map (top) and aerial photo (bottom) view of site AZ1: Residencia de Agua Fría. _____	14
Figure 9. AZ1: Residencia de Agua Fría. Photo source: Alfredo Mercado. _____	15
Figure 10. Detail of temperature record for first month at site AZ1. _____	15
Figure 11. Daily average temperatures for site AZ1 _____	16
Figure 12. Harmonic spectral determination of thermal diffusivity for depth intervals (a) 30–50 cm, (b) 30–70 cm, (c) 30–90 cm and (d) 30–110 cm at site AZ1. Only relatively noise-free frequencies are plotted, the number of which decreases with increasing sensor depth. The gradient in each case is theoretically equal to $1/\sqrt{\kappa}$. _____	17
Figure 13. Mean daily temperatures at 30 cm depth measured by a Heat Needle (green dots) at AZ1, and Terra and Aqua night time land surface temperatures (blue and orange dots, respectively). _____	17
Figure 14. Daily mean temperatures at 30 cm depth at AZ1 since 2002, inferred from Terra and Aqua night time land surface temperatures _____	18
Figure 15. Reduced ground temperatures for 50 cm (blue), 70 cm (red), 90 cm (green) and 110 cm (purple) at AZ1 over the period of the survey _____	18
Figure 16. Temperature increase versus the natural log of heating time for site AZ1. _____	19
Figure 17. Bullard plots of change in 'reduced ground temperature' (ΔT) versus thermal resistance (R) at monthly intervals for site AZ1. The equations of the lines of best fit are given in the top left corner of the plot. The gradients indicate 'reduced surface heat flow' in Wm^{-2} . R^2 = coefficient of determination. _____	20
Figure 18. 'Reduced surface heat flow' versus time for site AZ1 (red, left axis); Coefficient of determination (black, right axis). _____	21
Figure 19. Location in map (top) and aerial photo (bottom) view of site AZ2: Balneario Rancho Viejo. _____	22
Figure 20. AZ2: Balneario Rancho Viejo. Photo source: Anson Antriasian. _____	23
Figure 21. Detail of temperature record for first month at site AZ2. _____	23
Figure 22. Daily average temperature for site AZ2. _____	24
Figure 23. Harmonic spectral determination of thermal diffusivity for depth intervals (a) 30–50 cm, (b) 30–70 cm, (c) 30–90 cm and (d) 30–110 cm at site AZ2. Only relatively noise-free frequencies are plotted. The gradient in each case is theoretically equal to $1/\sqrt{\kappa}$. Uncertainties are greater than for AZ1. _____	25
Figure 24. Mean daily temperatures at 30 cm depth measured by a Heat Needle (green dots) at AZ2, and Terra and Aqua night time land surface temperatures (blue and orange dots, respectively). _____	25
Figure 25. Daily mean temperatures at 30 cm depth at AZ2 since 2002, inferred from Terra and Aqua night time land surface temperatures _____	26
Figure 26. Reduced ground temperatures for 50 cm (blue), 70 cm (red), 90 cm (green) and 110 cm (purple) at AZ2 over the period of the survey _____	26
Figure 27. Temperature increase versus the natural log of heating time for site AZ2. _____	27
Figure 28. Bullard plots of change in 'reduced ground temperature' (ΔT) versus thermal resistance (R) at monthly intervals for site AZ2. The equations of the lines of best fit are given in the top left corner of the plot. The gradients indicate 'reduced surface heat flow' in Wm^{-2} . R^2 = coefficient of determination. _____	28

Figure 29. 'Reduced surface heat flow' versus time for site AZ2 (red, left axis); Coefficient of determination (black, right axis).	29
Figure 30. Location in map (top) and aerial photo (bottom) view of site AZ4: Balneario La Cumbre.	30
Figure 31. AZ4: Balneario La Cumbre. Photo source: Alfredo Mercado.	31
Figure 32. Detail of temperature record for first month at site AZ4.	31
Figure 33. Daily average temperature for site AZ4.	32
Figure 34. Harmonic spectral determination of thermal diffusivity for depth intervals (a) 30–50 cm, (b) 30–70 cm, (c) 30–90 cm and (d) 30–110 cm at site AZ4. Only relatively noise-free frequencies are plotted. The gradient in each case is theoretically equal to $1/\sqrt{\kappa}$. All values are tightly constrained.	33
Figure 35. Mean daily temperatures at 30 cm depth measured by a Heat Needle (green dots) at AZ4, and Terra and Aqua night time land surface temperatures (blue and orange dots, respectively).	33
Figure 36. Daily mean temperatures at 30 cm depth at AZ4 since 2002, inferred from Terra and Aqua night time land surface temperatures	34
Figure 37. Reduced ground temperatures for 50 cm (blue), 70 cm (red), 90 cm (green) and 110 cm (purple) at AZ4 over the period of the survey	34
Figure 38. Temperature increase versus the natural log of heating time; raw plot for site AZ4.	35
Figure 39. Bullard plots of change in 'reduced ground temperature' (ΔT) versus thermal resistance (R) at monthly intervals for site AZ4. The equations of the lines of best fit are given in the top left corner of the plot. The gradients indicate 'reduced surface heat flow' in Wm^{-2} . R^2 = coefficient of determination.	36
Figure 40. 'Reduced surface heat flow' versus time for site AZ4 (red, left axis); Coefficient of determination (black, right axis).	37
Figure 41. Location in map (top) and aerial photo (bottom) view of site AZ6: Drilling pad for well AZ-41.	38
Figure 42. AZ6: Drilling pad for well AZ-41. Photo source: Alfredo Mercado.	39
Figure 43. Detail of temperature record for first month at site AZ6.	39
Figure 44. Daily average temperature for site AZ6.	40
Figure 45. Harmonic spectral determination of thermal diffusivity for depth intervals (a) 30–50 cm, (b) 30–70 cm, (c) 30–90 cm and (d) 30–110 cm at site AZ6. Only relatively noise-free frequencies are plotted. The gradient in each case is theoretically equal to $1/\sqrt{\kappa}$. All values are tightly constrained.	41
Figure 46. Mean daily temperatures at 30 cm depth measured by a Heat Needle (green dots) at AZ6, and Terra and Aqua night time land surface temperatures (blue and orange dots, respectively).	41
Figure 47. Daily mean temperatures at 30 cm depth at AZ6 since 2002, inferred from Terra and Aqua night time land surface temperatures	42
Figure 48. Reduced ground temperatures for 50 cm (blue), 70 cm (red), 90 cm (green) and 110 cm (purple) at AZ6 over the period of the survey	42
Figure 49. Temperature increase versus the natural log of heating time for site AZ6	43
Figure 50. Bullard plots of change in 'reduced ground temperature' (ΔT) versus thermal resistance (R) at monthly intervals for site AZ6. The equations of the lines of best fit are given in the top left corner of the plot. The gradients indicate 'reduced surface heat flow' in Wm^{-2} . R^2 = coefficient of determination.	44
Figure 51. 'Reduced surface heat flow' versus time for site AZ6 (red, left axis); Coefficient of determination (black, right axis).	45
Figure 52. Location in map (top) and aerial photo (bottom) view of site AZ7: Drilling pad for well AZ-26.	46
Figure 53. AZ7: Drilling pad for well AZ-26. Photo source: Alfredo Mercado.	47
Figure 54. Detail of temperature record for January 2015 at site AZ7.	47
Figure 55. Daily average temperature for site AZ7. Days with spurious data have been removed.	48
Figure 56. Harmonic spectral determination of thermal diffusivity for depth intervals (a) 30–50 cm, (b) 30–70 cm, (c) 30–90 cm and (d) 30–110 cm compiled over four discrete time intervals at site AZ6. Only relatively noise-free frequencies are plotted. The gradient in each case is theoretically equal to $1/\sqrt{\kappa}$.	50
Figure 57. Mean daily temperatures at 30 cm depth measured by a Heat Needle (green dots) at AZ7, and Terra and Aqua night time land surface temperatures (blue and orange dots, respectively).	51
Figure 58. Daily mean temperatures at 30 cm depth at AZ7 since 2002, inferred from Terra and Aqua night time land surface temperatures	51
Figure 59. Reduced ground temperatures for 50 cm (blue), 70 cm (red), 90 cm (green) and 110 cm (purple) at AZ7 over the period of the survey. Days with spurious data have been removed.	52
Figure 60. Temperature increase versus the natural log of heating time for site AZ7.	52
Figure 61. Bullard plots of change in 'reduced ground temperature' (ΔT) versus thermal resistance (R) at monthly intervals for site AZ7. The equations of the lines of best fit are given in the top left corner of the plot. The gradients indicate 'reduced surface heat flow' in Wm^{-2} . R^2 = coefficient of determination.	53

Figure 62. 'Reduced surface heat flow' versus time for site AZ7 (red, left axis); Coefficient of determination (black, right axis). Days with spurious data have been removed.	54
Figure 63. Location in map (top) and aerial photo (bottom) view of site AZ8: Poblado La Yerbabuena.	56
Figure 64. AZ8: Poblado La Yerbabuena. Photo source: Anson Antriasian.	56
Figure 65. Detail of temperature record for first month at site AZ8.	57
Figure 66. Daily average temperature for site AZ8.	57
Figure 67. Harmonic spectral determination of thermal diffusivity for depth intervals (a) 30–50 cm, (b) 30–70 cm, (c) 30–90 cm and (d) 30–110 cm at site AZ8. Only relatively noise-free frequencies are plotted. The gradient in each case is theoretically equal to $1/\sqrt{\kappa}$. All values are tightly constrained.	58
Figure 68. Mean daily temperatures at 30 cm depth measured by a Heat Needle (green dots) at AZ8, and Terra and Aqua night time land surface temperatures (blue and orange dots, respectively).	58
Figure 69. Daily mean temperatures at 30 cm depth at AZ8 since 2002, inferred from Terra and Aqua night time land surface temperatures	59
Figure 70. Reduced ground temperatures for 50 cm (blue), 70 cm (red), 90 cm (green) and 110 cm (purple) at AZ8 over the period of the survey	59
Figure 71. Temperature increase versus the natural log of heating time in March 2015 for site AZ8.	60
Figure 72. Bullard plots of change in 'reduced ground temperature' (ΔT) versus thermal resistance (R) at monthly intervals for site AZ8. The equations of the lines of best fit are given in the top left corner of the plot. The gradients indicate 'reduced surface heat flow' in Wm^{-2} . R^2 = coefficient of determination.	61
Figure 73. 'Reduced surface heat flow' versus time for site AZ8 (red, left axis); Coefficient of determination (black, right axis).	62
Figure 74. Reduced surface heat flow through time for all sites.	63
Figure 75. 'Static' reduced surface heat flow for all sites at the end of December 2014 (red). Published ¹¹ conductive heat flow values based on borehole thermal gradient measurements (yellow pins).	64
Figure 76. Wells locations, identified structures, thermal manifestations and Heat Needle sites in the Los Azufres geothermal field. Modified after Arellano et al. (2015).	65
Figure 77. An electrical resistivity depth-slice through a geothermal system in Iceland (After Árnason et al., 2010), representing how a future 'reduced surface heat flow' map might delineate and quantify the thermal signature of a geothermal system.	66

1.0 Introduction

The 'Heat Needle' is a tool developed by Hot Dry Rocks Pty Ltd ('HDR', Australia) to detect and quantify the geophysical component of conductive heat flow in the near-surface, a zone dominated by thermal 'noise' induced by solar cycles and weather patterns. Readers are referred to Beardsmore (2012)² and Beardsmore & Antriasian (2015)³ for a description of the Heat Needle hardware and calibration procedure.

This document reports on a calculation of 'reduced surface heat flow' for the Los Azufres geothermal region to the east of Morelia, Michoacán, Mexico. It builds on a field trial of Heat Needles at six sites around Los Azufres over a six-month period from September 2014 to March 2015 run under the auspices of the Mexican Center for Geothermal Energy Innovation (CEMIE-Geo)⁴. Readers are referred to the report on that project and Beardsmore *et al.* (2017)⁵ for a description of previous data processing algorithms and interpretations.

This document describes and applies a new processing algorithm⁶ incorporating additional data to improve the resolution of inferred surface heat flow by an order of magnitude over the previous report. HDR utilized the following data:

- Records of ambient temperature at the six sites around Los Azufres at the air-soil interface and at 10 cm, 30 cm, 50 cm, 70 cm, 90 cm and 110 cm depth at 15-minute intervals;
- Thermal conductivity for the six sites derived from the change in temperature of the ground as a response to constant heating over a one-hour period;

² Beardsmore, G.R. (2012). Towards a shallow heat flow probe for mapping thermal anomalies. Proceedings, Thirty-Seventh Workshop on Geothermal Reservoir Engineering Stanford University, Stanford, California, January 30–February 1, 2012. SGP-TR-194. 14pp.

³ Beardsmore, G.R. and Antriasian, A. (2015). Developing the 'Heat Needle'—a tool for cost effective heat flow mapping. Proceedings World Geothermal Congress 2015 Melbourne, Australia, 19-25 April 2015. 11pp.

⁴ Beardsmore, G.R. (2015). CEMIE-Geo Project 23: Testing probes for measuring shallow heat flow in geothermal zones, Report 2: Los Azufres geothermal region. Report prepared for Universidad Michoacana de San Nicolas de Hidalgo, October 2015. 56pp.

⁵ Beardsmore, G., Gutiérrez-Negrín, L., Garduño-Monroy, V., Espinoza-Ojeda, O.M., Almanza-Álvarez, S., Antriasian, A. and Egan, S. (2017). Trial Deployment of a surface heat flow probe over the Los Azufres Geothermal Region, Mexico. Proceedings, 42nd Workshop on Geothermal Reservoir Engineering Stanford University, Stanford, California, February 13–15, 2017. SGP-TR-212.

⁶ Australian Patent Application No. 2018900262—Method of Measuring Conductive Geophysical Heat Flow

- Night time land surface temperatures inferred from Terra (MOD11A1.006) and Aqua (MYD11A1.006) satellites⁷, for 1 km² pixels around each site.

The significant improvement in the precision of the surface heat flow measurement is due in large part to a new method, developed by HDR, to determine the mean value of thermal diffusivity (\pm standard error) of the ground between any pair of temperature sensors on a Heat Needle. The method involves application of Fourier transforms to convert the temperature time-series from the sensors into amplitude (A) and phase (ϕ) spectra. The phase shift ($\phi_2 - \phi_1$, radians) and amplitude decay (A_2/A_1) can be determined between any two sensors, S_1 and S_2 , for all harmonic components of the signals with detectable amplitudes. Heat Needles can resolve harmonic components with amplitudes as low as 5×10^{-6} K.

For pure thermal conduction, it can be shown that both $\ln(A_2/A_1)$ and phase shift have the same linear relationship with $\sqrt{(\Delta z^2 \cdot \pi \cdot f)}$, where Δz (m) is the distance between sensors and f (s^{-1}) is the harmonic frequency. The gradient of the relationship is $1/\sqrt{\kappa}$, where κ ($m^2 s^{-1}$) is thermal diffusivity. The Los Azufres data set conformed to the theoretical predictions for pure conduction for depth intervals 30–50 cm, 30–70 cm, 30–90 cm and 30–110 cm at all six sites. HDR calculated mean and standard error of thermal diffusivity for each interval.

Another key development that allows HDR to discriminate geophysical heat flow from diurnal, meteorological and annual thermal noise is the recognition of a correlation between mean daily ground temperatures measured with a Heat Needle and MOD11A1.006 and MYD11A1.006 night time land surface temperature products generated from NASA's Terra and Aqua satellites⁷ (Figure 1). The observed correlation allows a first-pass estimate of ground temperature history to be derived from the historical land surface temperatures measured by the satellites. The data provide daily temporal resolution for more than 10 years at any given survey site (Figure 2).

⁷ The MOD11A1.006 and MYD11A1.006 datasets were retrieved from the online Application for Extracting and Exploring Analysis Ready Samples (AppEEARS), courtesy of the NASA EOSDIS Land Processes Distributed Active Archive Center (LP DAAC), USGS/Earth Resources Observation and Science (EROS) Center, Sioux Falls, South Dakota, <https://lpdaacsvc.cr.usgs.gov/appeears/>.

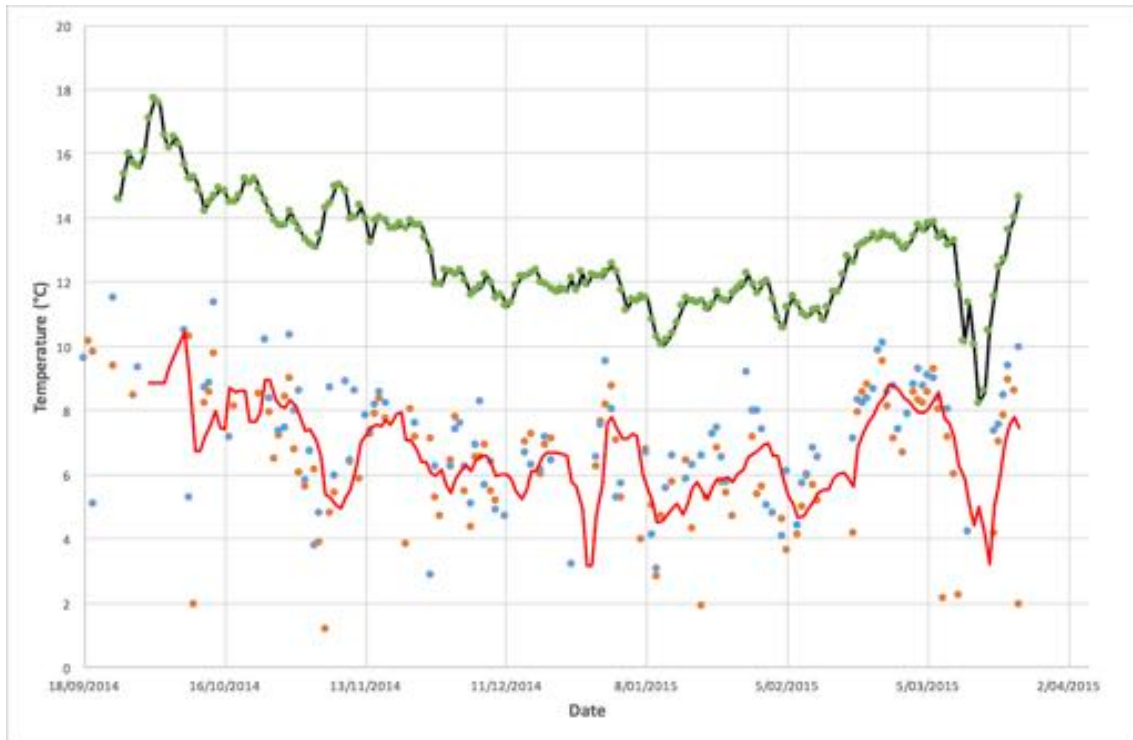


Figure 1. Mean daily temperatures at 30 cm depth measured by a Heat Needle (green dots and line), and Terra and Aqua night time land surface temperatures (blue and orange dots, respectively). Correlation between the Heat Needle data and the 7-point moving average of the satellite data (red line) indicate a mean offset of about 6°C.

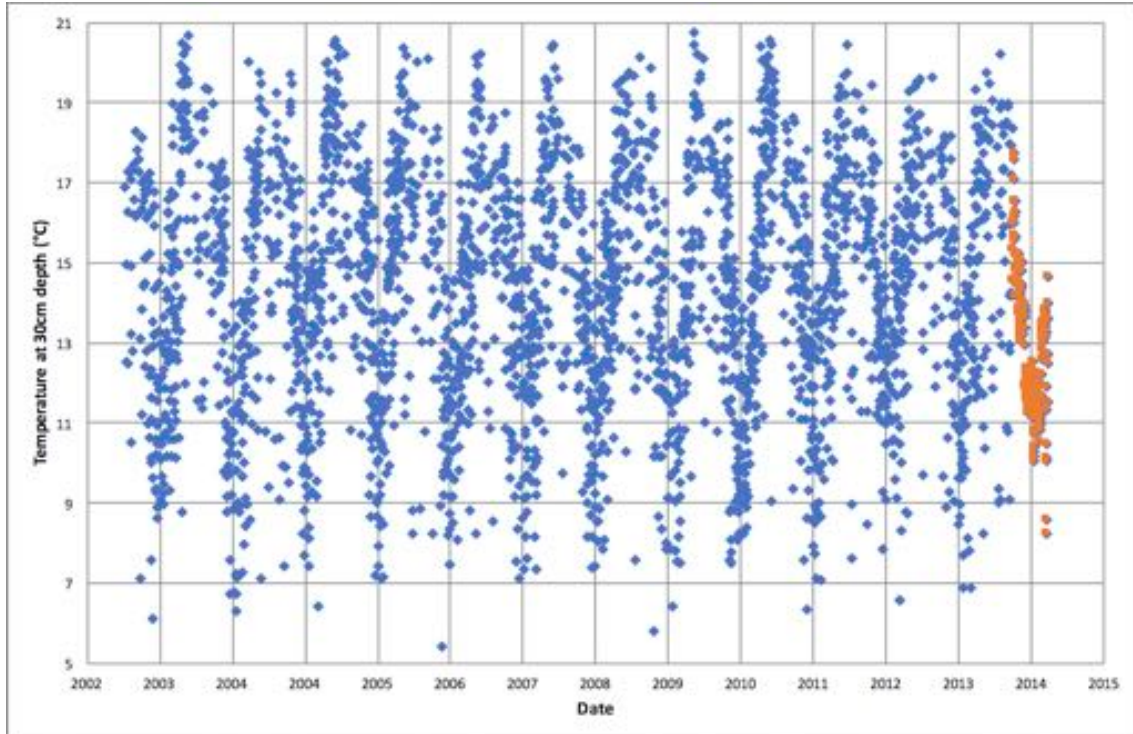


Figure 2. More than 10 years of mean daily temperatures at 30 cm depth (blue dots) at a Heat Needle survey location estimated through correlation with satellite-derived night time land surface temperatures. Actual temperatures measured by the Heat Needle are at the end of the record (orange dots).

The third critical step to discriminate the geophysical component of surface heat flow is to forward model the diffusion of the near-surface temperature signal into the ground. Thermal diffusion is a function of time and the thermal diffusivity of the ground, both of which are provided by the Heat Needle data. The temperature of a half-space under initial isothermal conditions is perturbed by fluctuations in surface temperature. The degree of perturbation can be predicted for any given sensor depth and record time (eg Figure 3).

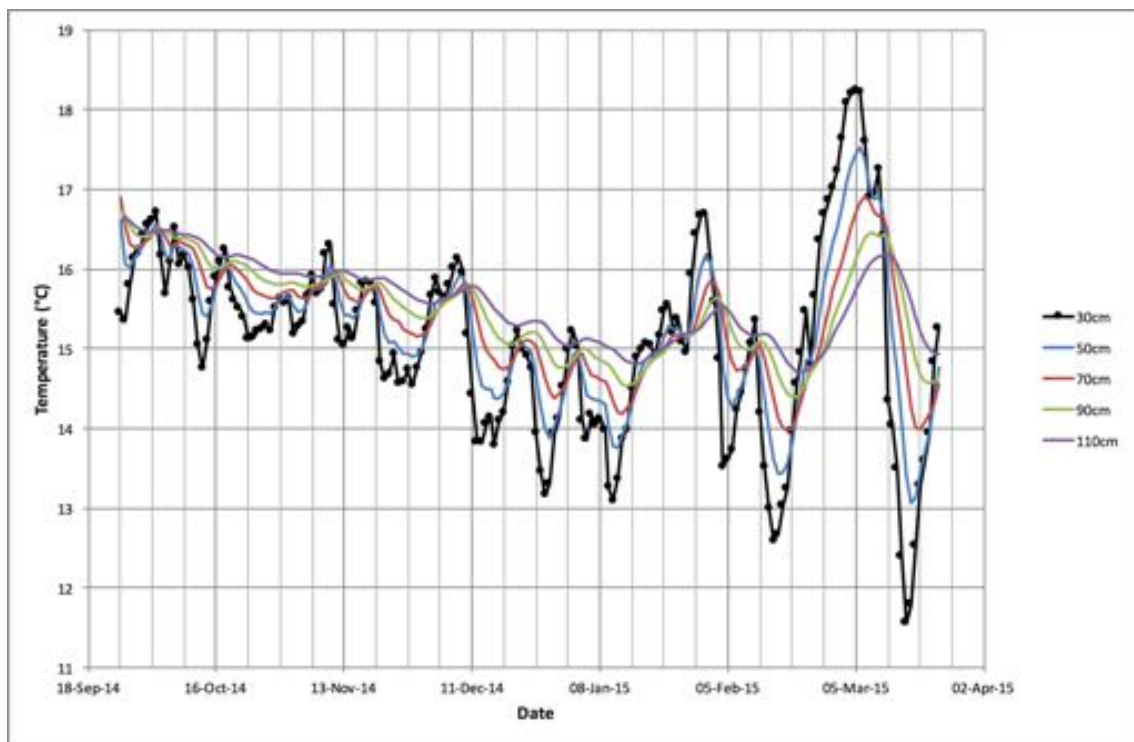


Figure 3. Temperatures observed by a Heat Needle at 30 cm depth (black dots and line). Temperatures predicted for 50 cm (blue), 70 cm (red), 90 cm (green) and 110 cm (purple) for the diffusion of the historical temperature signal from 30 cm to those depths.

The next step is to subtract the predicted perturbation signal from the observed ground temperature records at each depth. Figure 4 illustrates the predicted and observed daily average ground temperatures for two depths at a Heat Needle site. The differences between curves can be calculated for each day and depth. ‘Reduced ground temperature’ (Figure 5) is what remains when the thermal perturbation due the surface temperature history is removed from the observed ground temperature record. The simplest interpretation of ‘reduced ground temperature’ is that it defines the geophysical component of thermal gradient.

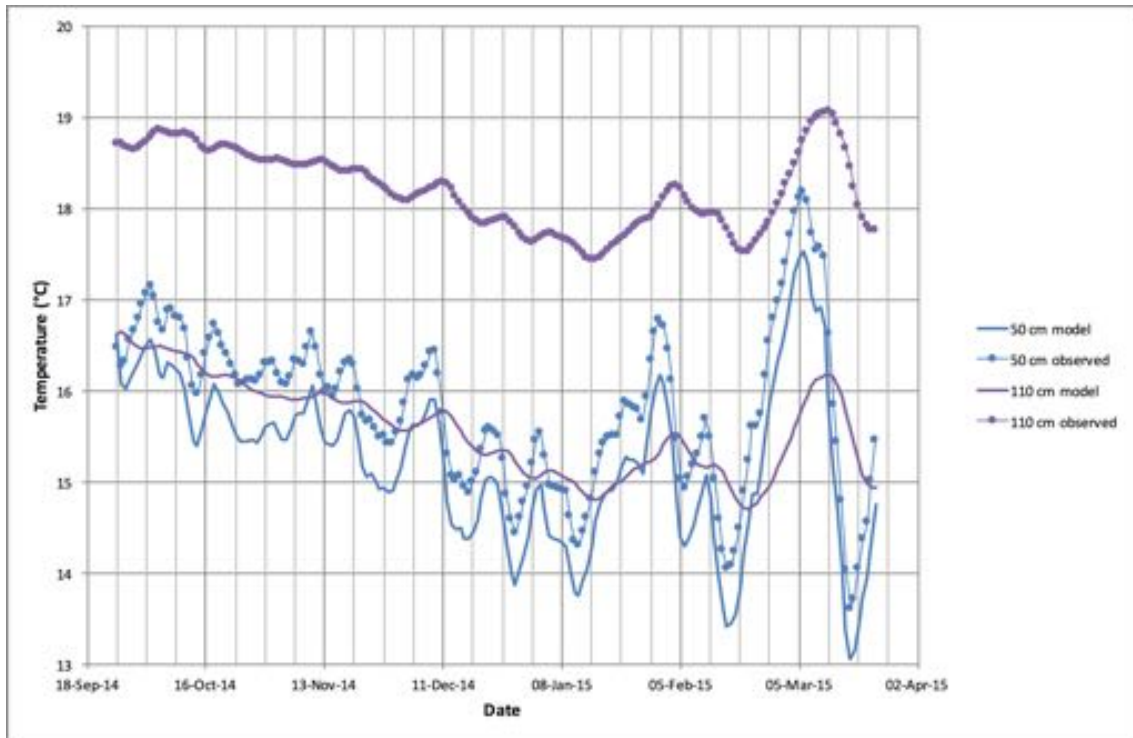


Figure 4. Detecting constant offsets between observed (dots) and predicted (lines) temperatures at 50 cm (blue) and 110 cm (purple) for a Heat Needle site.

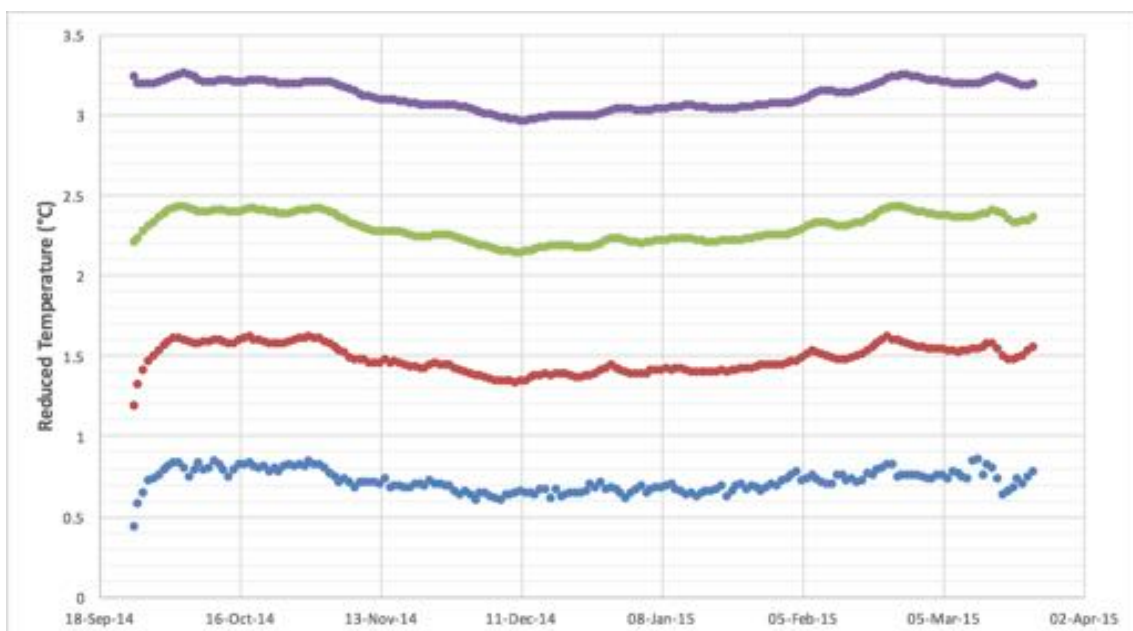


Figure 5. Reduced ground temperature signals at 50 cm (blue), 70 cm (red), 90 cm (green) and 110 cm (purple) for a Heat Needle site. The ground at 110 cm at this site is constantly $3.1 \pm 0.1^\circ\text{C}$ warmer than can be explained by the diffusion of surface temperature fluctuations.

It can be shown that random errors in the surface temperature history created by correlation with satellite data become insignificant to the calculated subsurface

thermal perturbation several weeks into the Heat Needle survey. That is, the sum effect of all historic random errors cancel each other out after about a month.

An increase in ‘reduced ground temperature’ with depth defines a thermal gradient. When the gradient is calculated as a function of thermal resistance ($\sum z/\lambda$, where z = depth and λ = thermal conductivity), it defines ‘**reduced surface heat flow**’.

‘Reduced surface heat flow’ can be estimated for each day of a Heat Needle survey, and its variation through time can highlight temporal changes in subterranean heat sources and sinks (eg Figure 6).



Figure 6. Reduced surface heat flow through time deduced from a Heat Needle record. The values in the first weeks of the survey are influenced by random errors in the surface temperature history, but equilibrate to a static $2.9 \pm 0.1 \text{ Wm}^{-2}$. No significant temporal changes in ‘reduced surface heat flow’ are seen in this case.

This document illustrates the most precise geophysical heat flow measurements produced using a near-surface instrument to date, and demonstrates that the Heat Needle is a credible alternative to ‘gradient wells’ or ‘heat flow wells’ for geothermal energy exploration. A regional Heat Needle survey at 1 km^{-1} site spacing could potentially delineate the full extent and magnitude of a geothermal system for about the same cost as a single gradient well.

2.0 Survey sites

This section illustrates the locations of the six Heat Needle sites to the east of Morelia, Michoacán, Mexico. Section 3 details the results.

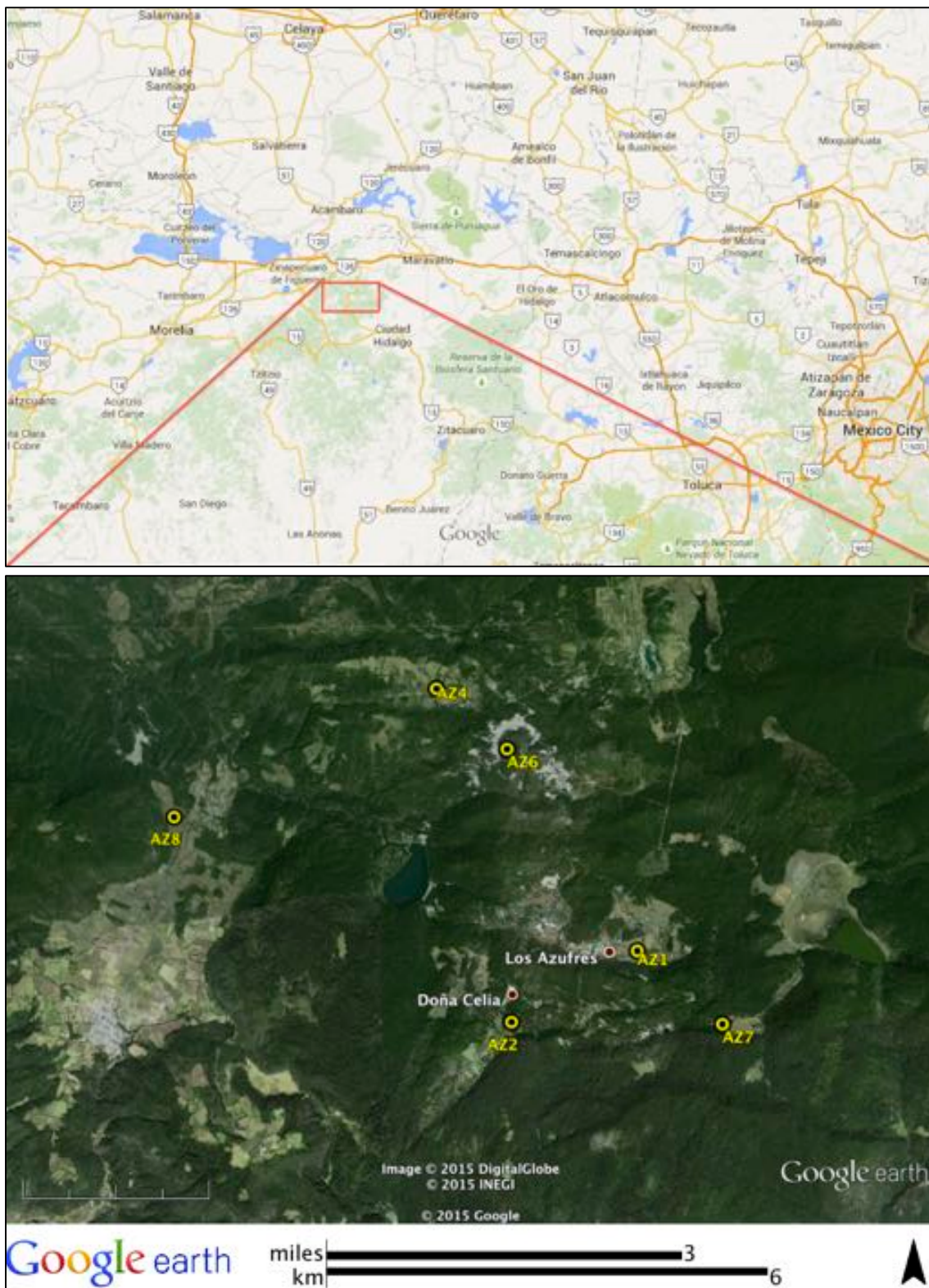


Figure 7. Locations of Heat Needle survey sites (yellow circles) east of Morelia, Michoacán, Mexico.

Site	Site name and description	Latitude Longitude	UTM Zone 14Q Coordinates Elevation	Google Earth image (± 5 m)
AZ1	Residencia de Agua Fría Grassy expanse within the Los Azufres geothermal field.	19.79055 °N 100.66055 °W	2189157 mN 326050 mE 2,884 \pm 7 m	 AZ1 location Grounds of CFTI administrative buildings
AZ2	Balneario Rancho Viejo Inside the grounds of a private spa, installed about 3 m from a 1 m deep and 3 m wide flowing creek.	19.78203 °N 100.67619 °W	2188230 mN 324402 mE 2,776 \pm 9 m	 AZ2
AZ4	Balneario La Cumbre Inside the boundary of a small private spa.	19.82160 °N 100.68566 °W	2192620 mN 323454 mE 2,799 \pm 13 m	 AZ4
AZ6	Drilling pad for well AZ-41 At the edge of the pad of geothermal well AZ-41.	19.81407 °N 100.67686 °W	2191778 mN 324367 mE 3,050 \pm 11 m	 AZ6

AZ7	<p>Drilling pad for well AZ-26</p> <p>On the pad of geothermal well AZ-26.</p>	<p>19.78202 °N 100.65013 °W</p>	<p>2188202 mN 327133 mE 2,937 ± 7 m</p>	 <p>Aerial satellite view of a drilling pad (AZ7) located in a forested area. The pad is a cleared, circular area with a central structure and a small pond. A red pin marks the location. The image includes a scale bar (42 m) and a north arrow.</p>
AZ8	<p>Poblado La Yerbabuena</p> <p>Adjacent to a seismic station on the outskirts of the village of La Yerbabuena. Outside the known geothermal field.</p>	<p>19.80659 °N 100.71952 °W</p>	<p>2190995 mN 319890 mE 2,558 ± 12 m</p>	 <p>Aerial satellite view of the Poblado La Yerbabuena area. The image shows a large, cleared, brownish area, likely a seismic station or drilling site, with a red pin marking the location. The surrounding area is a mix of cleared land and vegetation. The image includes a scale bar (70 m) and a north arrow.</p>

2.1 Site AZ1: Residencia de Agua Fría

2.1.1 Location

Latitude 19.79055°N, Longitude 100.66055°W

UTM coordinates: 14Q 326050mE 2189157mN Elevation: 2,884±7 m

The Heat Needle was installed inside the grounds of CFE (the state utility that operates the field and power plants) within the geothermal field (Figure 8, Figure 9). It recorded ground temperature data from 24 September 2014 to 24 March 2015.

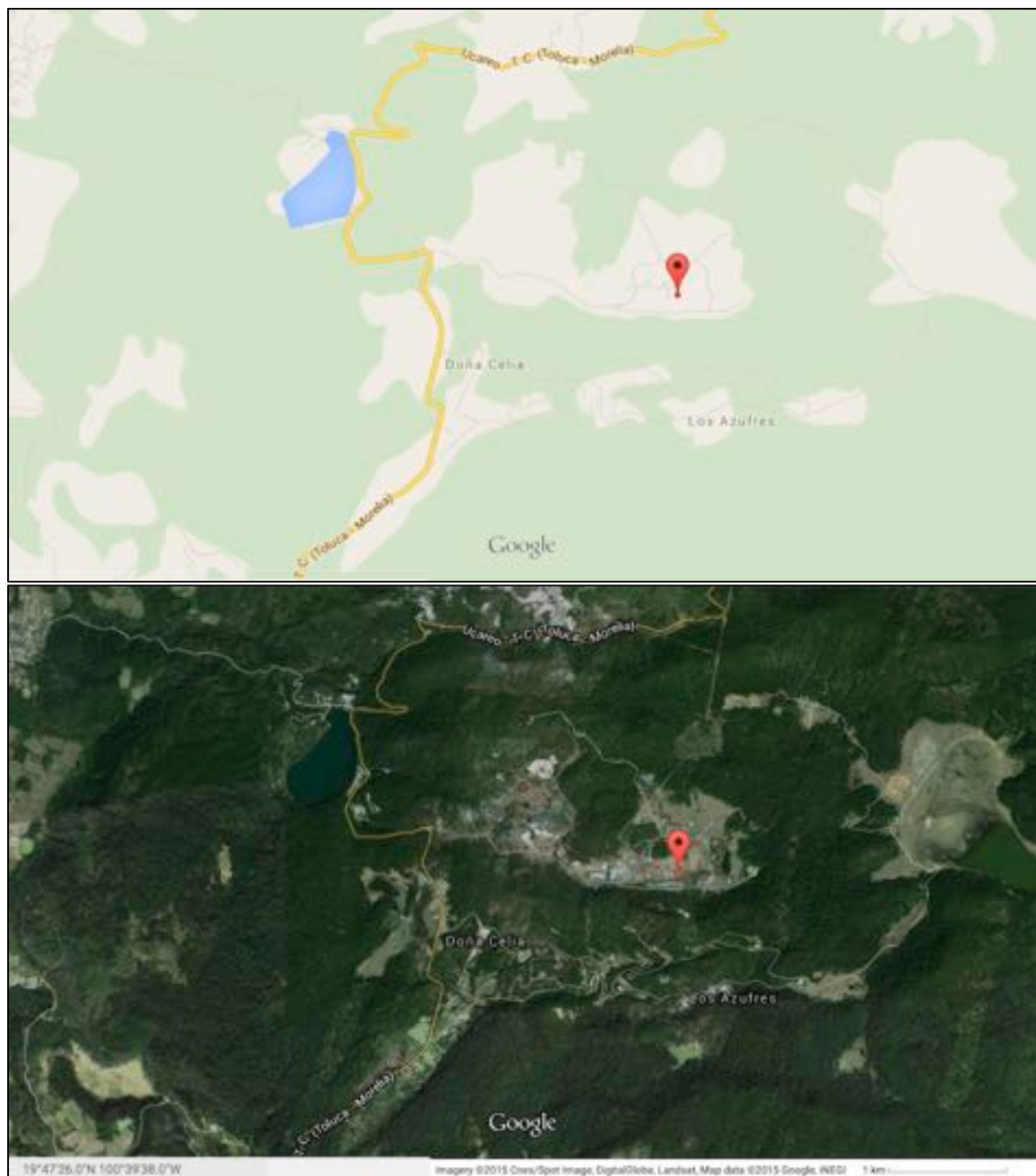


Figure 8. Location in map (top) and aerial photo (bottom) view of site AZ1: Residencia de Agua Fría.

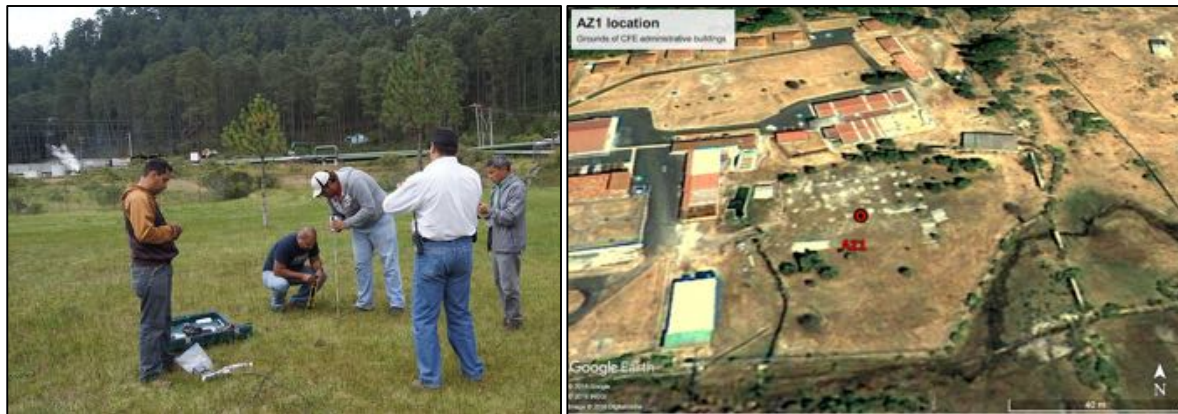


Figure 9. AZ1: Residencia de Agua Fría. Photo source: Alfredo Mercado.

2.1.2 Temperature records

A full temperature record was collected for the 181-day period. Processing of the raw temperature data included the following steps:

1. Conversion of digital records to temperatures
2. Correction of recorded times for drift in internal clock
3. Re-sampling of records to precise quarter-hour times by interpolation
4. Calculation of daily average temperatures

Figure 10 and Figure 11 show examples of the temperature records.

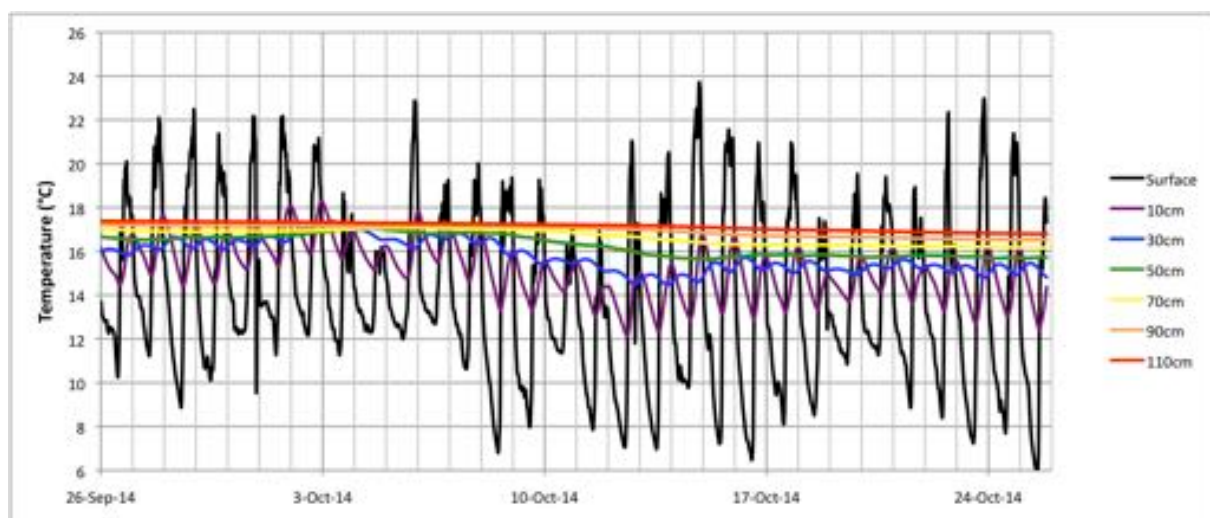


Figure 10. Detail of temperature record for first month at site AZ1.

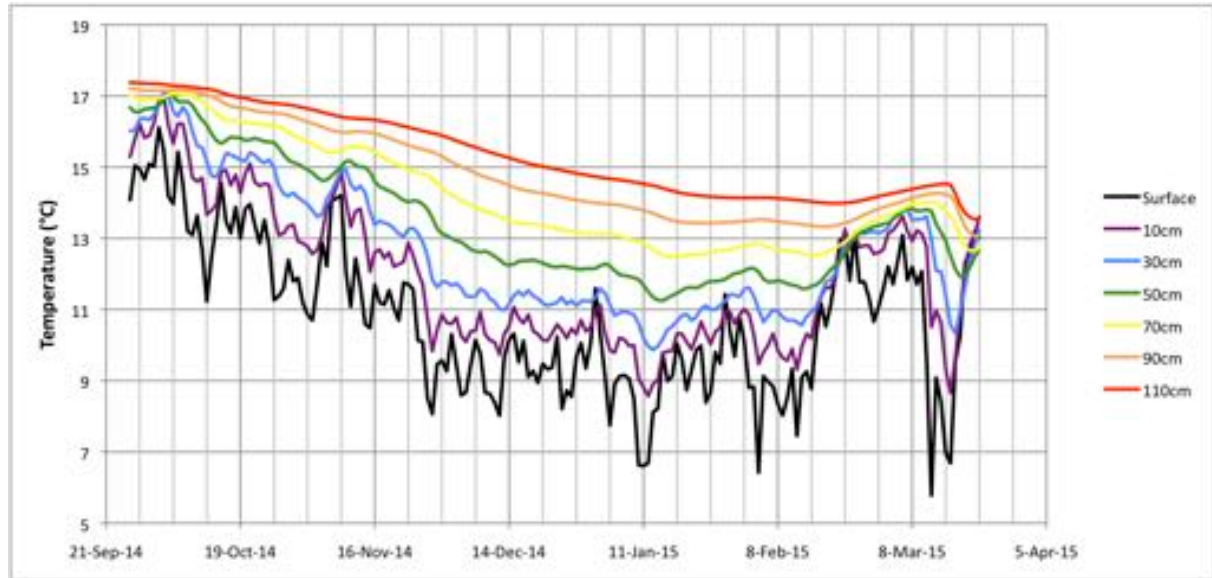


Figure 11. Daily average temperatures for site AZ1

2.1.3 Thermal diffusivity

HDR calculated mean and standard error of thermal diffusivity over the depth intervals 30–50 cm, 30–70 cm, 30–90 cm and 30–110 cm following the method summarized in Section 1.0. Figure 12 illustrates plots of $\ln(A_2/A_1)$ and phase shift (radians) versus $\sqrt{(\Delta z^2 \cdot \pi f)}$ for the four depth intervals. The gradients are theoretically equal to $1/\sqrt{\kappa}$, so the results indicate:

30–50 cm	$\kappa = 2.281 \pm 0.014 \times 10^{-7} \text{ m}^2\text{s}^{-1}$
30–70 cm	$\kappa = 2.020 \pm 0.021 \times 10^{-7} \text{ m}^2\text{s}^{-1}$
30–90 cm	$\kappa = 1.839 \pm 0.032 \times 10^{-7} \text{ m}^2\text{s}^{-1}$
30–110 cm	$\kappa = 1.887 \pm 0.053 \times 10^{-7} \text{ m}^2\text{s}^{-1}$

2.1.4 Temperature history and ‘reduced ground temperature’

A visual comparison between Aqua and Terra night time land surface temperatures and mean daily temperatures measured by the Heat Needle at 30 cm depth (Figure 13) suggests a mean offset of around 6°C. A daily mean temperature history for 30 cm depth (Figure 14) generated using a constant offset of 6.2°C from the mean satellite night time land surface temperatures was found to produce the most stable ‘reduced ground temperature’ curves (Figure 15) over the period 31 October 2014 – 31 January 2015. The inferred average surface temperature at 30 cm depth over the period of satellite coverage was 13.25°C.

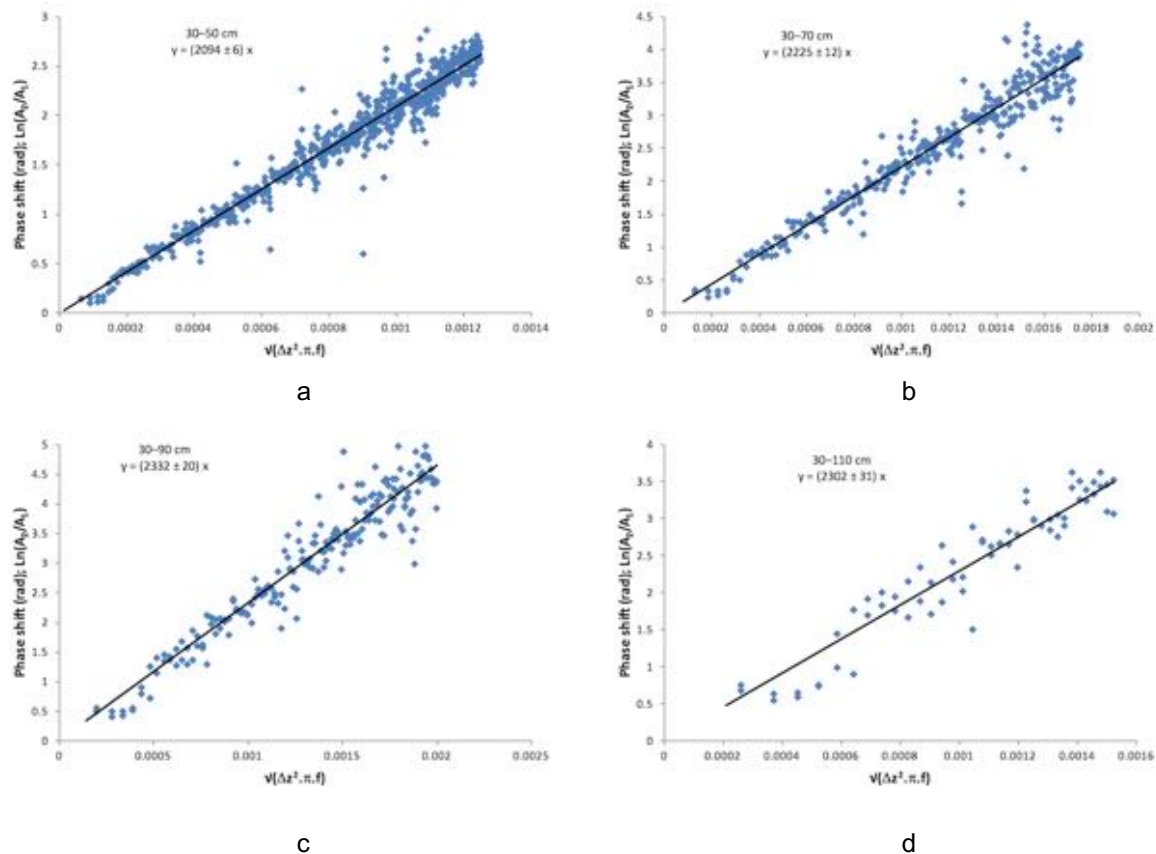


Figure 12. Harmonic spectral determination of thermal diffusivity for depth intervals (a) 30–50 cm, (b) 30–70 cm, (c) 30–90 cm and (d) 30–110 cm at site AZ1. Only relatively noise-free frequencies are plotted, the number of which decreases with increasing sensor depth. The gradient in each case is theoretically equal to $1/\sqrt{\kappa}$.

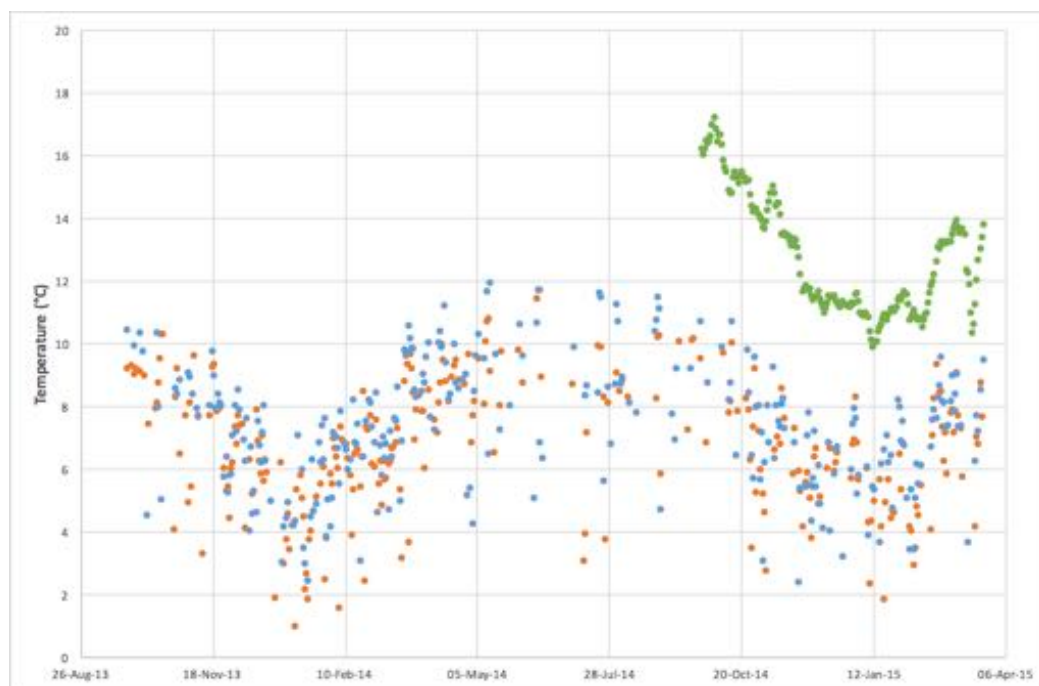


Figure 13. Mean daily temperatures at 30 cm depth measured by a Heat Needle (green dots) at AZ1, and Terra and Aqua night time land surface temperatures (blue and orange dots, respectively).

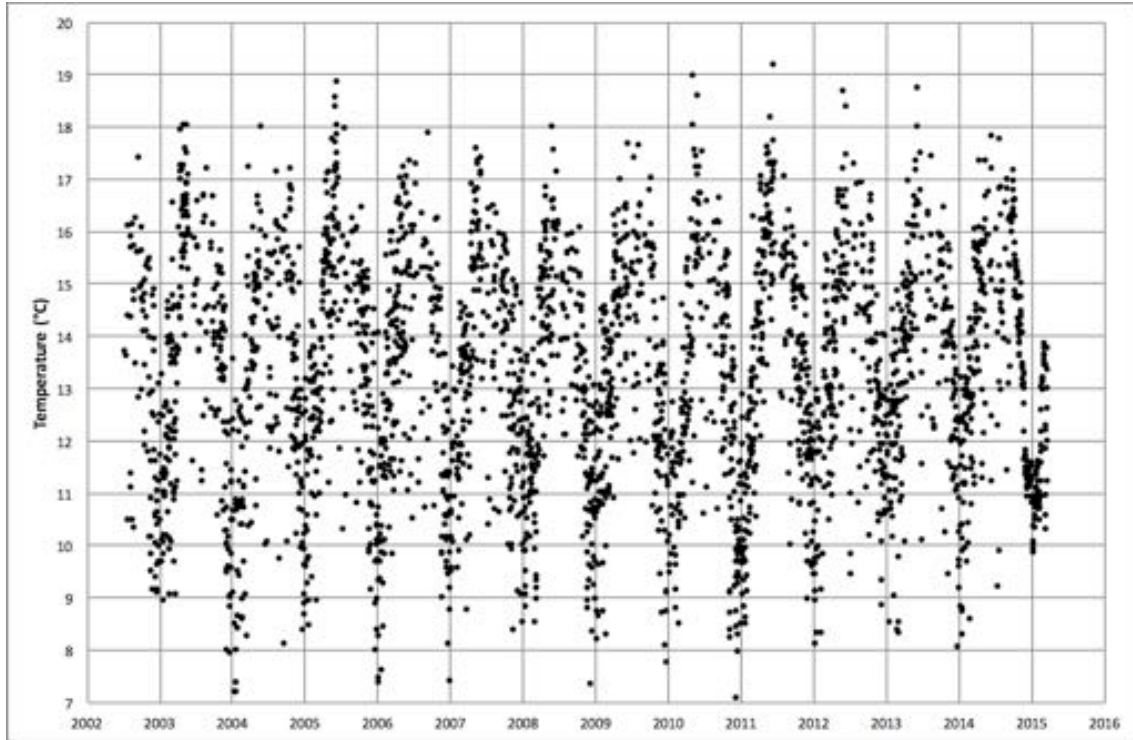


Figure 14. Daily mean temperatures at 30 cm depth at AZ1 since 2002, inferred from Terra and Aqua night time land surface temperatures

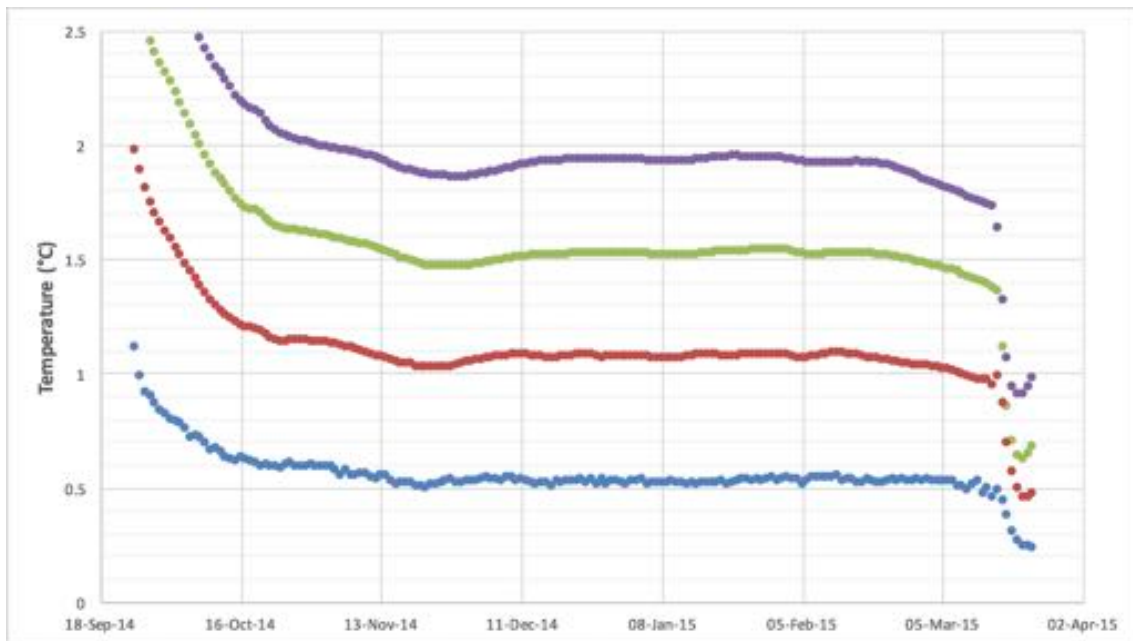


Figure 15. Reduced ground temperatures for 50 cm (blue), 70 cm (red), 90 cm (green) and 110 cm (purple) at AZ1 over the period of the survey

2.1.5 Thermal conductivity and thermal resistance

A successful thermal conductivity measurement was carried out over the time interval (UTC time) 16:53–17:53 on 24 March 2015. Assuming an ‘infinite line source’ of heat at a rate of 14.90 ± 0.04 W/m, the resulting log-linear temperature increases observed at sensor depths (Figure 16) implied mean thermal conductivities of:

30 cm	0.54 ± 0.01^8 W/mK
50 cm	0.641 ± 0.003 W/mK
70 cm	0.659 ± 0.003 W/mK
90 cm	0.751 ± 0.003 W/mK
110 cm	0.75 ± 0.1^9 W/mK

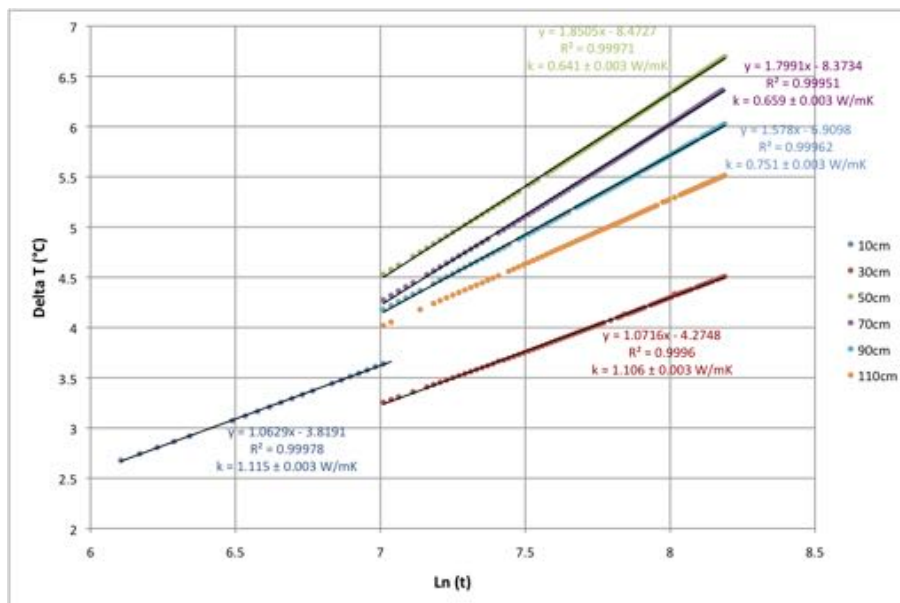


Figure 16. Temperature increase versus the natural log of heating time for site AZ1.

Thermal resistance is the integral of physical depth divided by thermal conductivity. The thermal resistance from 30 cm to each deeper sensor can be estimated from the thermal conductivity values above:

⁸ The record at 10 cm was not used in subsequent data analyses. Conductivity at 30 cm is influenced by transient near-surface effects, and chosen to optimise the intersection of subsequent Bullard plots with the origin.

⁹ The sensor at 110 cm did not meet the ‘infinite line source’ approximation, so that sensor did not yield a reliable conductivity estimate by that method. The value for 110 cm was deduced by maximising the linearity of subsequent Bullard plots.

50 cm	$0.100/0.543 + 0.100/0.641 =$	$0.340 \text{ m}^2\text{K/W}$
70 cm	$0.340 + 0.100/0.641 + 0.100/0.659 =$	$0.648 \text{ m}^2\text{K/W}$
90 cm	$0.648 + 0.100/0.659 + 0.100/0.751 =$	$0.933 \text{ m}^2\text{K/W}$
110 cm	$0.933 + 0.100/0.751 + 0.100/0.75 =$	$1.199 \text{ m}^2\text{K/W}$

In a steady state conductive setting, temperature increases linearly with thermal resistance at a gradient equal to the conductive heat flow. A straight line of best fit provides an estimate of the mean conductive heat flow at any given moment. Figure 17 shows a sample of Bullard plots of 'change in reduced temperature' versus thermal resistance at one-month intervals during the recording period. The gradient of each plot indicates the 'reduced surface heat flow' at that time, while the coefficient of determination (R^2) indicates the degree of linearity. The plots display high linearity for times after the first month.

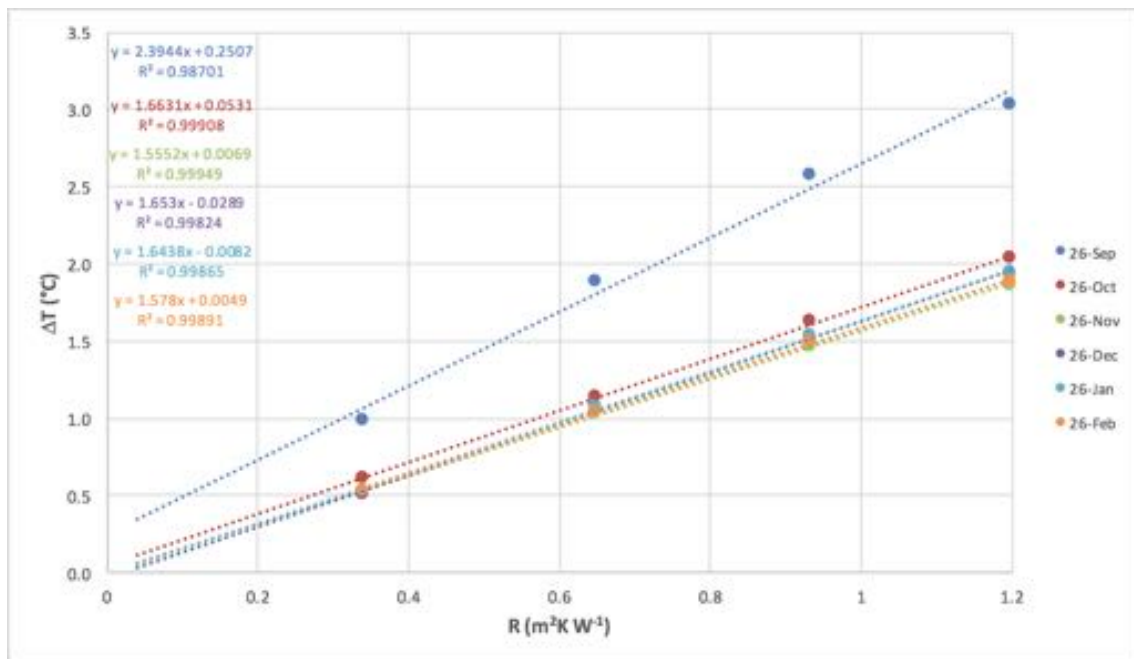


Figure 17. Bullard plots of change in 'reduced ground temperature' (ΔT) versus thermal resistance (R) at monthly intervals for site AZ1. The equations of the lines of best fit are given in the top left corner of the plot. The gradients indicate 'reduced surface heat flow' in Wm^{-2} . R^2 = coefficient of determination.

2.1.6 Reduced surface heat flow through time

Variation in 'reduced surface heat flow' through time is derived from the gradient of the Bullard plot for successive days. The red line on Figure 18 shows 'reduced surface heat flow' as a function of time for AZ1. It indicates relatively constant geophysical

heat flow at $1.63 \pm 0.01 \text{ Wm}^{-2}$ over the three-month period from 1 November 2014 to 31 January 2015.



Figure 18. ‘Reduced surface heat flow’ versus time for site AZ1 (red, left axis); Coefficient of determination (black, right axis).

2.1.7 Summary

The reduced surface heat flow at this location is estimated at $1.63 \pm 0.01 \text{ W/m}^2$. This is about 25 times the mean global continental heat flow (e.g. Beardsmore and Cull, 2001¹⁰), which indicates an anomalous, significant heat source beneath this site. Reductions in reduced surface heat flow in late November (temporary) and late February (open ended) suggest non-conductive components of heat transfer in the shallow sub-surface at those times. Possible mechanisms include transpiration through deep grass roots, infiltration of meteoric water, or evaporation from the soil.

¹⁰ Beardsmore, G.R. and Cull, J.P. (2001). *Crustal Heat Flow: A Guide to Measurement and Modelling*. Cambridge University Press: Cambridge, UK. 321pp.

2.2 Site AZ2: Balneario Rancho Viejo

2.2.1 Location

Latitude 19.78203°N, Longitude 100.67619°W

UTM coordinates: 14Q 324402mE 2188230mN Elevation: 2,776±9 m

The Heat Needle was placed within a private spa operating within the geothermal field (Figure 19, Figure 20), about 3 m from a 1 m deep and 3 m wide flowing creek. It recorded ground temperature data from 24 September 2014 to 24 March 2015.

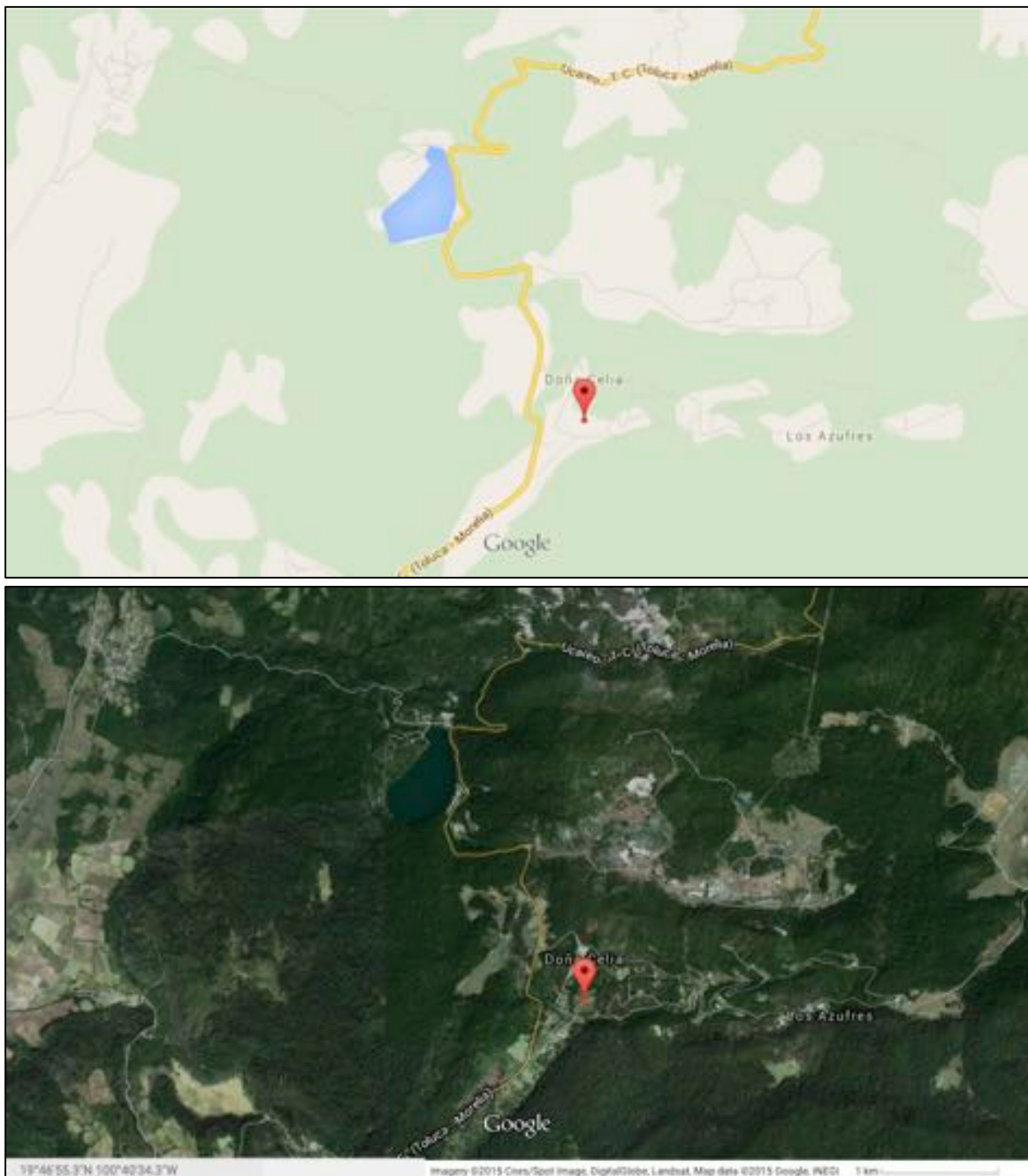


Figure 19. Location in map (top) and aerial photo (bottom) view of site AZ2: Balneario Rancho Viejo.



Figure 20. AZ2: Balneario Rancho Viejo. Photo source: Anson Antriasian.

2.2.2 Temperature records

A full temperature record was collected for the 181-day period. Processing of the raw temperature data included the following steps:

1. Conversion of digital records to temperatures
2. Correction of recorded times for drift in internal clock
3. Re-sampling of records to precise quarter-hour times by interpolation
4. Calculation of daily average temperatures

Figure 21 and Figure 22 show examples of the temperature records.

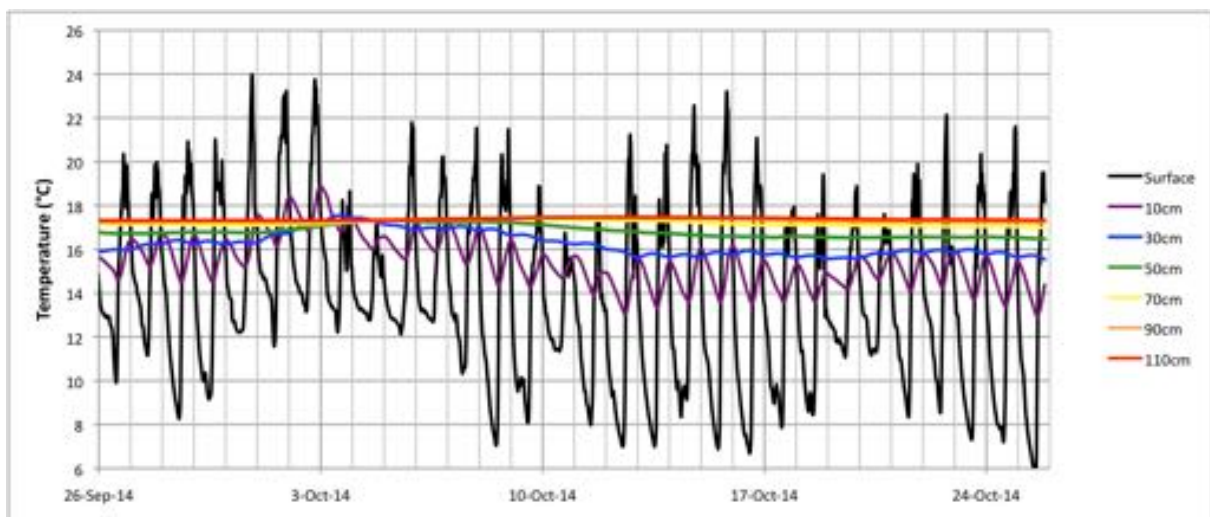


Figure 21. Detail of temperature record for first month at site AZ2.

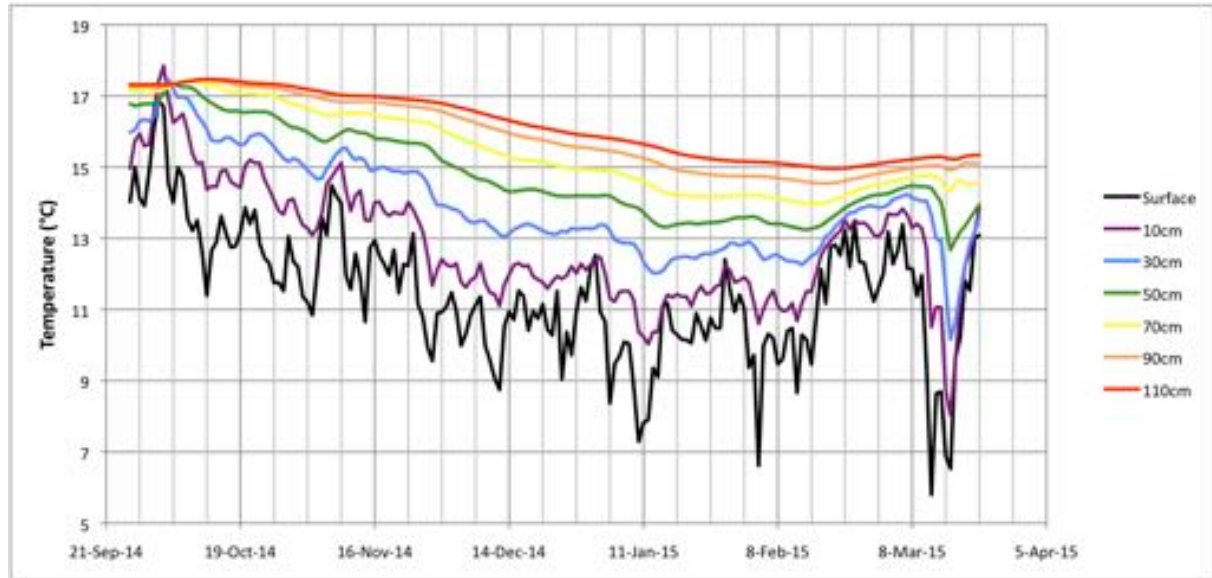


Figure 22. Daily average temperature for site AZ2.

2.2.3 Thermal diffusivity

HDR calculated mean and standard error of thermal diffusivity over the depth intervals 30–50 cm, 30–70 cm, 30–90 cm and 30–110 cm following the method summarized in Section 1.0. Figure 23 illustrates plots of $\ln(A_2/A_1)$ and phase shift (radians) versus $\sqrt{(\Delta z^2 \cdot \pi f)}$ for the four depth intervals. The gradients are theoretically equal to $1/\sqrt{\kappa}$, so the results indicate:

30–50 cm	$\kappa = 2.082 \pm 0.022 \times 10^{-7} \text{ m}^2\text{s}^{-1}$
30–70 cm	$\kappa = 1.984 \pm 0.066 \times 10^{-7} \text{ m}^2\text{s}^{-1}$
30–90 cm	$\kappa = 2.070 \pm 0.073 \times 10^{-7} \text{ m}^2\text{s}^{-1}$
30–110 cm	$\kappa = 2.163 \pm 0.173 \times 10^{-7} \text{ m}^2\text{s}^{-1}$

2.2.4 Temperature history and ‘reduced ground temperature’

A visual comparison between Aqua and Terra night time land surface temperatures and mean daily temperatures measured by the Heat Needle at 30 cm depth (Figure 24) suggests a mean offset of around 6°C. A daily mean temperature history for 30 cm depth (Figure 25) generated using a constant offset of 6.7°C from the mean satellite night time land surface temperatures was found to produce the most stable ‘reduced ground temperature’ curves (Figure 26) over the period 28 October – 28 December 2014. The inferred average surface temperature at 30 cm depth over the period of satellite coverage was 14.25°C.

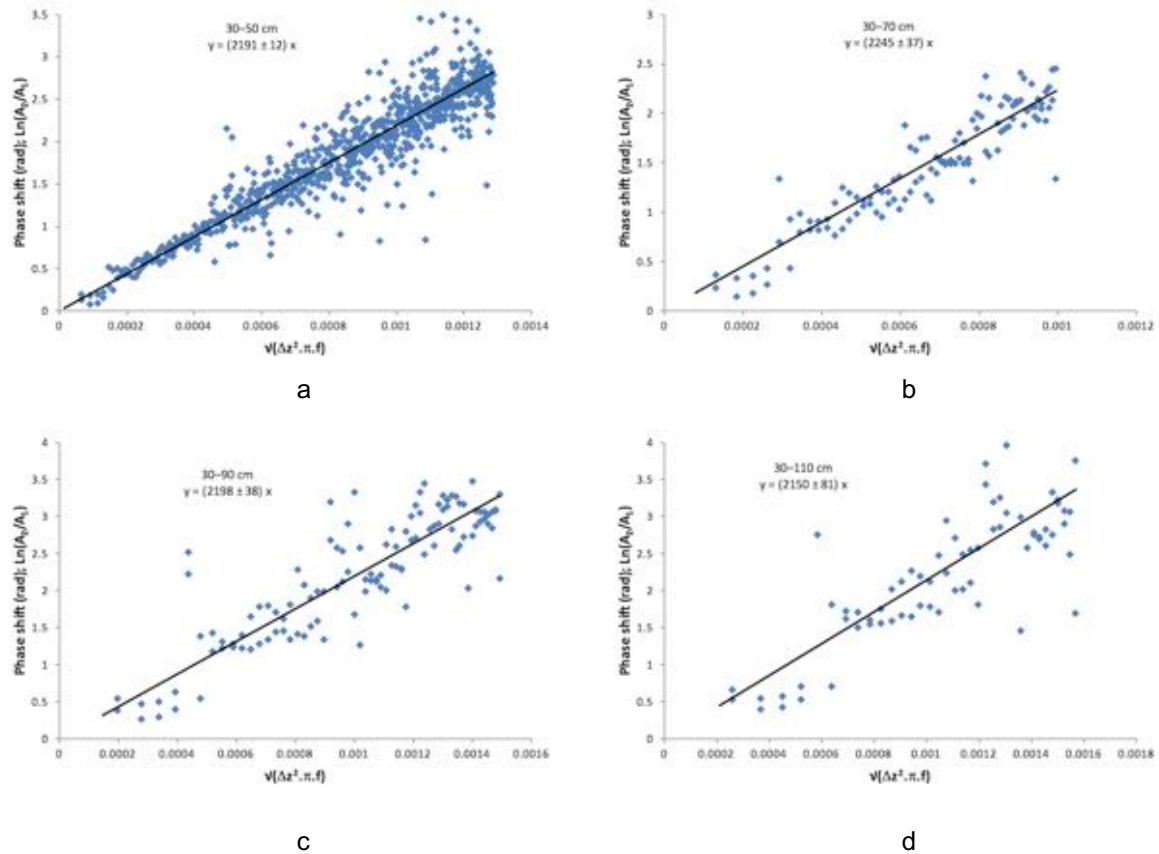


Figure 23. Harmonic spectral determination of thermal diffusivity for depth intervals (a) 30–50 cm, (b) 30–70 cm, (c) 30–90 cm and (d) 30–110 cm at site AZ2. Only relatively noise-free frequencies are plotted. The gradient in each case is theoretically equal to $1/\sqrt{\kappa}$. Uncertainties are greater than for AZ1.

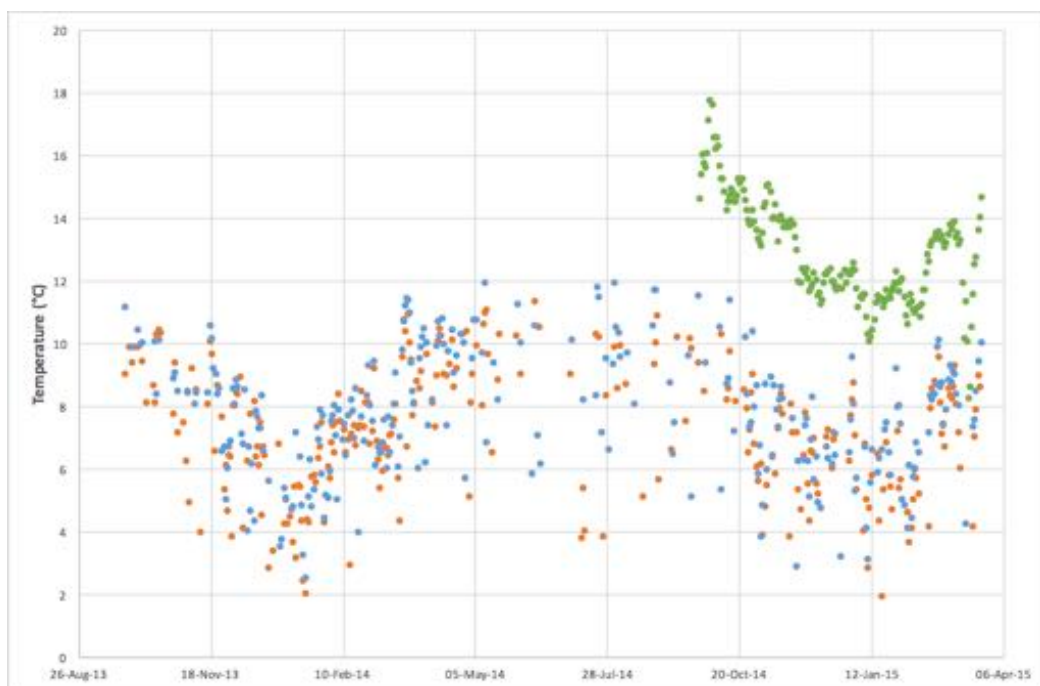


Figure 24. Mean daily temperatures at 30 cm depth measured by a Heat Needle (green dots) at AZ2, and Terra and Aqua night time land surface temperatures (blue and orange dots, respectively).

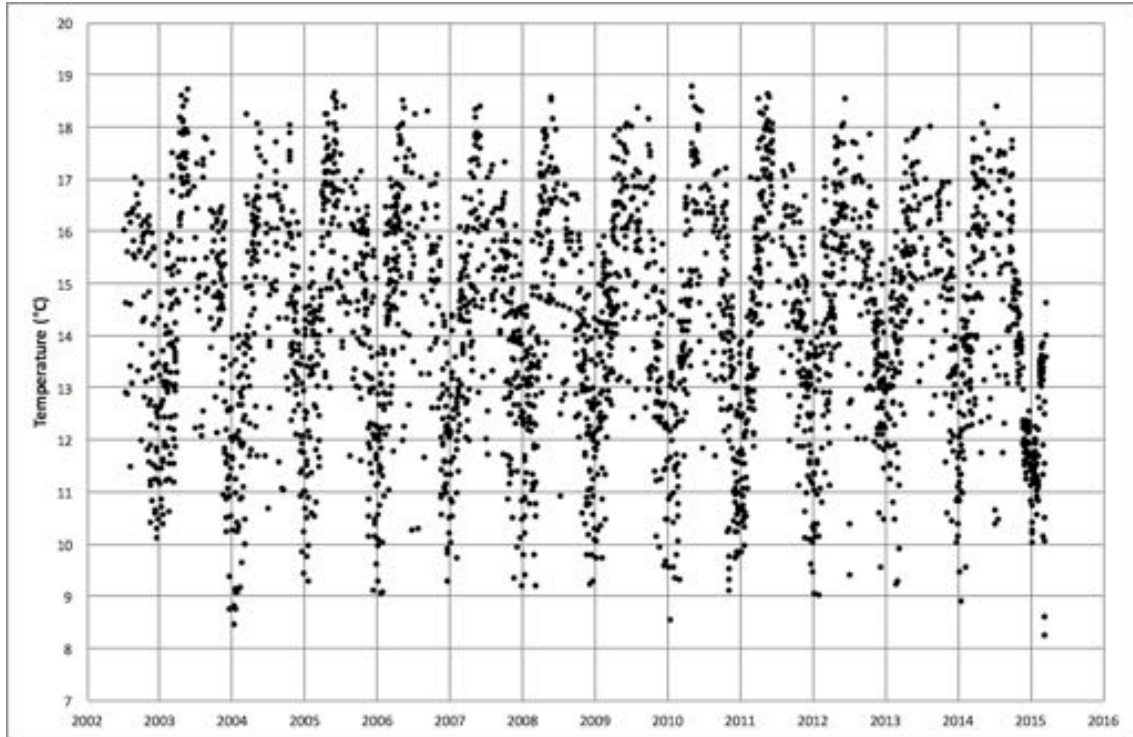


Figure 25. Daily mean temperatures at 30 cm depth at AZ2 since 2002, inferred from Terra and Aqua night time land surface temperatures

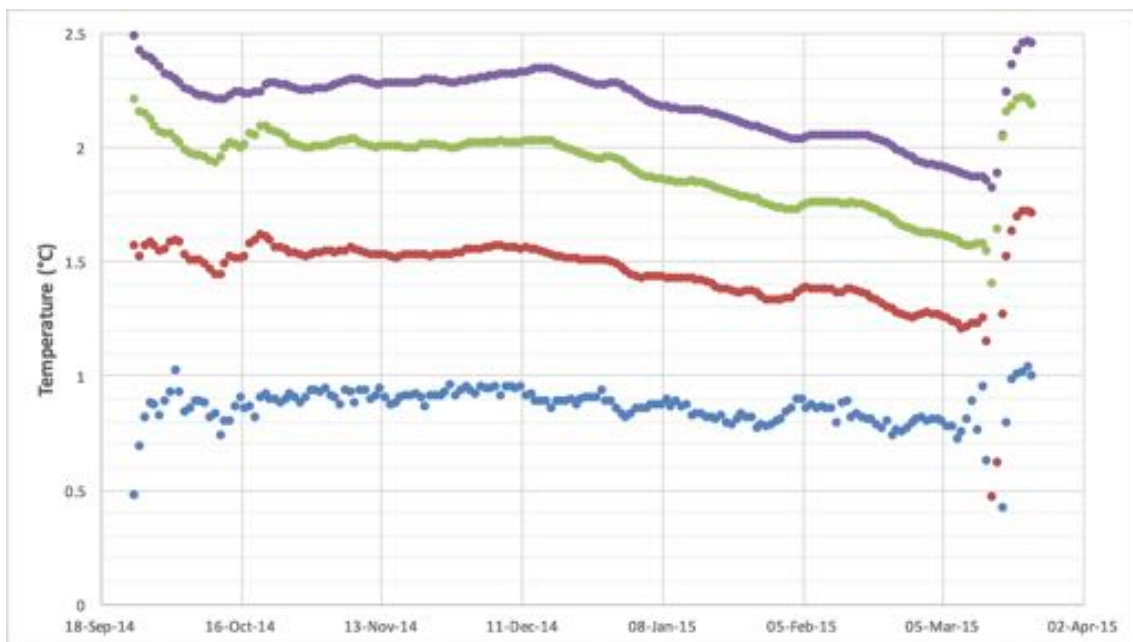


Figure 26. Reduced ground temperatures for 50 cm (blue), 70 cm (red), 90 cm (green) and 110 cm (purple) at AZ2 over the period of the survey

2.2.5 Thermal conductivity and thermal resistance

A successful thermal conductivity measurement was carried out over the time interval (UTC time) 19:10–20:10 on 24 March 2015. Assuming an ‘infinite line source’ of heat at a rate of 14.90 ± 0.04 W/m, the resulting log-linear temperature increases observed at sensor depths (Figure 27) imply thermal conductivities of:

30 cm	0.31 ± 0.01^8 W/mK
50 cm	0.697 ± 0.003 W/mK
70 cm	0.837 ± 0.003 W/mK
90 cm	0.877 ± 0.003 W/mK
110 cm	3.5 ± 0.1^9 W/mK

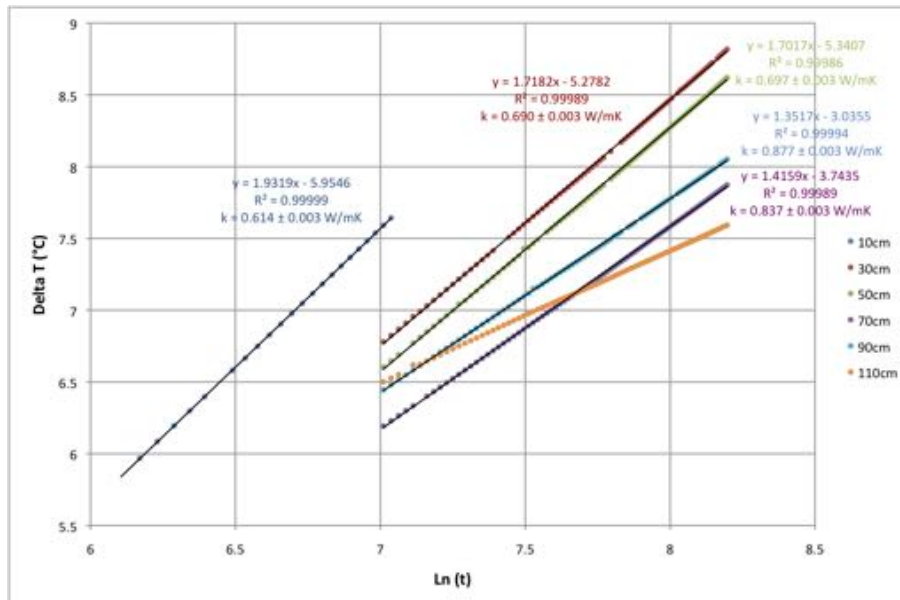


Figure 27. Temperature increase versus the natural log of heating time for site AZ2.

Thermal resistance is the integral of physical depth divided by thermal conductivity. The thermal resistance from 30 cm to each deeper sensor can be estimated from the thermal conductivity values above:

50 cm	$0.100/0.311 + 0.100/0.697 = 0.465$ m ² K/W
70 cm	$0.465 + 0.100/0.697 + 0.100/0.837 = 0.728$ m ² K/W
90 cm	$0.728 + 0.100/0.837 + 0.100/0.877 = 0.961$ m ² K/W
110 cm	$0.961 + 0.100/0.877 + 0.100/3.5 = 1.104$ m ² K/W

In a steady state conductive setting, temperature increases linearly with thermal resistance at a gradient equal to the conductive heat flow. A straight line of best fit provides an estimate of the mean conductive heat flow at any given moment. Figure 28 shows a sample of Bullard plots of ‘change in reduced temperature’ versus thermal resistance at one-month intervals during the recording period. The gradient of each plot indicates the ‘reduced surface heat flow’ at that time, while the coefficient of determination (R^2) indicates the degree of linearity. The plots are less linear than for AZ1, suggesting an influence of non-conductive processes.

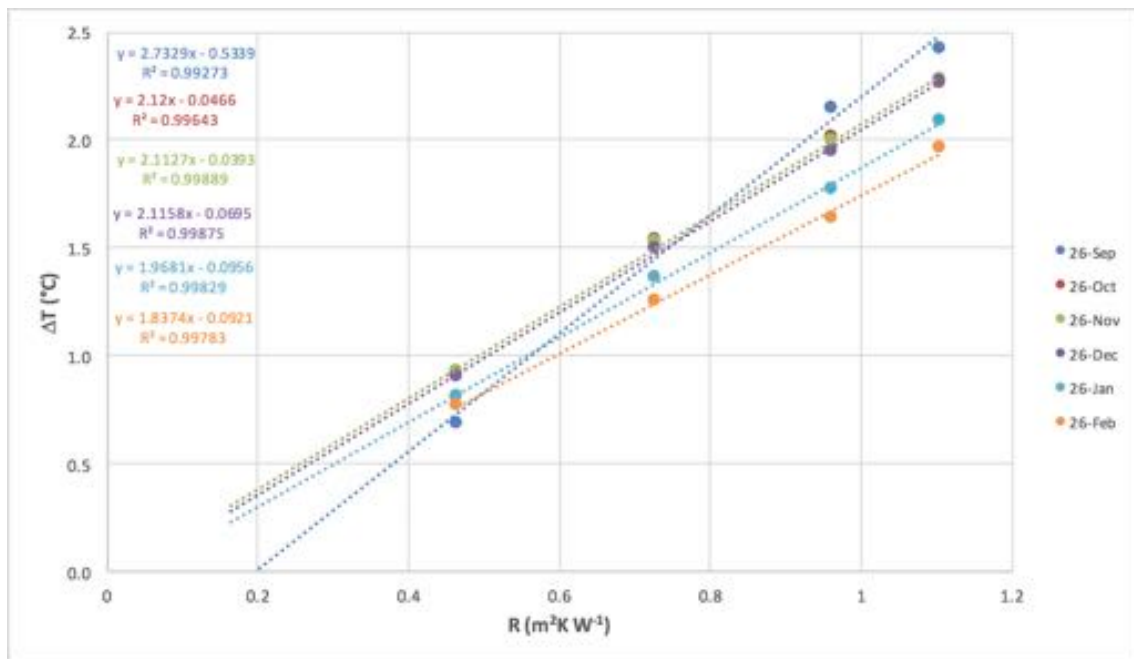


Figure 28. Bullard plots of change in ‘reduced ground temperature’ (ΔT) versus thermal resistance (R) at monthly intervals for site AZ2. The equations of the lines of best fit are given in the top left corner of the plot. The gradients indicate ‘reduced surface heat flow’ in Wm^{-2} . R^2 = coefficient of determination.

2.2.6 Reduced surface heat flow through time

Variation in ‘reduced surface heat flow’ through time is derived from the gradient of the Bullard plot for successive days. The red line on Figure 29 shows ‘reduced surface heat flow’ as a function of time for AZ2. It indicates relatively constant geophysical heat flow at $2.15 \pm 0.05 \text{ Wm}^{-2}$ over the three-month period from 1 October to 31 December 2014, followed by a gradual decline of 25% over the succeeding two and a half months, then a sudden recover to pre-Christmas levels.



Figure 29. ‘Reduced surface heat flow’ versus time for site AZ2 (red, left axis); Coefficient of determination (black, right axis).

2.2.7 Summary

The reduced surface heat flow at this location is estimated at $2.15 \pm 0.05 \text{ W/m}^2$. This is more than 30 times the mean global continental heat flow (e.g. Beardsmore and Cull, 2001¹⁰), which indicates an anomalous, significant heat source beneath this site. The volatile, gradual decline in reduced surface heat flow from late-December to mid-March suggests a non-conductive component of heat transfer in the shallow sub-surface over that period. This is supported by the relatively high scatter in the thermal diffusivity plots (Figure 23). Given the site’s proximity to a flowing stream, a possible mechanism for the reduction in heat flow is the gradual infiltration of relatively cool meteoric water from the stream into the surrounding soil.

2.3 Site AZ4: Balneario La Cumbre

2.3.1 Location

Latitude 19.82160°N, Longitude 100.68566°W

UTM coordinates: 14Q 323454mE 2192620mN

Elevation: 2,799±13 m

The Heat Needle was placed inside a small private spa (Figure 30, Figure 31). It recorded ground temperature data from 24 September 2014 to 24 March 2015.

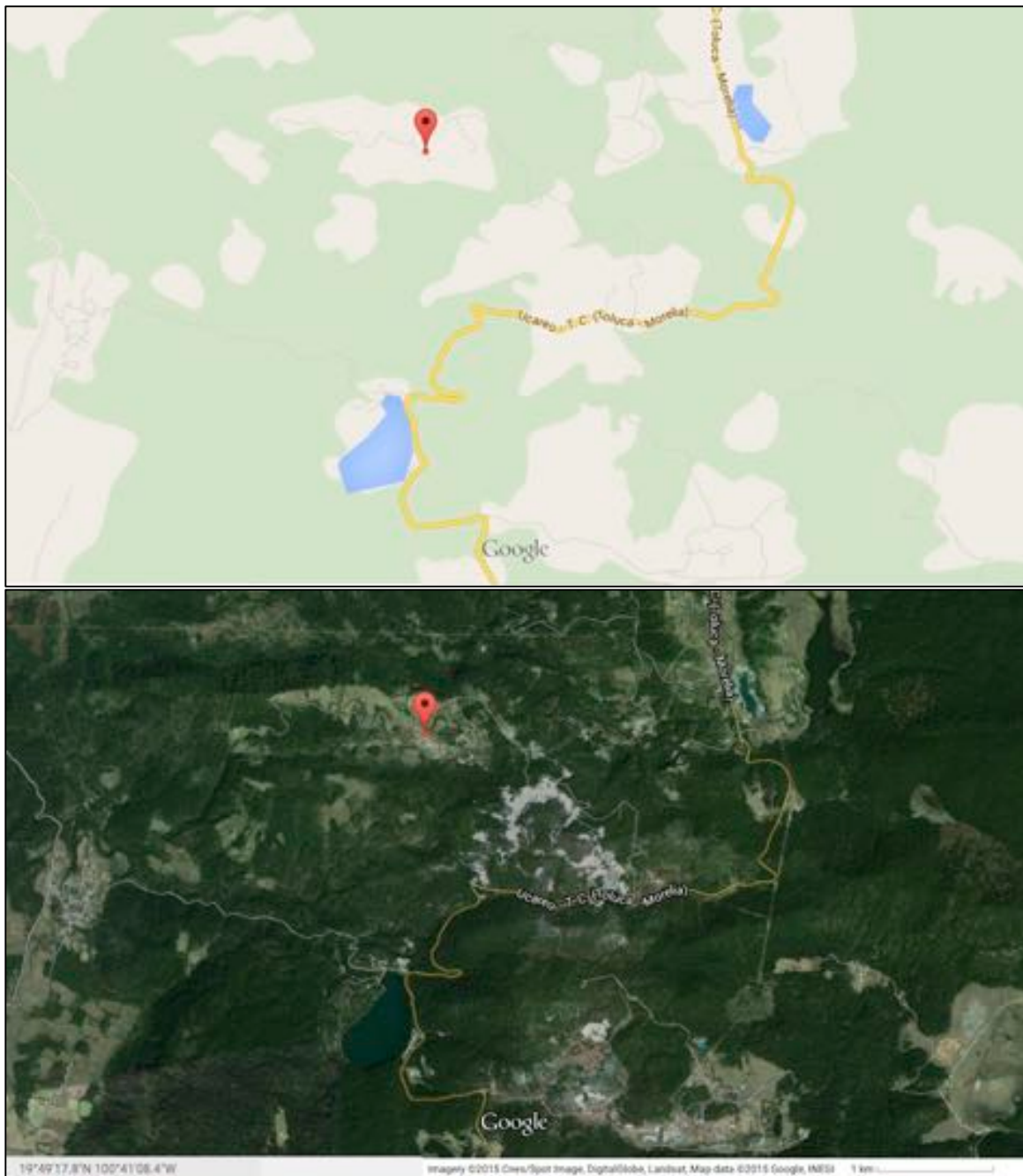


Figure 30. Location in map (top) and aerial photo (bottom) view of site AZ4: Balneario La Cumbre.



Figure 31. AZ4: Balneario La Cumbre. Photo source: Alfredo Mercado.

2.3.2 Temperature records

A full temperature record was collected for the 181-day period. Processing of the raw temperature data included the following steps:

1. Conversion of digital records to temperatures
2. Correction of recorded times for drift in internal clock
3. Re-sampling of records to precise quarter-hour times by interpolation
4. Calculation of daily average temperatures

Figure 32 and Figure 33 show examples of the temperature records.

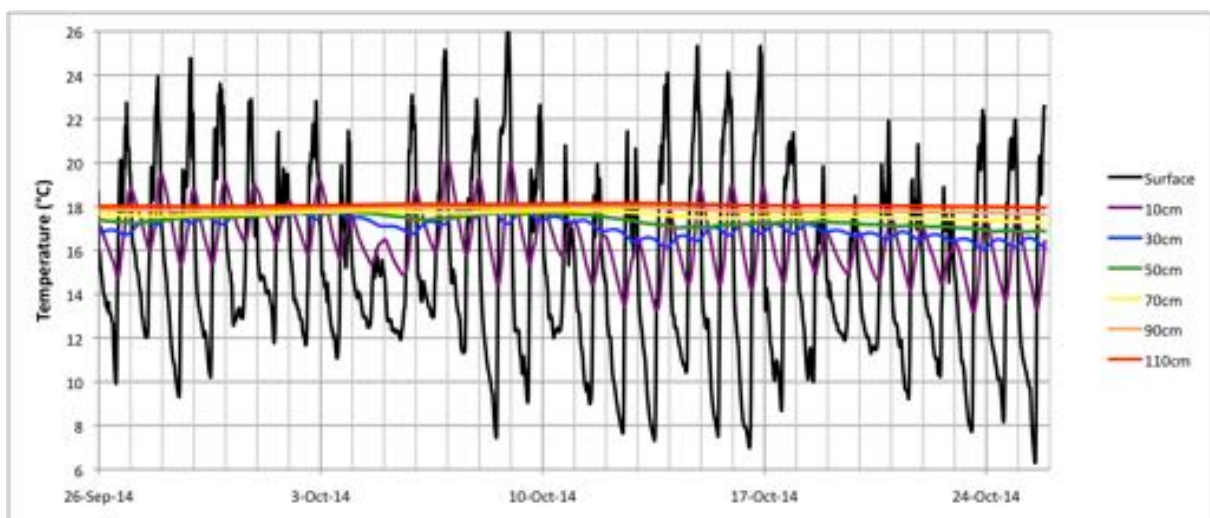


Figure 32. Detail of temperature record for first month at site AZ4.

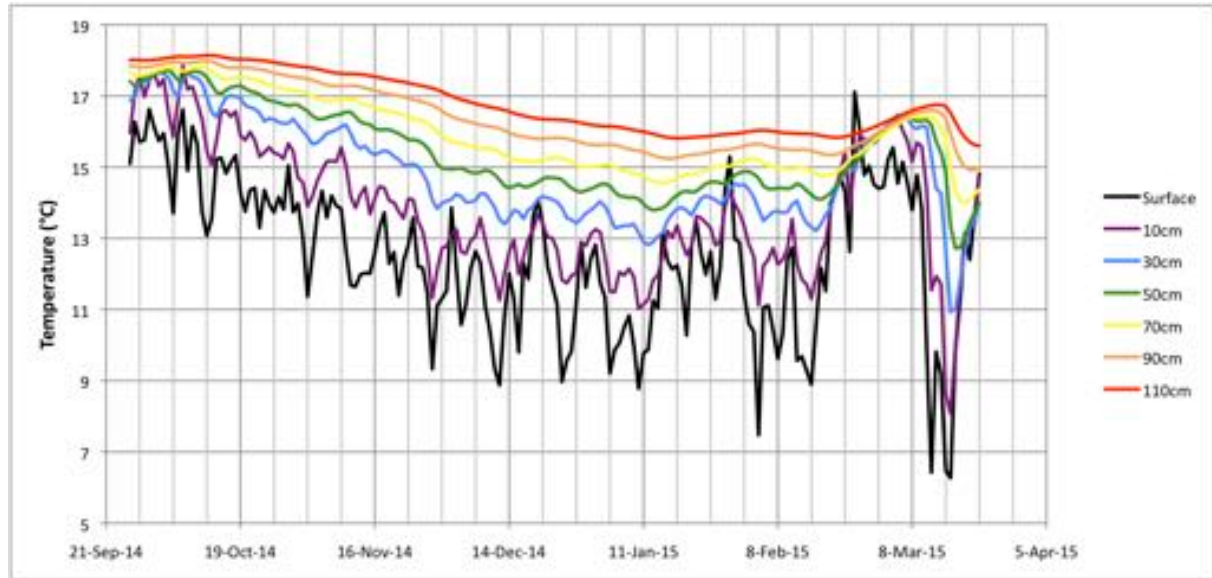


Figure 33. Daily average temperature for site AZ4.

2.3.3 Thermal diffusivity

HDR calculated mean and standard error of thermal diffusivity over the depth intervals 30–50 cm, 30–70 cm, 30–90 cm and 30–110 cm following the method summarized in Section 1.0. Figure 34 illustrates plots of $\ln(A_2/A_1)$ and phase shift (radians) versus $\sqrt{(\Delta z^2 \cdot \pi \cdot f)}$ for the four depth intervals. The gradients are theoretically equal to $1/\sqrt{\kappa}$, so the results indicate:

30–50 cm	$\kappa = 3.186 \pm 0.012 \times 10^{-7} \text{ m}^2\text{s}^{-1}$
30–70 cm	$\kappa = 3.346 \pm 0.019 \times 10^{-7} \text{ m}^2\text{s}^{-1}$
30–90 cm	$\kappa = 3.393 \pm 0.026 \times 10^{-7} \text{ m}^2\text{s}^{-1}$
30–110 cm	$\kappa = 3.409 \pm 0.029 \times 10^{-7} \text{ m}^2\text{s}^{-1}$

2.3.4. Temperature history and ‘reduced ground temperature’

A visual comparison between Aqua and Terra night time land surface temperatures and mean daily temperatures measured by the Heat Needle at 30 cm depth (Figure 35) suggests a mean offset of around 7°C. A daily mean temperature history for 30 cm depth (Figure 36) generated using a constant offset of 6.7°C from the mean satellite night time land surface temperatures was found to produce the most stable ‘reduced ground temperature’ curves (Figure 37) over the period 1 November 2014 – 28 February 2015. The inferred average temperature at 30 cm depth over the period of satellite coverage was 15.00°C.

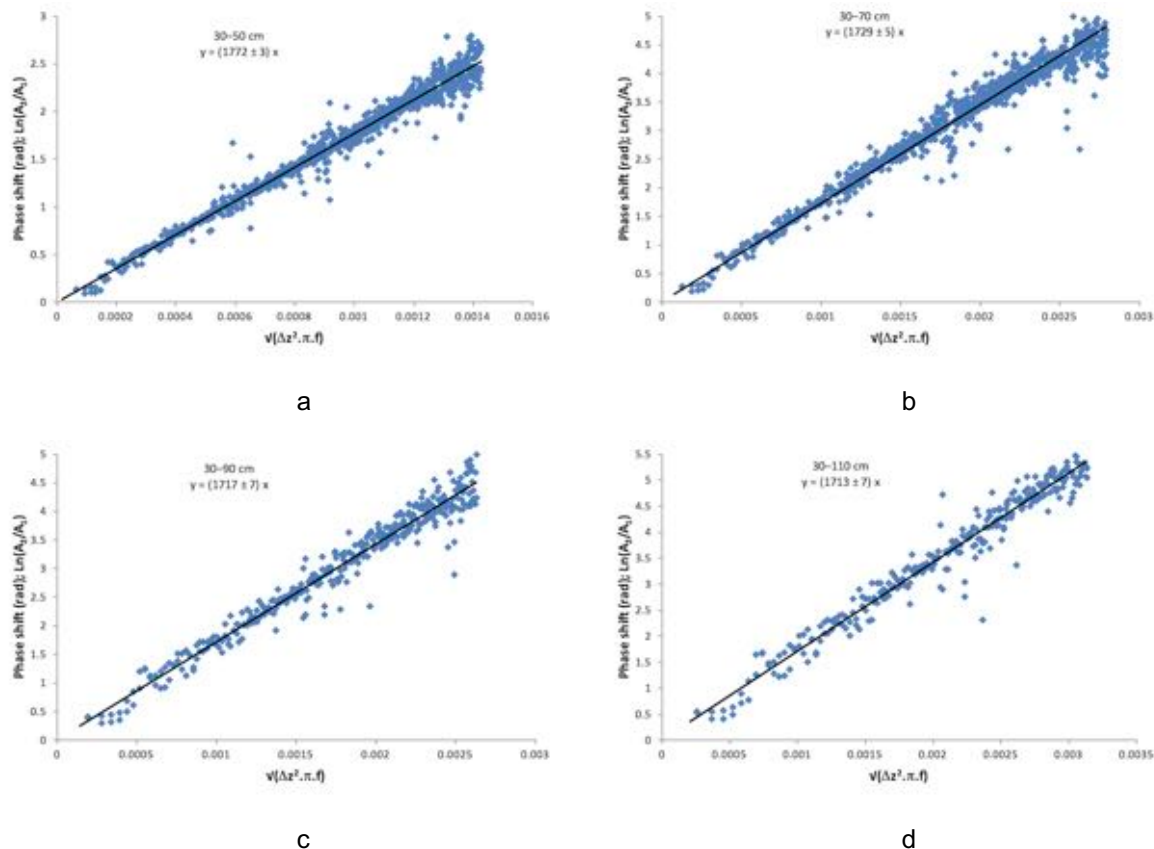


Figure 34. Harmonic spectral determination of thermal diffusivity for depth intervals (a) 30–50 cm, (b) 30–70 cm, (c) 30–90 cm and (d) 30–110 cm at site AZ4. Only relatively noise-free frequencies are plotted. The gradient in each case is theoretically equal to $1/\sqrt{k}$. All values are tightly constrained.

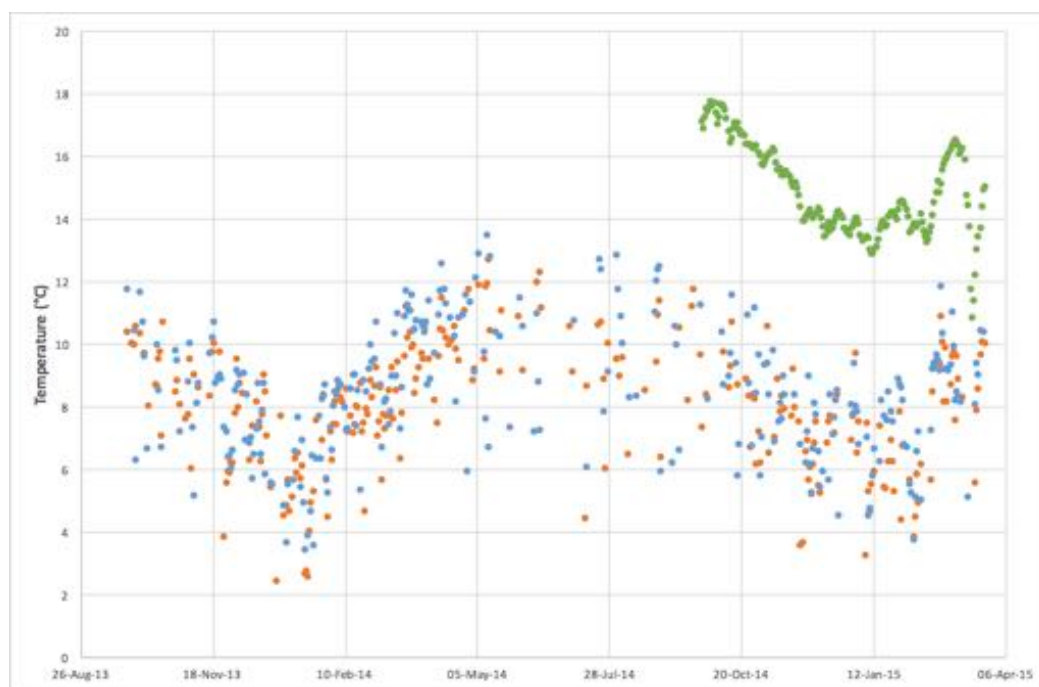


Figure 35. Mean daily temperatures at 30 cm depth measured by a Heat Needle (green dots) at AZ4, and Terra and Aqua night time land surface temperatures (blue and orange dots, respectively).

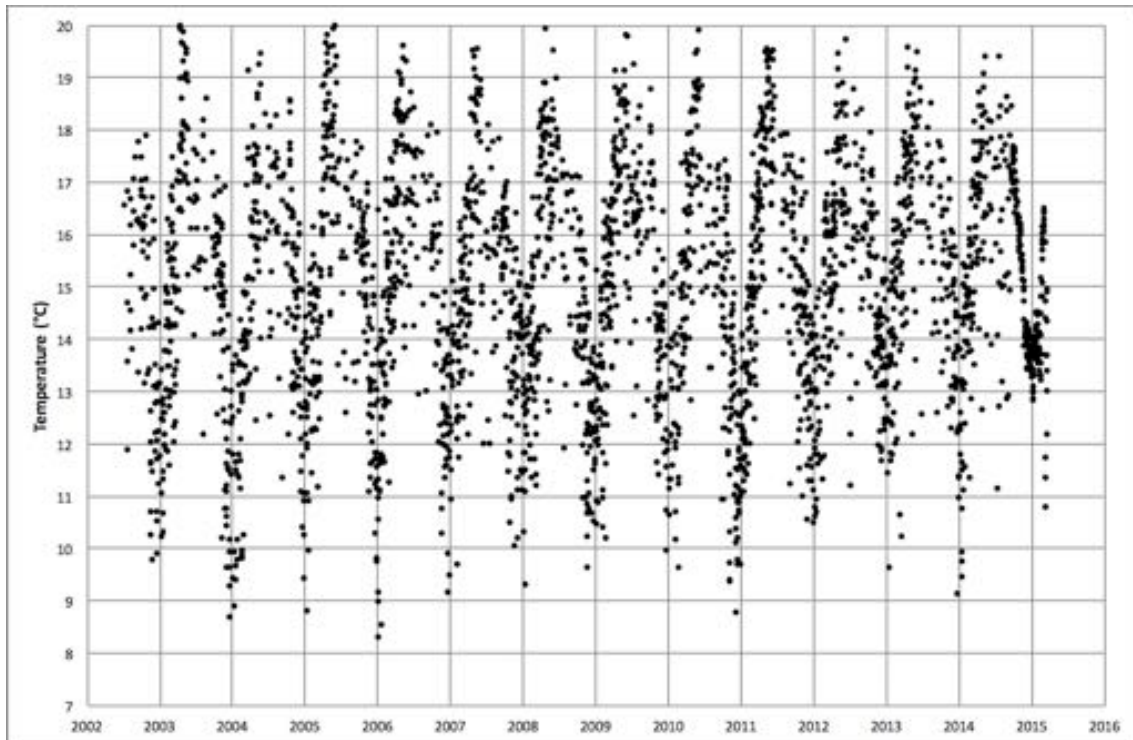


Figure 36. Daily mean temperatures at 30 cm depth at AZ4 since 2002, inferred from Terra and Aqua night time land surface temperatures

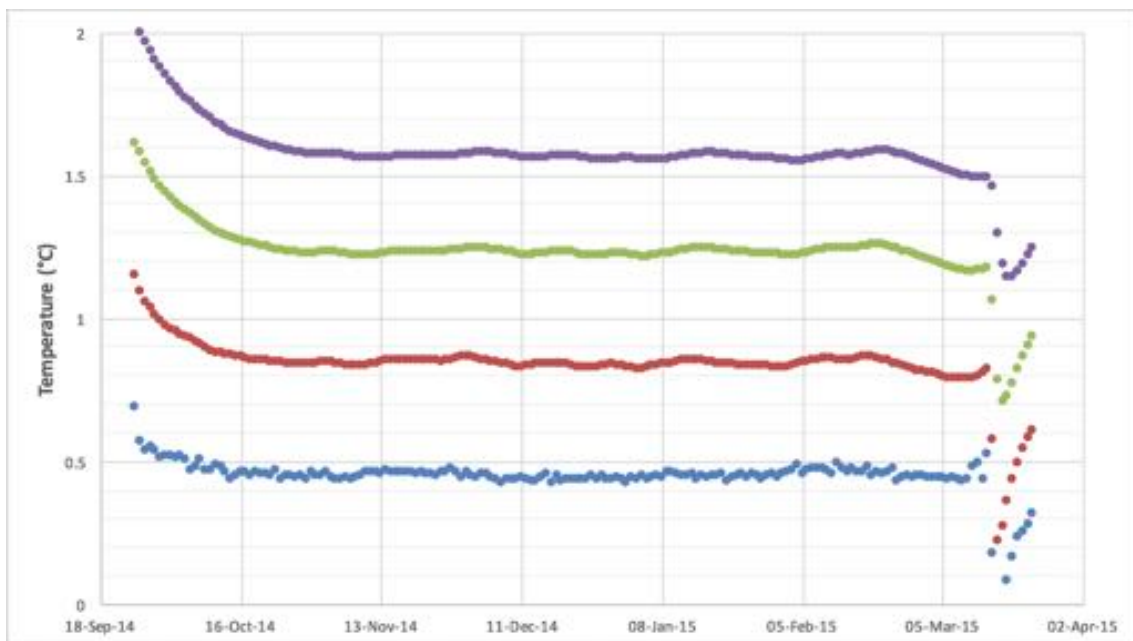


Figure 37. Reduced ground temperatures for 50 cm (blue), 70 cm (red), 90 cm (green) and 110 cm (purple) at AZ4 over the period of the survey

2.3.5 Thermal conductivity and thermal resistance

A successful thermal conductivity measurement was carried out over the time interval (UTC time) 23:53 on 24 March 2015 – 00:53 on 25 March 2015. Assuming an ‘infinite line source’ of heat at a rate of 14.90 ± 0.04 W/m, the resulting log-linear temperature increases observed at sensor depths (Figure 38) imply thermal conductivities of:

30 cm	0.71 ± 0.01^8 W/mK
50 cm	1.062 ± 0.003 W/mK
70 cm	0.937 ± 0.003 W/mK
90 cm	0.979 ± 0.003 W/mK
110 cm	1.4 ± 0.1^9 W/mK

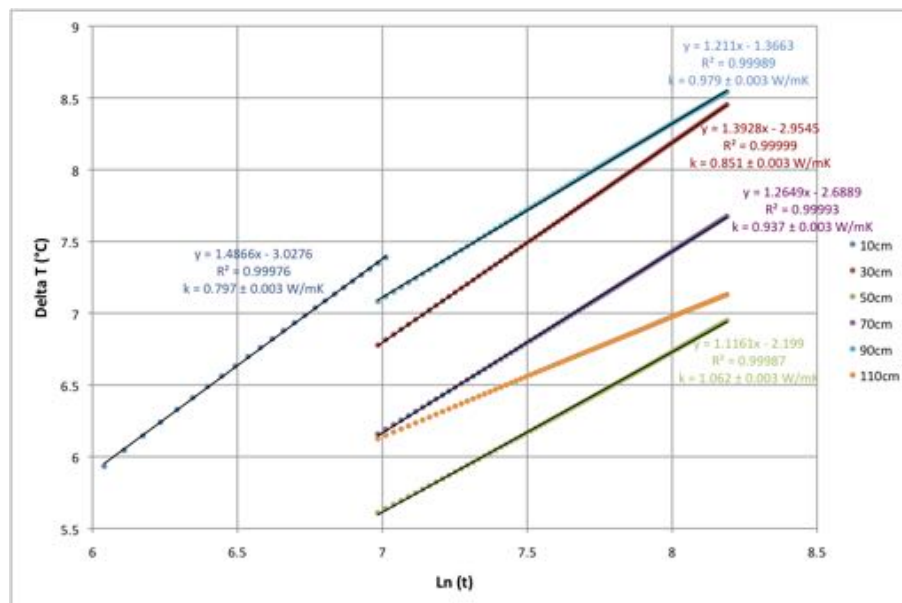


Figure 38. Temperature increase versus the natural log of heating time; raw plot for site AZ4.

Thermal resistance is the integral of physical depth divided by thermal conductivity. The thermal resistance from 30 cm to each deeper sensor can be estimated from the thermal conductivity values above:

50 cm	$0.100/0.71 + 0.100/1.062 =$	$0.235 \text{ m}^2\text{K/W}$
70 cm	$0.235 + 0.100/1.062 + 0.100/0.937 =$	$0.436 \text{ m}^2\text{K/W}$
90 cm	$0.436 + 0.100/0.937 + 0.100/0.979 =$	$0.645 \text{ m}^2\text{K/W}$
110 cm	$0.645 + 0.100/0.979 + 0.100/1.4 =$	$0.818 \text{ m}^2\text{K/W}$

In a steady state conductive setting, temperature increases linearly with thermal resistance at a gradient equal to the conductive heat flow. A straight line of best fit provides an estimate of the mean conductive heat flow at any given moment. Figure 39 shows a sample of Bullard plots of ‘change in reduced temperature’ versus thermal resistance at one-month intervals during the recording period. The gradient of each plot indicates the ‘reduced surface heat flow’ at that time, while the coefficient of determination (R^2) indicates the degree of linearity. The plots are highly linear, suggesting dominant conductive processes.

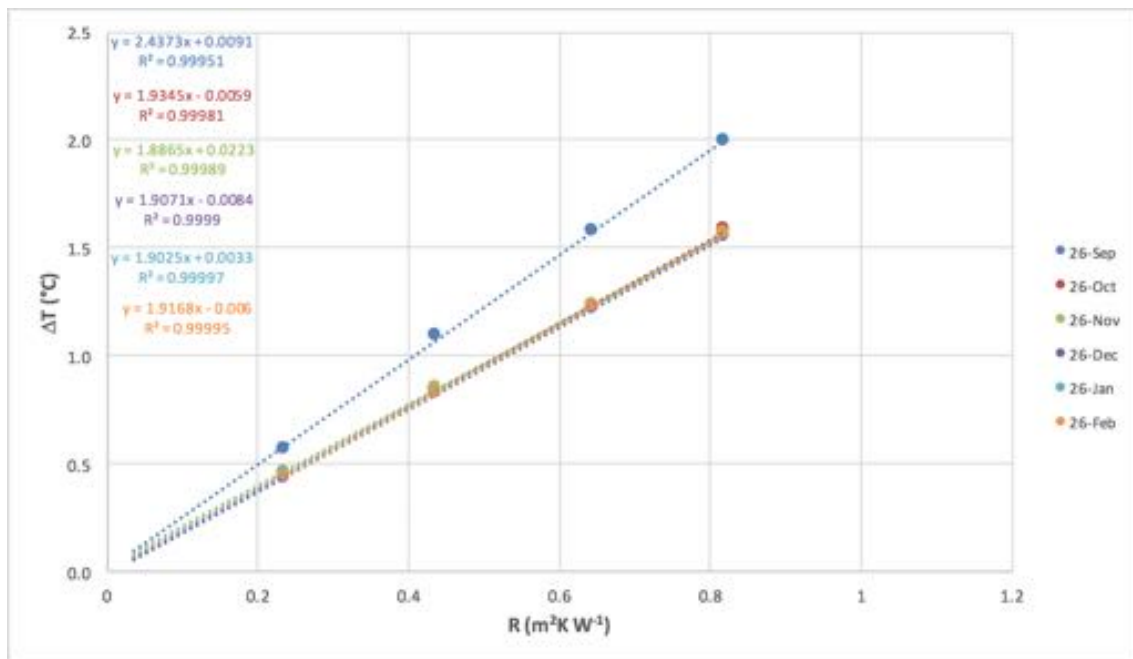


Figure 39. Bullard plots of change in ‘reduced ground temperature’ (ΔT) versus thermal resistance (R) at monthly intervals for site AZ4. The equations of the lines of best fit are given in the top left corner of the plot. The gradients indicate ‘reduced surface heat flow’ in Wm^{-2} . R^2 = coefficient of determination.

2.3.6 Reduced surface heat flow through time

Variation in ‘reduced surface heat flow’ through time is derived from the gradient of the Bullard plot for successive days. The red line on Figure 40 shows ‘reduced surface heat flow’ as a function of time for AZ4. It indicates relatively constant geophysical heat flow at $1.90 \pm 0.05 \text{ Wm}^{-2}$ over the four-month period from 1 November 2014 to 28 February 2015.



Figure 40. ‘Reduced surface heat flow’ versus time for site AZ4 (red, left axis); Coefficient of determination (black, right axis).

2.3.7 Summary

The reduced surface heat flow at this location is estimated at $1.90 \pm 0.05 \text{ W/m}^2$. This is about 30 times the mean global continental heat flow (e.g. Beardsmore and Cull, 2001¹⁰), which indicates an anomalous, significant heat source beneath this site. The thermal diffusivity values are very tightly constrained and the Bullard plots are highly linear, indicating stable conductive conditions over a four-month period.

2.4 Site AZ6: Drilling Pad for Well AZ-41

2.4.1 Location

Latitude 19.81407°N, Longitude 100.67686°W

UTM coordinates: 14Q 324367mE 2191778mN

Elevation: 3,050±11 m

The Heat Needle was placed on the pad of geothermal well AZ-41 (Figure 41, Figure 42). It recorded ground temperature data from 24 September 2014 to 24 March 2015.

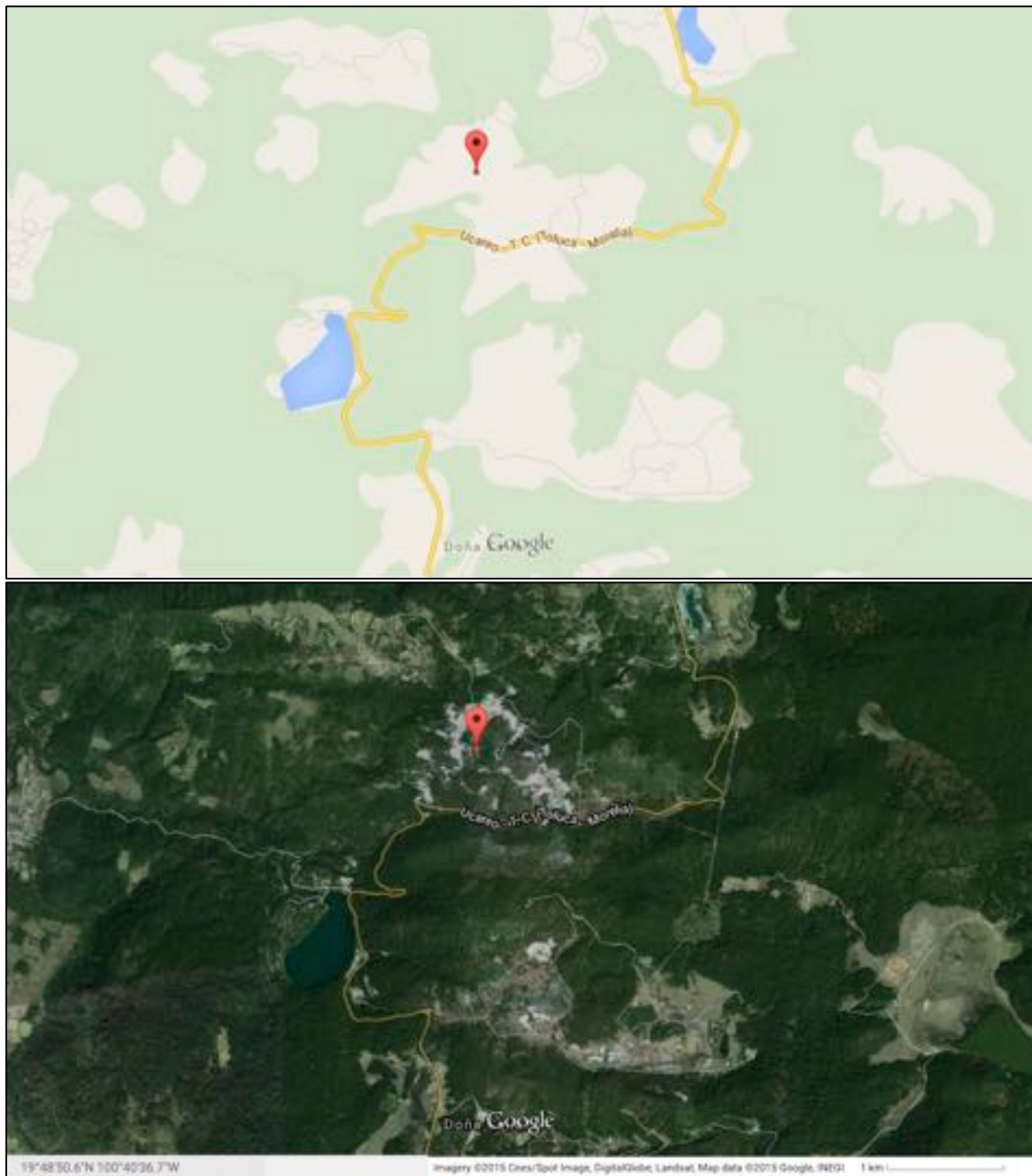


Figure 41. Location in map (top) and aerial photo (bottom) view of site AZ6: Drilling pad for well AZ-41.



Figure 42. AZ6: Drilling pad for well AZ-41. Photo source: Alfredo Mercado.

2.4.2 Temperature records

A full temperature record was collected for the 181-day period. Processing of the raw temperature data included the following steps:

1. Conversion of digital records to temperatures
2. Correction of recorded times for drift in internal clock
3. Re-sampling of records to precise quarter-hour times by interpolation
4. Calculation of daily average temperatures

Figure 43 and Figure 44 show examples of the temperature records.

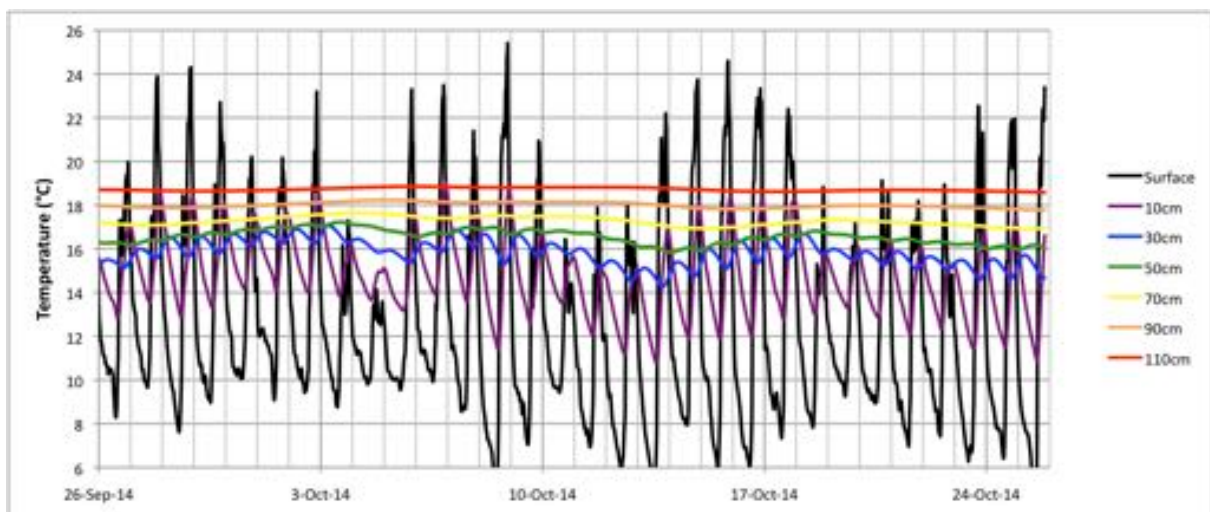


Figure 43. Detail of temperature record for first month at site AZ6.

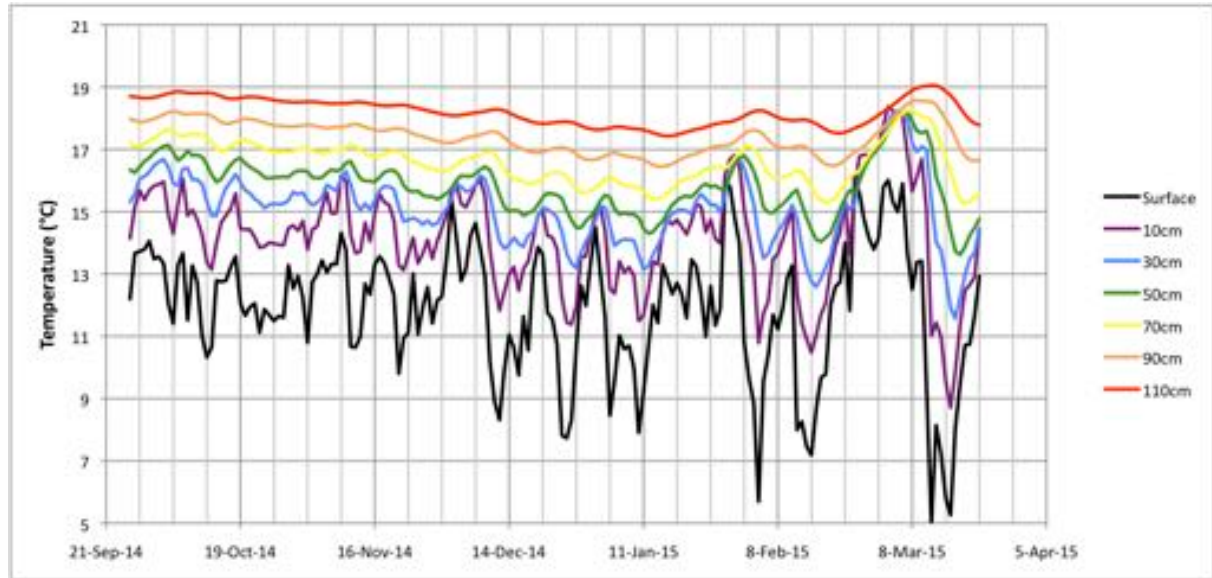


Figure 44. Daily average temperature for site AZ6.

2.4.3 Thermal diffusivity

HDR calculated mean and standard error of thermal diffusivity over the depth intervals 30–50 cm, 30–70 cm, 30–90 cm and 30–110 cm following the method summarized in Section 1.0. Figure 45 illustrates plots of $\ln(A_2/A_1)$ and phase shift (radians) versus $\sqrt{(\Delta z^2 \cdot \pi \cdot f)}$ for the four depth intervals. The gradients are theoretically equal to $1/\sqrt{\kappa}$, so the results indicate:

30–50 cm	$\kappa = 4.651 \pm 0.006 \times 10^{-7} \text{ m}^2\text{s}^{-1}$
30–70 cm	$\kappa = 4.444 \pm 0.008 \times 10^{-7} \text{ m}^2\text{s}^{-1}$
30–90 cm	$\kappa = 4.204 \pm 0.011 \times 10^{-7} \text{ m}^2\text{s}^{-1}$
30–110 cm	$\kappa = 4.044 \pm 0.021 \times 10^{-7} \text{ m}^2\text{s}^{-1}$

2.4.4. Temperature history and ‘reduced ground temperature’

A visual comparison between Aqua and Terra night time land surface temperatures and mean daily temperatures measured by the Heat Needle at 30 cm depth (Figure 46) suggests a mean offset of around 8°C. However, a daily mean temperature history for 30 cm depth (Figure 47) generated using a constant offset of 6.4°C from the mean satellite night time land surface temperatures was found to produce the most stable ‘reduced ground temperature’ curves (Figure 48) over the period 1 November 2014 – 31 January 2015. The inferred average temperature at 30 cm depth over the period of satellite coverage was 14.13°C.

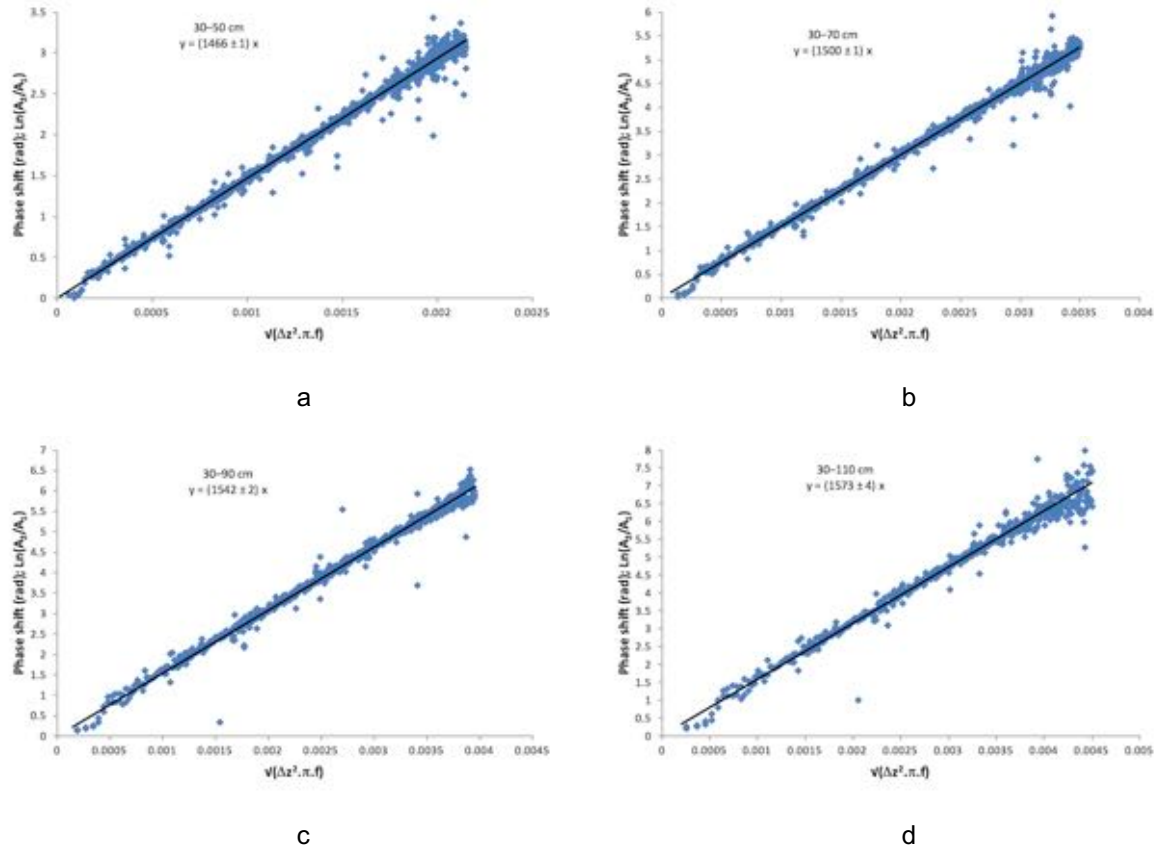


Figure 45. Harmonic spectral determination of thermal diffusivity for depth intervals (a) 30–50 cm, (b) 30–70 cm, (c) 30–90 cm and (d) 30–110 cm at site AZ6. Only relatively noise-free frequencies are plotted. The gradient in each case is theoretically equal to $1/\sqrt{k}$. All values are tightly constrained.

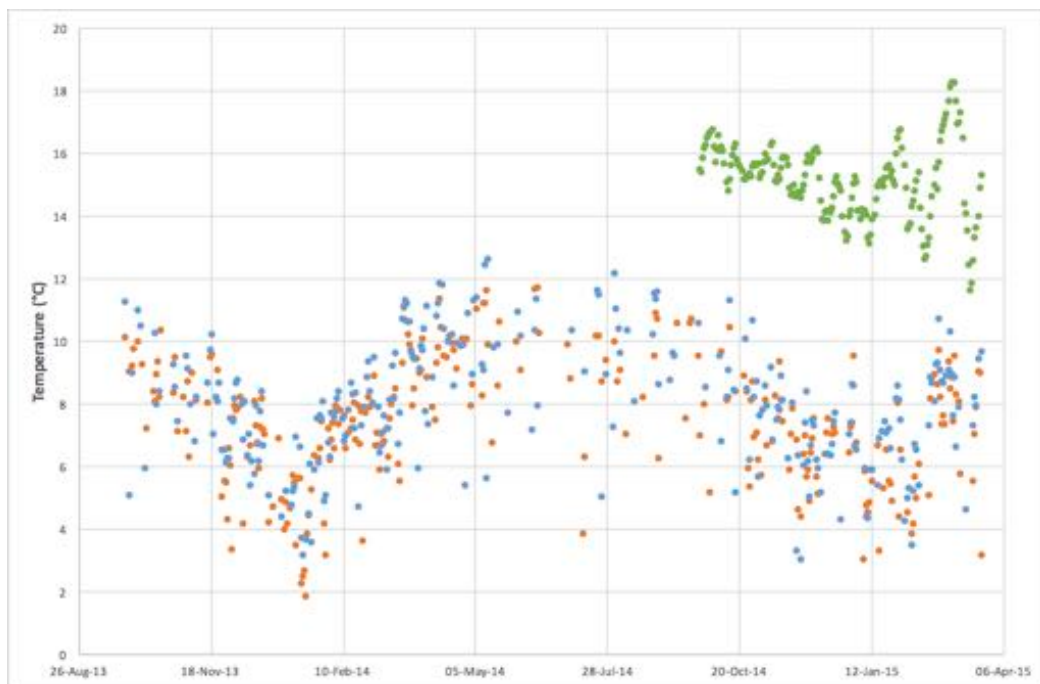


Figure 46. Mean daily temperatures at 30 cm depth measured by a Heat Needle (green dots) at AZ6, and Terra and Aqua night time land surface temperatures (blue and orange dots, respectively).

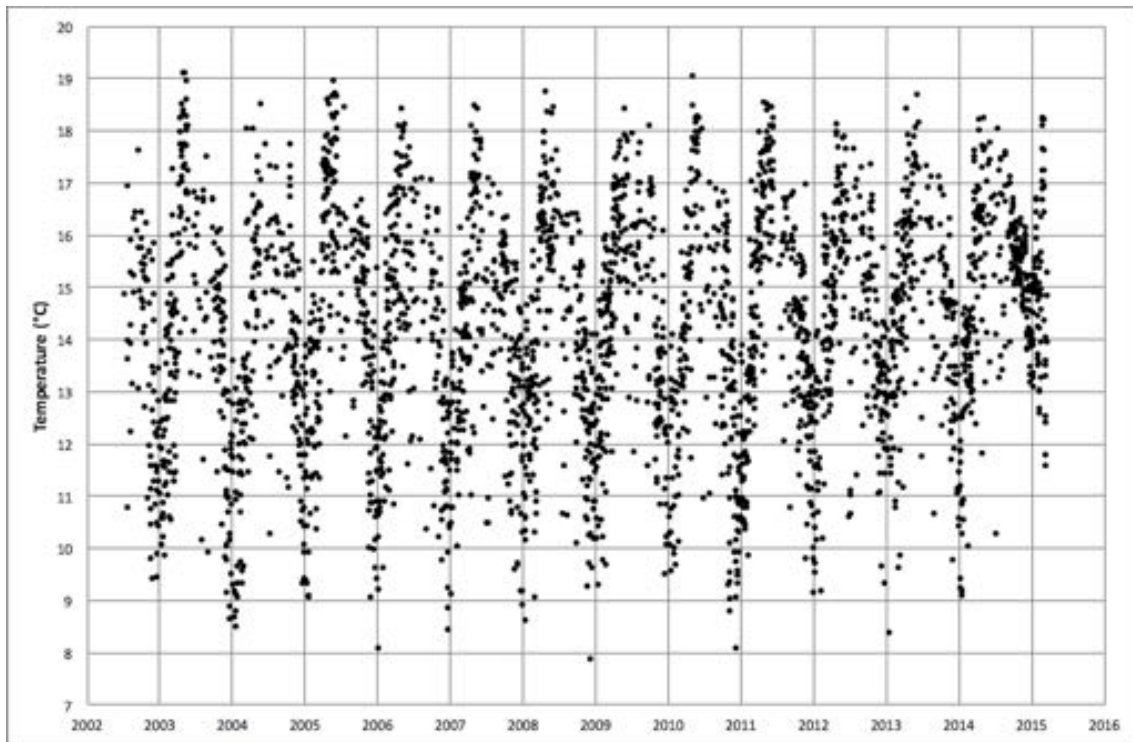


Figure 47. Daily mean temperatures at 30 cm depth at AZ6 since 2002, inferred from Terra and Aqua night time land surface temperatures

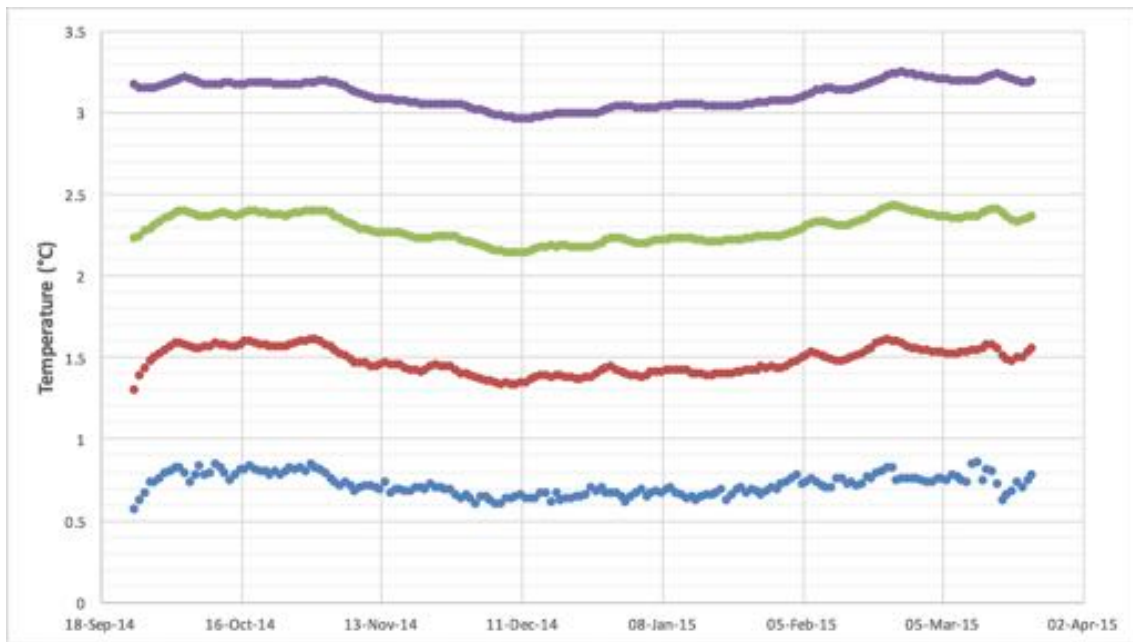


Figure 48. Reduced ground temperatures for 50 cm (blue), 70 cm (red), 90 cm (green) and 110 cm (purple) at AZ6 over the period of the survey

2.4.5 Thermal conductivity and thermal resistance

A successful thermal conductivity measurement was carried out over the time interval (UTC time) 23:11 on 24 March 2015 – 00:11 on 25 March 2015. Assuming an ‘infinite line source’ of heat at a rate of 14.90 ± 0.04 W/m, the resulting log-linear temperature increases observed at sensor depths (Figure 49) imply thermal conductivities of:

30 cm	0.82 ± 0.01^8 W/mK
50 cm	0.922 ± 0.003 W/mK
70 cm	0.779 ± 0.003 W/mK
90 cm	0.679 ± 0.003 W/mK
110 cm	0.85 ± 0.05^9 W/mK

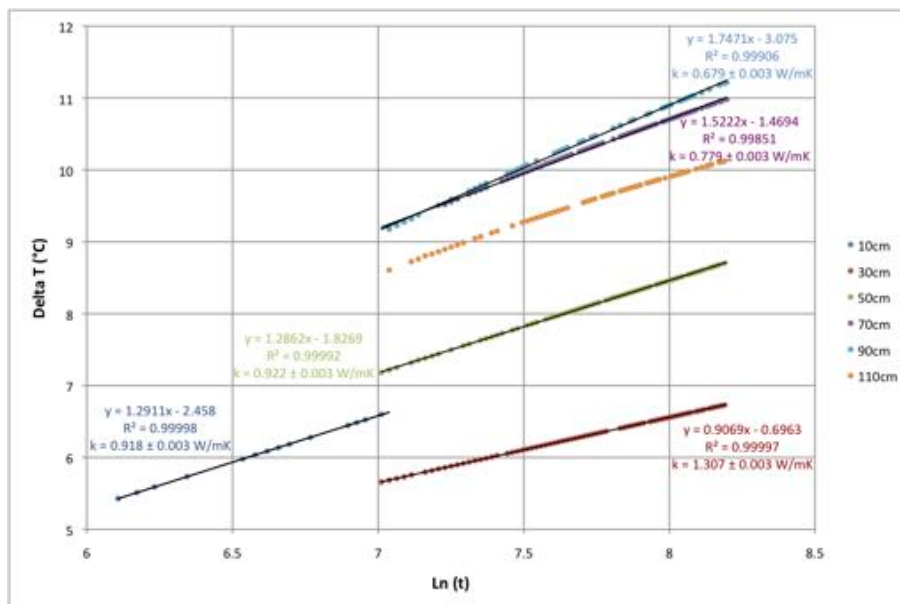


Figure 49. Temperature increase versus the natural log of heating time for site AZ6

Thermal resistance is the integral of physical depth divided by thermal conductivity. The thermal resistance from 30 cm to each deeper sensor can be estimated from the thermal conductivity values above:

50 cm	$0.100/0.82 + 0.100/0.922 =$	$0.230 \text{ m}^2\text{K/W}$
70 cm	$0.230 + 0.100/0.922 + 0.100/0.779 =$	$0.467 \text{ m}^2\text{K/W}$
90 cm	$0.467 + 0.100/0.779 + 0.100/0.679 =$	$0.742 \text{ m}^2\text{K/W}$
110 cm	$0.742 + 0.100/0.679 + 0.100/0.85 =$	$1.007 \text{ m}^2\text{K/W}$

In a steady state conductive setting, temperature increases linearly with thermal resistance at a gradient equal to the conductive heat flow. A straight line of best fit

provides an estimate of the mean conductive heat flow at any given moment. Figure 50 shows a sample of Bullard plots of ‘change in reduced temperature’ versus thermal resistance at one-month intervals during the recording period. The gradient of each plot indicates the ‘reduced surface heat flow’ at that time, while the coefficient of determination (R^2) indicates the degree of linearity. The plots are highly linear, suggesting dominant conductive processes.

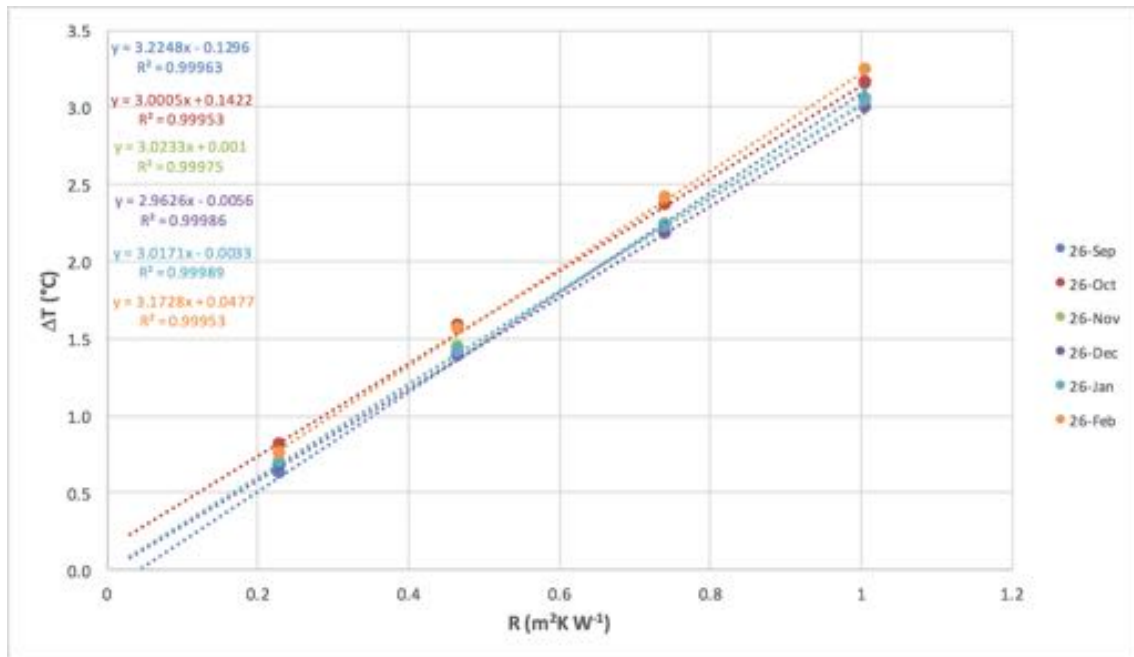


Figure 50. Bullard plots of change in ‘reduced ground temperature’ (ΔT) versus thermal resistance (R) at monthly intervals for site AZ6. The equations of the lines of best fit are given in the top left corner of the plot. The gradients indicate ‘reduced surface heat flow’ in W m^{-2} . R^2 = coefficient of determination.

2.4.6 Reduced surface heat flow through time

Variation in ‘reduced surface heat flow’ through time is derived from the gradient of the Bullard plot for successive days. The red line on Figure 51 shows ‘reduced surface heat flow’ as a function of time for AZ6. It indicates relatively constant geophysical heat flow at $3.05 \pm 0.05 \text{ W m}^{-2}$ over the four-month period from 1 November 2014 to 28 February 2015.



Figure 51. ‘Reduced surface heat flow’ versus time for site AZ6 (red, left axis); Coefficient of determination (black, right axis).

2.4.7 Summary

The reduced surface heat flow at this location is estimated at $3.05 \pm 0.05 \text{ W/m}^2$. This is almost 50 times the mean global continental heat flow (e.g. Beardsmore and Cull, 2001¹⁰), which indicates an anomalous, significant heat source beneath this site. The thermal diffusivity values are very tightly constrained and the Bullard plots are highly linear, indicating stable conductive conditions over a four-month period.

2.5 Site AZ7: Drilling Pad for Well AZ-26

2.5.1 Location

Latitude 19.78202°N, Longitude 100.65013°W

UTM coordinates: 14Q 327133mE 2188202mN Elevation: 2,937±7 m

The Heat Needle was placed on the pad of geothermal well AZ-26 (Figure 52, Figure 53). It recorded from 24 September 2014 to 24 March 2015, but many of the ground temperature data were null or corrupted. HDR filtered these from the record.

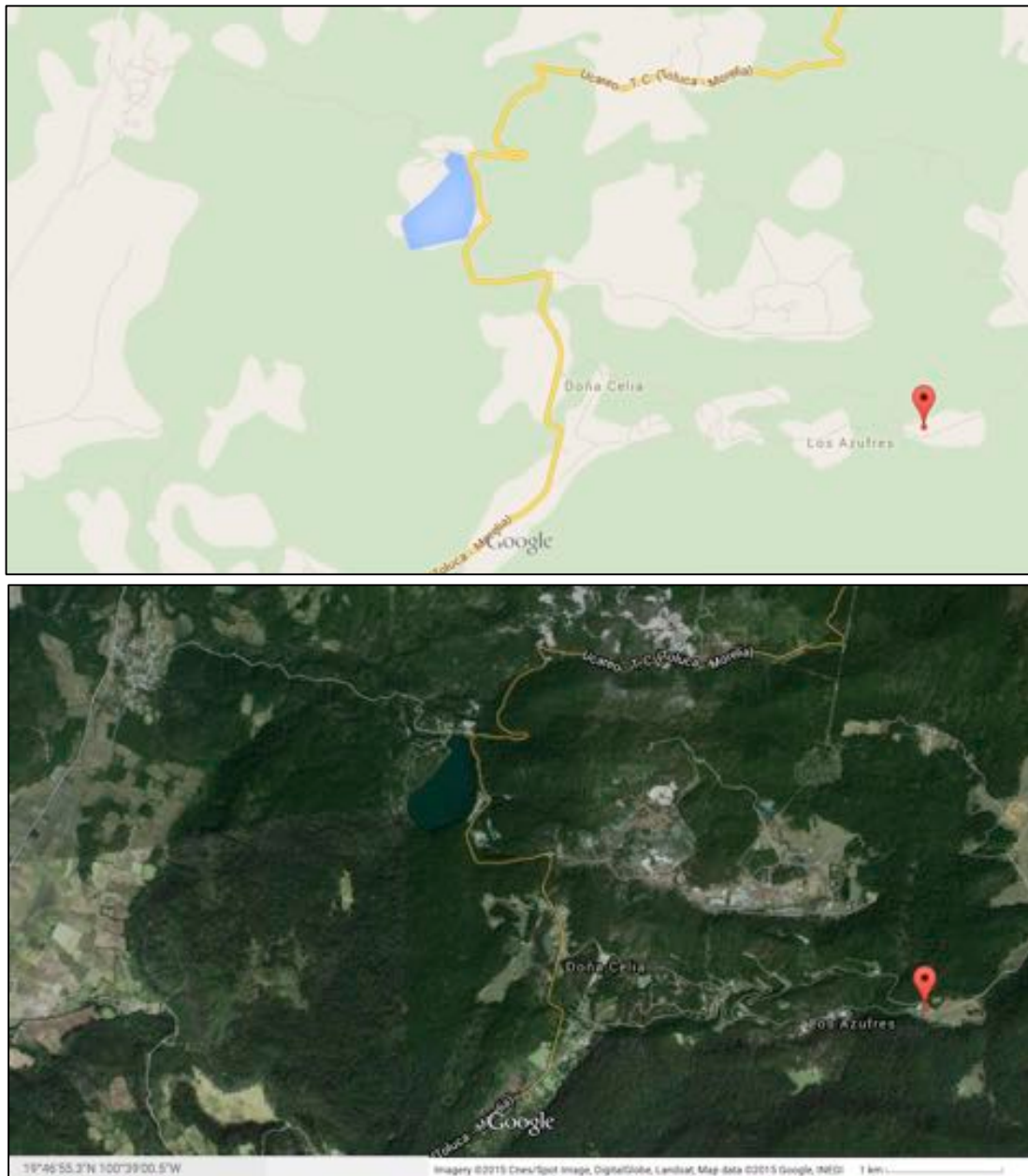


Figure 52. Location in map (top) and aerial photo (bottom) view of site AZ7: Drilling pad for well AZ-26.



Figure 53. AZ7: Drilling pad for well AZ-26. Photo source: Alfredo Mercado.

2.5.2 Temperature records

The Heat Needle recorded for 181-day period. Time stamps were correctly recorded but many of the temperature data were corrupted or recorded as null, particularly in the first six weeks of the recording period. Processing of the raw temperature data included the following steps:

1. Conversion of digital records to temperatures
2. Correction of recorded times for drift in internal clock
3. Re-sampling of viable data to precise quarter-hour times by interpolation
4. Removal of spurious temperature data
5. Calculation of daily average temperatures where possible

Figure 54 and Figure 55 show examples of the temperature records.

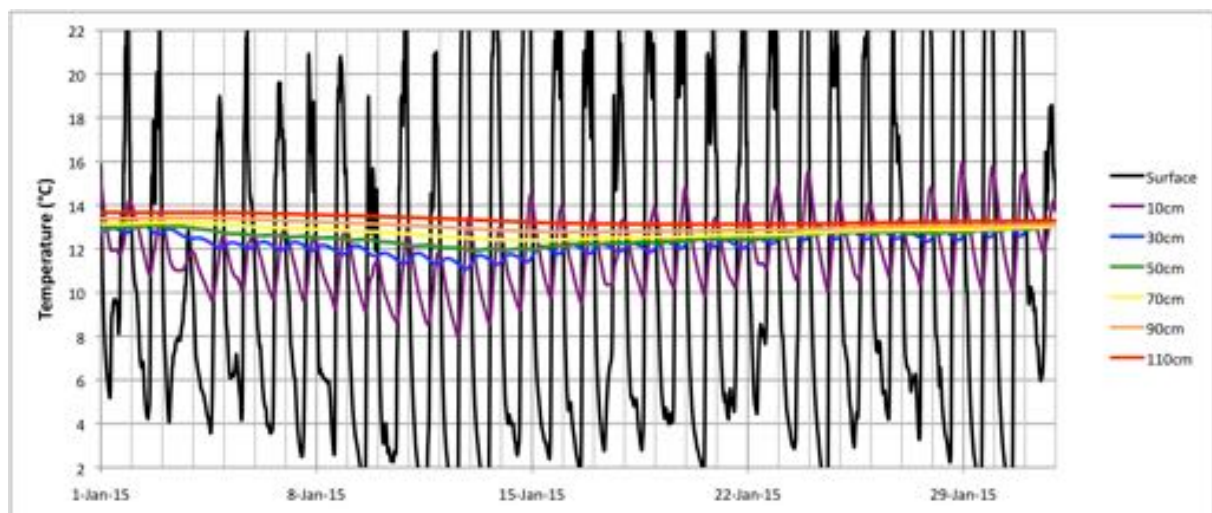


Figure 54. Detail of temperature record for January 2015 at site AZ7.

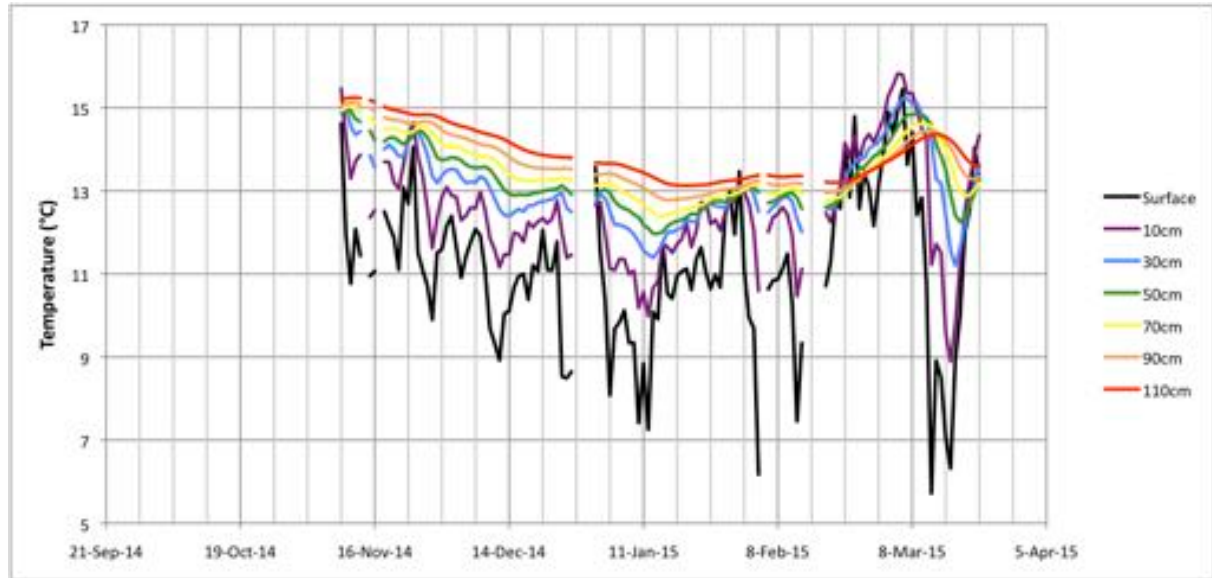


Figure 55. Daily average temperature for site AZ7. Days with spurious data have been removed.

2.5.3 Thermal diffusivity

HDR calculated mean and standard error of thermal diffusivity over the depth intervals 30–50 cm, 30–70 cm, 30–90 cm and 30–110 cm following the method summarized in Section 1.0. Given the breaks in the temperature record, spectra had to be calculated for three separate sub-sets of the survey period (18 November – 27 December 2014; 31 December 2014 – 03 February 2015; 15 February – 23 March 2015) and then compiled into a single set. Figure 56 illustrates plots of $\ln(A_2/A_1)$ and phase shift (radians) versus $\sqrt{(\Delta z^2 \cdot \pi \cdot f)}$ for the four depth intervals of the compiled spectra. The gradients are theoretically equal to $1/\sqrt{\kappa}$, so the results indicate:

$$30\text{--}50 \text{ cm} \quad \kappa = 4.185 \pm 0.025 \times 10^{-7} \text{ m}^2\text{s}^{-1}$$

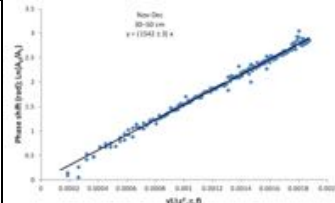
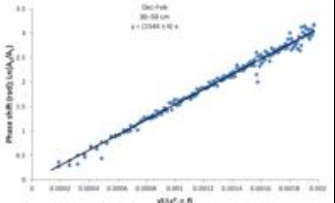
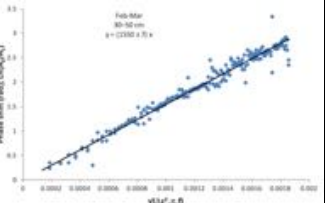
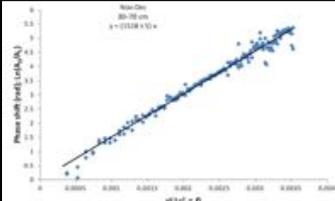
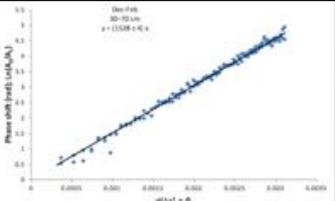
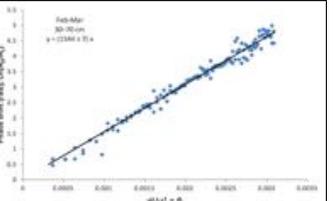
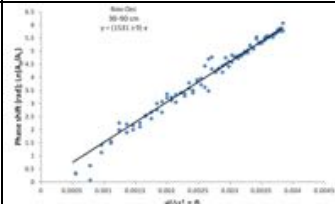
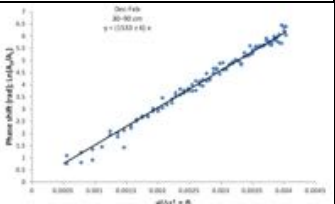
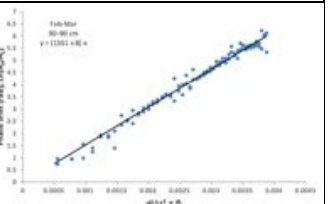
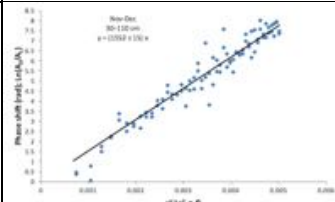
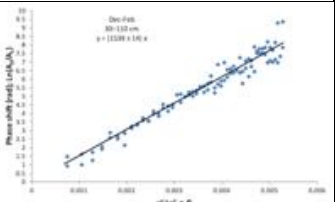
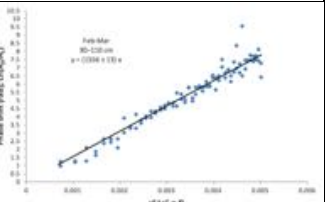
$$30\text{--}70 \text{ cm} \quad \kappa = 4.273 \pm 0.030 \times 10^{-7} \text{ m}^2\text{s}^{-1}$$

$$30\text{--}90 \text{ cm} \quad \kappa = 4.228 \pm 0.042 \times 10^{-7} \text{ m}^2\text{s}^{-1}$$

$$30\text{--}110 \text{ cm} \quad \kappa = 4.169 \pm 0.076 \times 10^{-7} \text{ m}^2\text{s}^{-1}$$

The thermal diffusivity spectra and calculated thermal diffusivities for each of the three discrete time intervals of uninterrupted temperature data can be compared to each other and to the compiled mean values above. The table below shows the harmonic spectra graphs and the calculated thermal diffusivities for each of the three time intervals over the four depth intervals. The graphs and values illustrate that recording periods less than six weeks in length provided adequate data to delineate

thermal diffusivity values to within 2% of values obtained from a much longer recording period (109 days combined).

	18 November – 27 December 2014 (39 days)	31 December 2014 – 03 February 2015 (34 days)	15 February – 23 March 2015 (36 days)
30–50 cm	 $4.204 \pm 0.018 \times 10^{-7} \text{ m}^2\text{s}^{-1}$	 $4.190 \pm 0.020 \times 10^{-7} \text{ m}^2\text{s}^{-1}$	 $4.160 \pm 0.037 \times 10^{-7} \text{ m}^2\text{s}^{-1}$
30–70 cm	 $4.340 \pm 0.030 \times 10^{-7} \text{ m}^2\text{s}^{-1}$	 $4.283 \pm 0.023 \times 10^{-7} \text{ m}^2\text{s}^{-1}$	 $4.195 \pm 0.036 \times 10^{-7} \text{ m}^2\text{s}^{-1}$
30–90 cm	 $4.267 \pm 0.049 \times 10^{-7} \text{ m}^2\text{s}^{-1}$	 $4.258 \pm 0.033 \times 10^{-7} \text{ m}^2\text{s}^{-1}$	 $4.158 \pm 0.042 \times 10^{-7} \text{ m}^2\text{s}^{-1}$
30–110 cm	 $4.151 \pm 0.081 \times 10^{-7} \text{ m}^2\text{s}^{-1}$	 $4.225 \pm 0.076 \times 10^{-7} \text{ m}^2\text{s}^{-1}$	 $4.132 \pm 0.072 \times 10^{-7} \text{ m}^2\text{s}^{-1}$

2.5.4. Temperature history and ‘reduced ground temperature’

A visual comparison between Aqua and Terra night time land surface temperatures and mean daily temperatures measured by the Heat Needle at 30 cm depth (Figure 57) suggests a mean offset of around 7°C. A daily mean temperature history for 30 cm depth (Figure 58) generated using a constant offset of 7.2°C from the mean satellite night time land surface temperatures was found to produce relatively constant ‘reduced ground temperature’ curves (Figure 59) over the period 1 December 2014 – 28 February 2015. The inferred average temperature at 30 cm depth over the period of satellite coverage was 14.90°C.

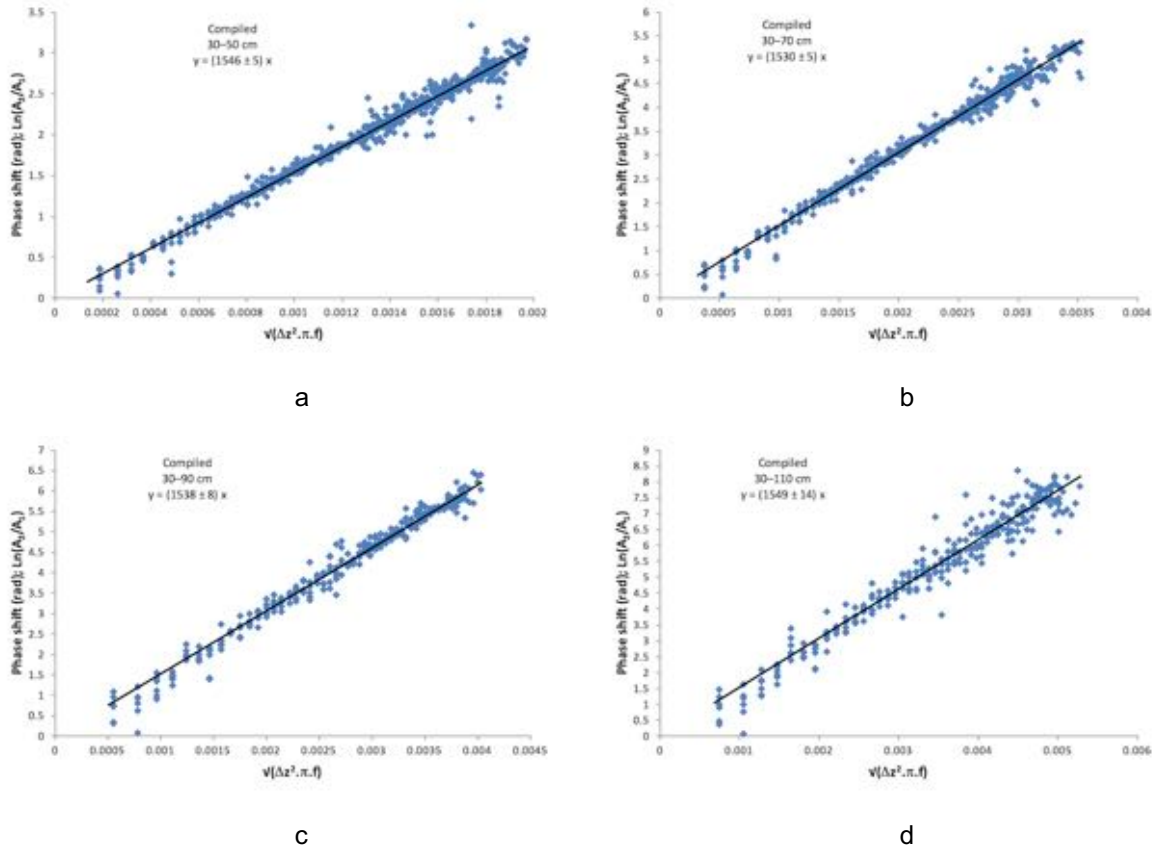


Figure 56. Harmonic spectral determination of thermal diffusivity for depth intervals (a) 30–50 cm, (b) 30–70 cm, (c) 30–90 cm and (d) 30–110 cm compiled over four discrete time intervals at site AZ7. Only relatively noise-free frequencies are plotted. The gradient in each case is theoretically equal to $1/\sqrt{\kappa}$.

2.5.5 Thermal conductivity and thermal resistance

A successful thermal conductivity measurement was carried out over the time interval (UTC time) 20:58–21:58 on 24 March 2015. Assuming an ‘infinite line source’ of heat at a rate of 14.90 ± 0.04 W/m, the resulting log-linear temperature increases observed at sensor depths (Figure 60) imply thermal conductivities of:

30 cm	1.25 ± 0.05^8 W/mK
50 cm	1.248 ± 0.003 W/mK
70 cm	1.187 ± 0.003 W/mK
90 cm	0.997 ± 0.003 W/mK
110 cm	1.0 ± 0.1^9 W/mK

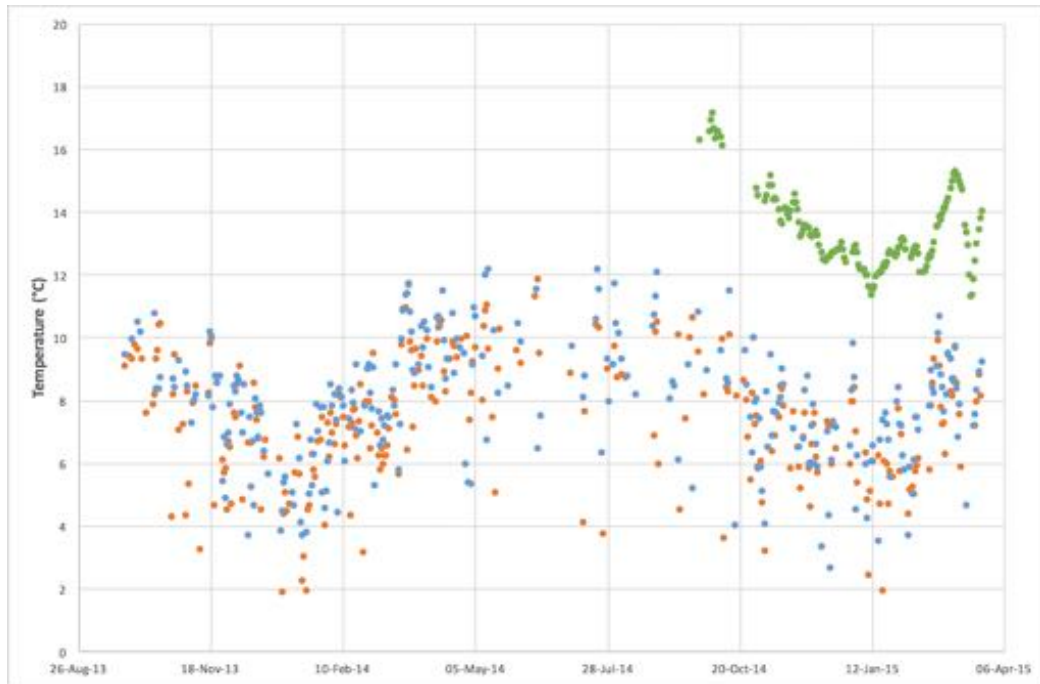


Figure 57. Mean daily temperatures at 30 cm depth measured by a Heat Needle (green dots) at AZ7, and Terra and Aqua night time land surface temperatures (blue and orange dots, respectively).

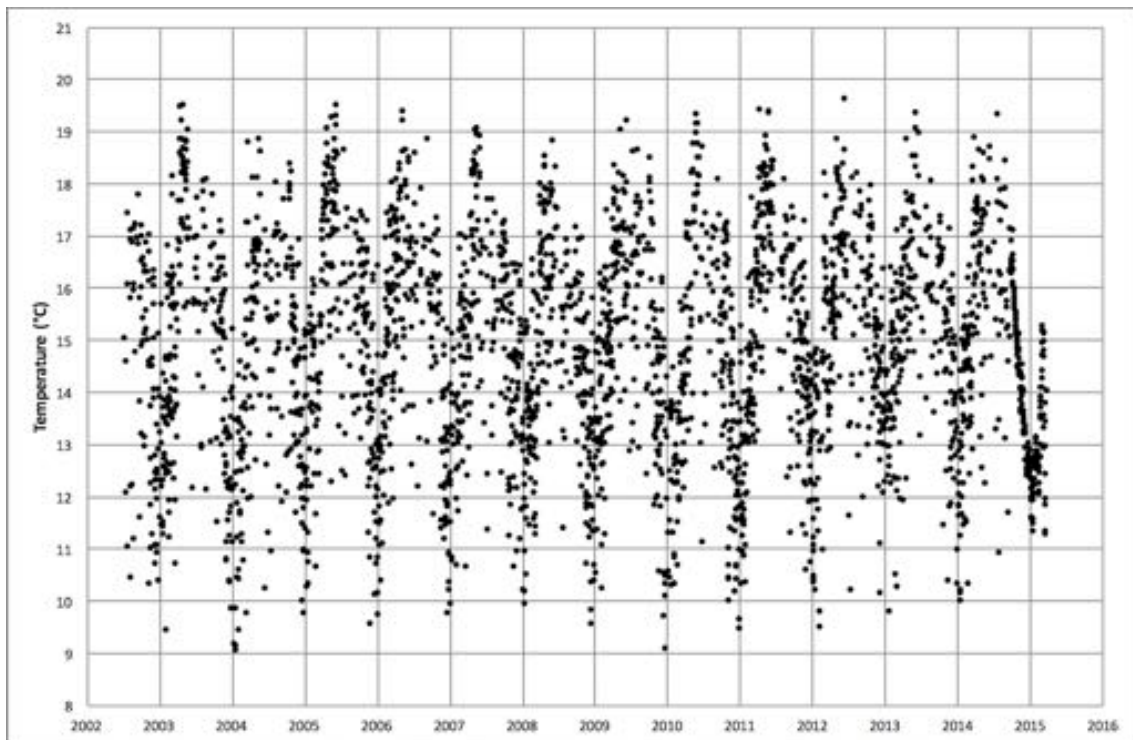


Figure 58. Daily mean temperatures at 30 cm depth at AZ7 since 2002, inferred from Terra and Aqua night time land surface temperatures

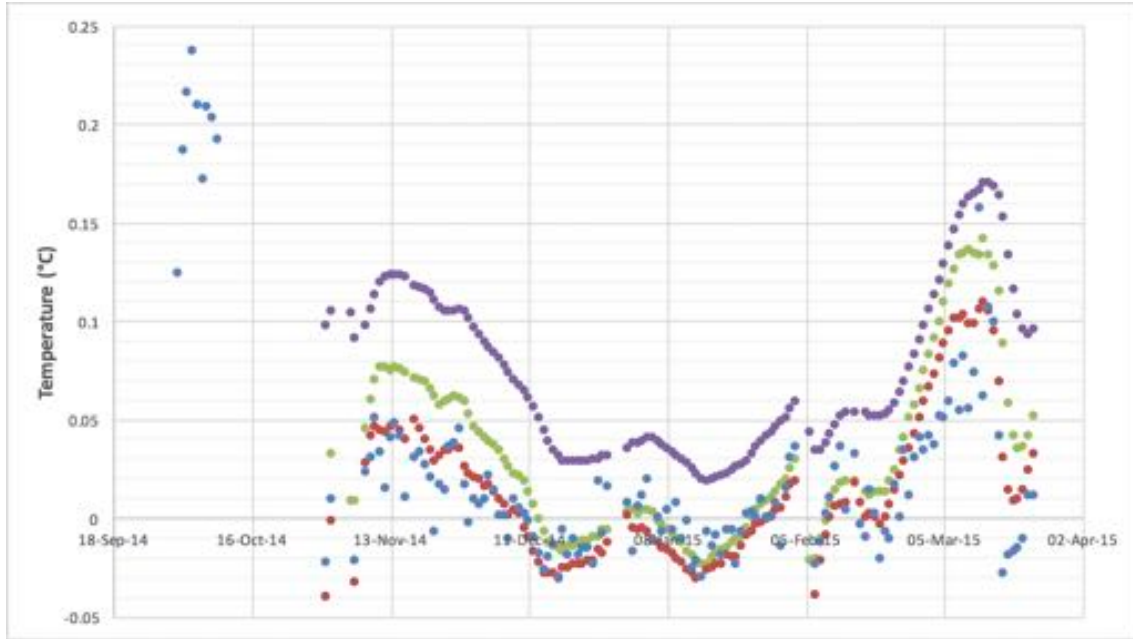


Figure 59. Reduced ground temperatures for 50 cm (blue), 70 cm (red), 90 cm (green) and 110 cm (purple) at AZ7 over the period of the survey. Days with spurious data have been removed.

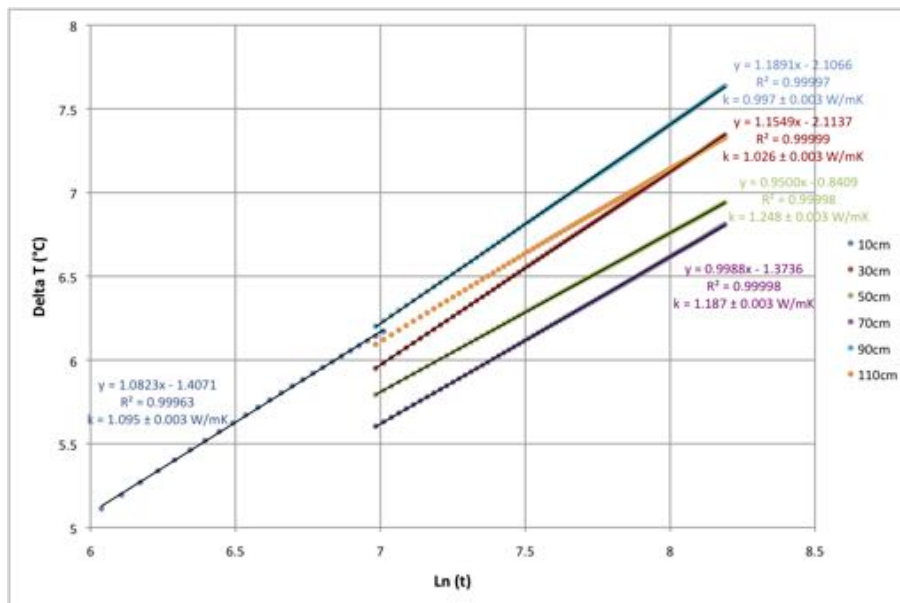


Figure 60. Temperature increase versus the natural log of heating time for site AZ7.

Thermal resistance is the integral of physical depth divided by thermal conductivity. The thermal resistance from 30 cm to each deeper sensor can be estimated from the thermal conductivity values above:

$$50 \text{ cm} \quad 0.100/1.25 + 0.100/1.248 = \quad 0.160 \text{ m}^2\text{K/W}$$

$$70 \text{ cm} \quad 0.160 + 0.100/1.248 + 0.100/1.187 = 0.325 \text{ m}^2\text{K/W}$$

$$90 \text{ cm} \quad 0.325 + 0.100/1.187 + 0.100/0.997 = 0.509 \text{ m}^2\text{K/W}$$

$$110 \text{ cm} \quad 0.509 + 0.100/0.997 + 0.100/1.0 = 0.709 \text{ m}^2\text{K/W}$$

In a steady state conductive setting, temperature increases linearly with thermal resistance at a gradient equal to the conductive heat flow. A straight line of best fit provides an estimate of the mean conductive heat flow at any given moment. Figure 61 shows a sample of Bullard plots of ‘change in reduced temperature’ versus thermal resistance at one-month intervals during the recording period. The gradient of each plot indicates the ‘reduced surface heat flow’ at that time, while the coefficient of determination (R^2) indicates the degree of linearity. The plots are linear to within 0.01°C of the mean values, suggesting dominant conductive processes.

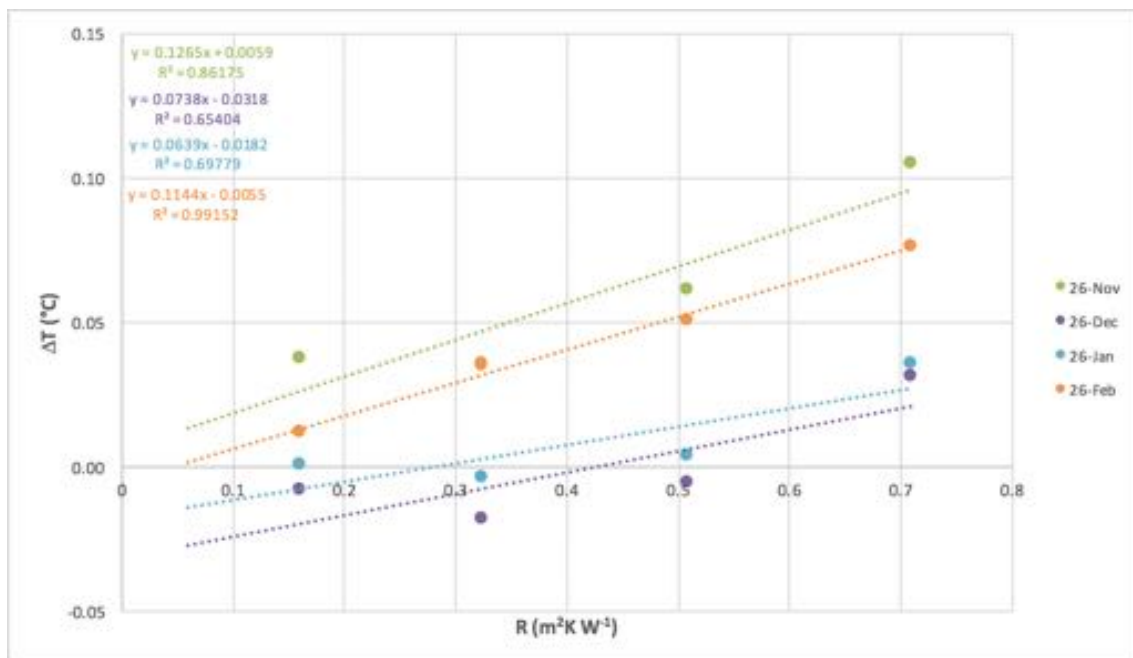


Figure 61. Bullard plots of change in ‘reduced ground temperature’ (ΔT) versus thermal resistance (R) at monthly intervals for site AZ7. The equations of the lines of best fit are given in the top left corner of the plot. The gradients indicate ‘reduced surface heat flow’ in Wm^{-2} . R^2 = coefficient of determination.

2.5.6 Reduced surface heat flow through time

Variation in ‘reduced surface heat flow’ through time is derived from the gradient of the Bullard plot for successive days. The red line on Figure 62 shows ‘reduced surface heat flow’ as a function of time for AZ7. It indicates relatively constant geophysical heat flow at $0.10 \pm 0.05 \text{ Wm}^{-2}$ over the three-month period from 1 December 2014 to 28 February 2015.

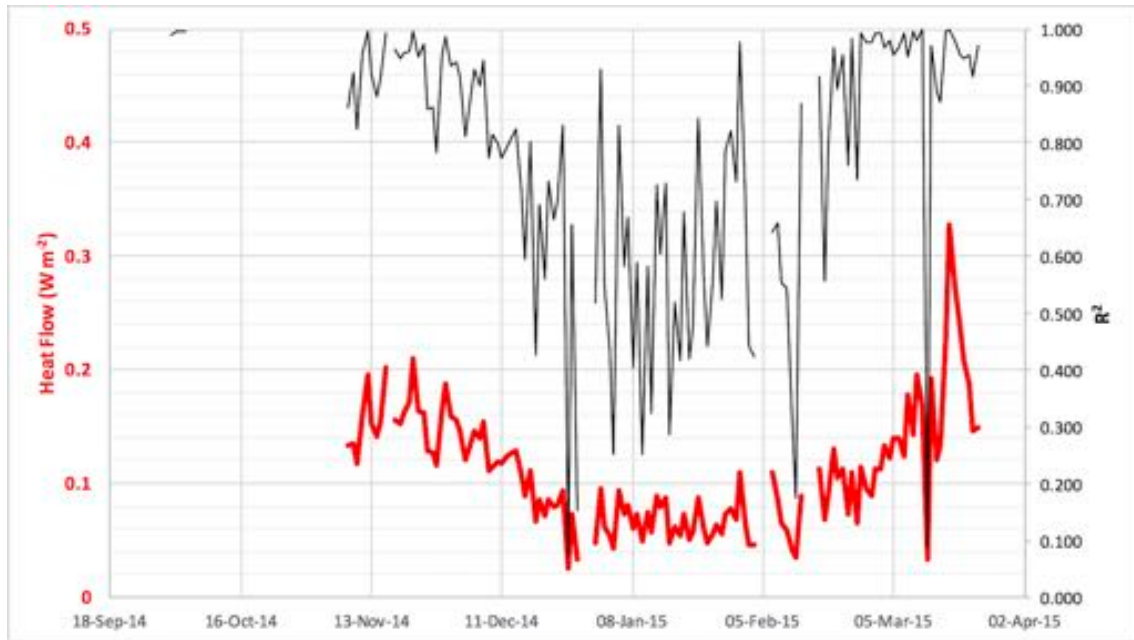


Figure 62. ‘Reduced surface heat flow’ versus time for site AZ7 (red, left axis); Coefficient of determination (black, right axis). Days with spurious data have been removed.

2.5.7 Summary

The reduced surface heat flow at this location is estimated at $0.10 \pm 0.05 \text{ W/m}^2$.

Mean global continental heat flow lies within this uncertainty range (e.g. Beardsmore and Cull, 2001¹⁰), so the Heat Needle records provide no evidence of an anomalous, significant heat source beneath this site. The thermal diffusivity values are very tightly constrained and the Bullard plots are highly linear within $\pm 0.01^\circ\text{C}$, indicating stable conductive conditions over a three-month period. The result is surprising given the site’s location adjacent to a production well tapping a geothermal reservoir at about 1,000 m depth. It points to thermal decoupling of the top meter of soil with respect to deeper layers. The AZ7 site lies on an artificial mound on top of alluvium near the edge of a valley, so infiltration and shallow flow of meteoric water is a credible mechanism for homogenization of the shallow mean ground temperature at this site.

2.6 Site AZ8: Poblado La Yerbabuena

2.6.1 Location

Latitude 19.80659°N, Longitude 100.71952°W

UTM coordinates: 14Q 319890mE 2190995mN Elevation: 2,558±12 m

The Heat Needle was placed adjacent to a seismic station on the outskirts of the village of La Yerbabuena (Figure 63, Figure 64). The location was outside the geothermal field with the goal to measure background heat flow, expected to be lower than in the geothermal field. The Heat Needle recorded ground temperature data from 23 September 2014 to 23 March 2015.

2.6.2 Temperature records

A full temperature record was collected for the 181-day period. Processing of the raw temperature data included the following steps:

1. Conversion of digital records to temperatures
2. Correction of recorded times for drift in internal clock
3. Re-sampling of records to precise quarter-hour times by interpolation
4. Calculation of daily average temperatures

Figure 65 and Figure 66 show examples of the resulting temperature records.

2.6.3 Thermal diffusivity

HDR calculated mean and standard error of thermal diffusivity over the depth intervals 30–50 cm, 30–70 cm, 30–90 cm and 30–110 cm following the method summarized in Section 1.0. Figure 67 illustrates plots of $\ln(A_2/A_1)$ and phase shift (radians) versus $\sqrt{(\Delta z^2 \cdot \pi \cdot f)}$ for the four depth intervals. The gradients are theoretically equal to $1/\sqrt{\kappa}$, so the results indicate:

30–50 cm	$\kappa = 3.005 \pm 0.010 \times 10^{-7} \text{ m}^2\text{s}^{-1}$
30–70 cm	$\kappa = 2.857 \pm 0.013 \times 10^{-7} \text{ m}^2\text{s}^{-1}$
30–90 cm	$\kappa = 2.887 \pm 0.030 \times 10^{-7} \text{ m}^2\text{s}^{-1}$
30–110 cm	$\kappa = 2.740 \pm 0.028 \times 10^{-7} \text{ m}^2\text{s}^{-1}$

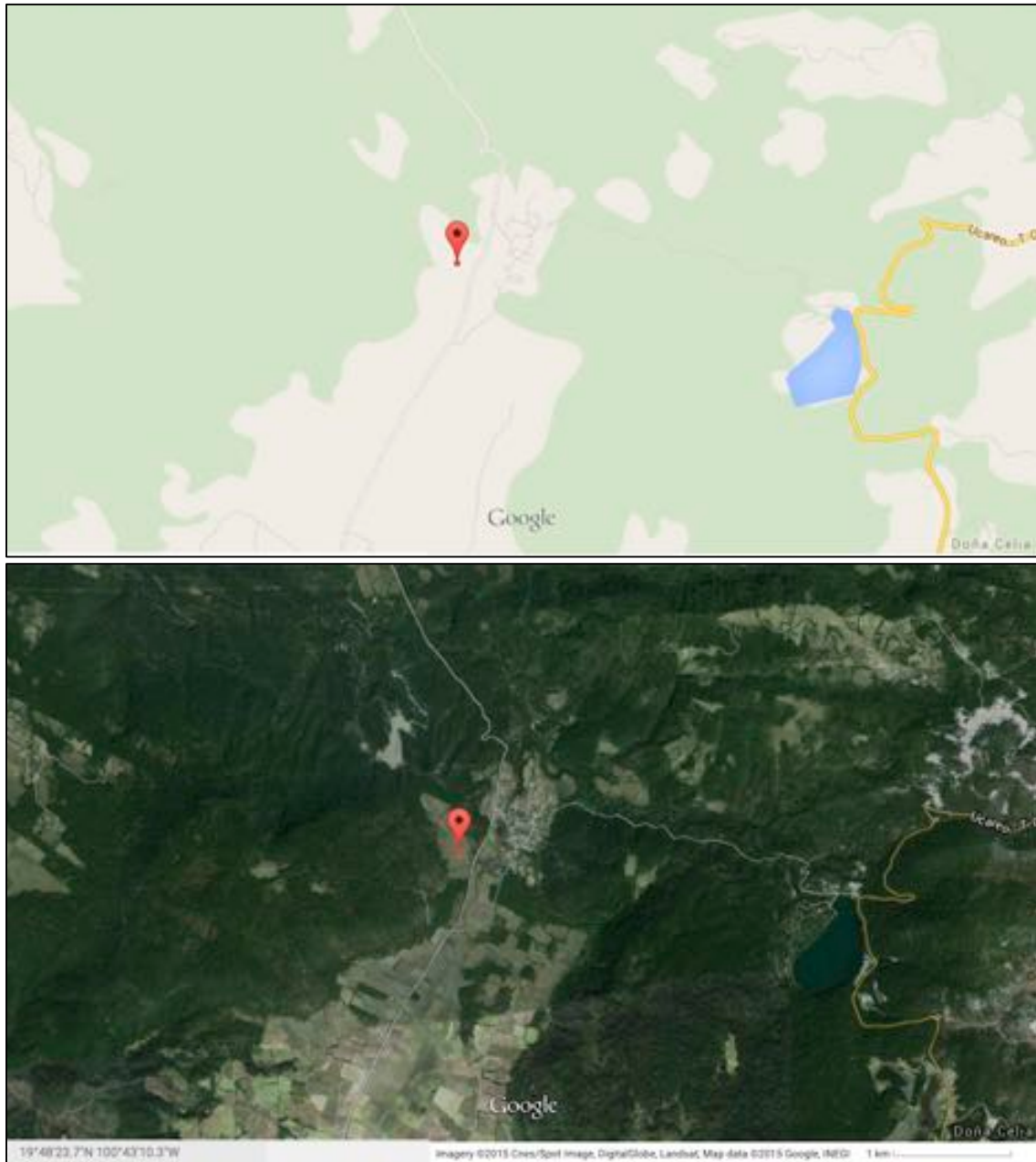


Figure 63. Location in map (top) and aerial photo (bottom) view of site AZ8: Poblado La Yerbabuena.



Figure 64. AZ8: Poblado La Yerbabuena. Photo source: Anson Antriasian.

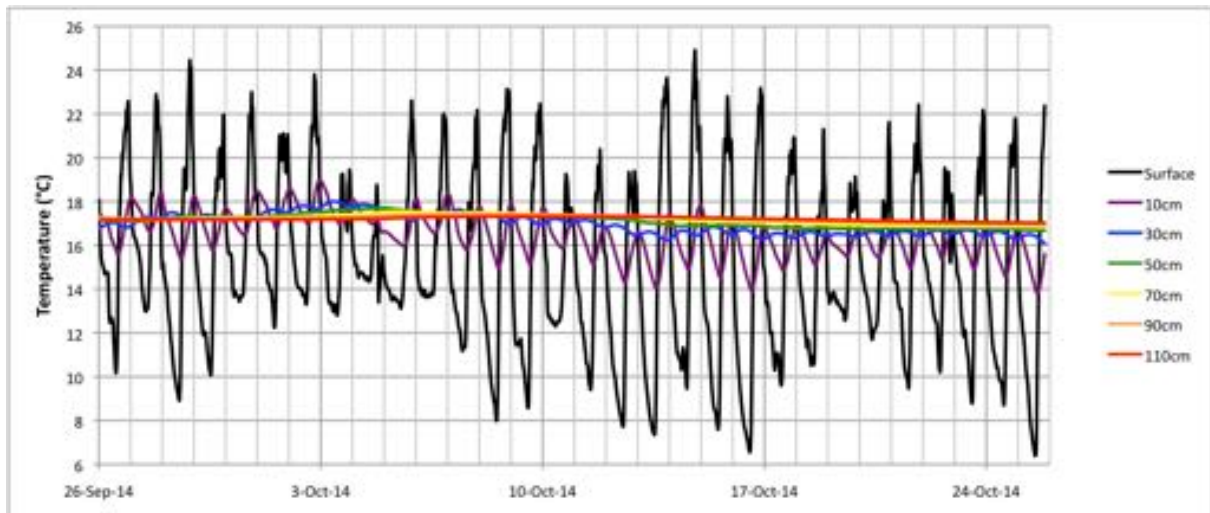


Figure 65. Detail of temperature record for first month at site AZ8.

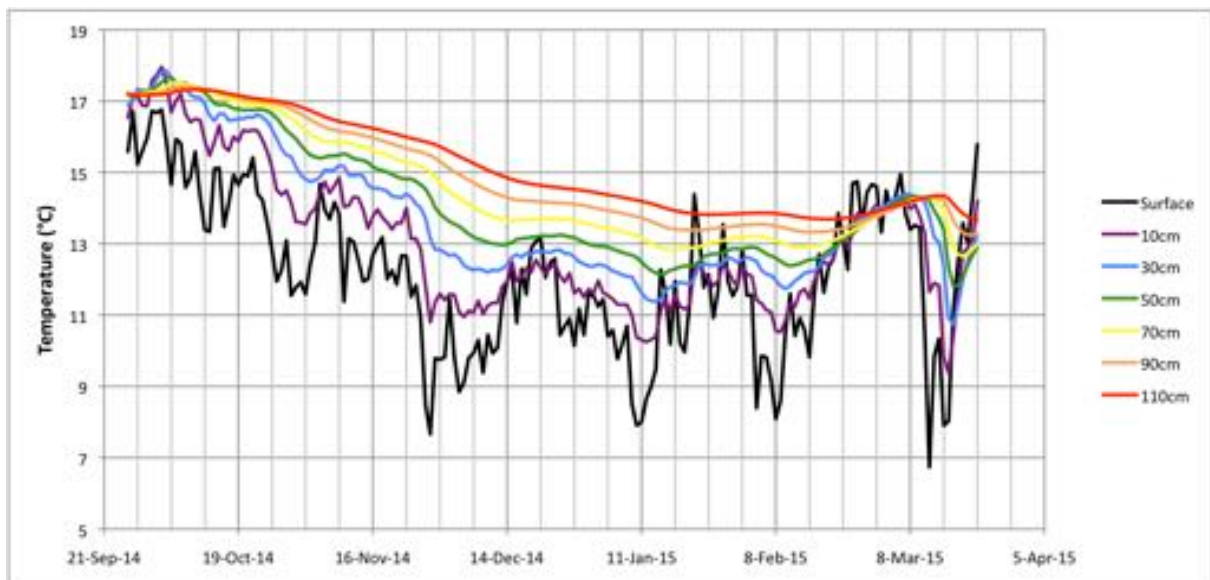


Figure 66. Daily average temperature for site AZ8.

2.6.4. Temperature history and 'reduced ground temperature'

A visual comparison between Aqua and Terra night time land surface temperatures and mean daily temperatures measured by the Heat Needle at 30 cm depth (Figure 68) suggests a mean offset of around 6°C. A daily mean temperature history for 30 cm depth (Figure 69) generated using a constant offset of 7.0°C from the mean satellite night time land surface temperatures was found to produce the most stable 'reduced ground temperature' curves (Figure 70) over the period 1 November 2014 – 31 January 2015. The inferred average temperature at 30 cm depth over the period of satellite coverage was 15.65°C.

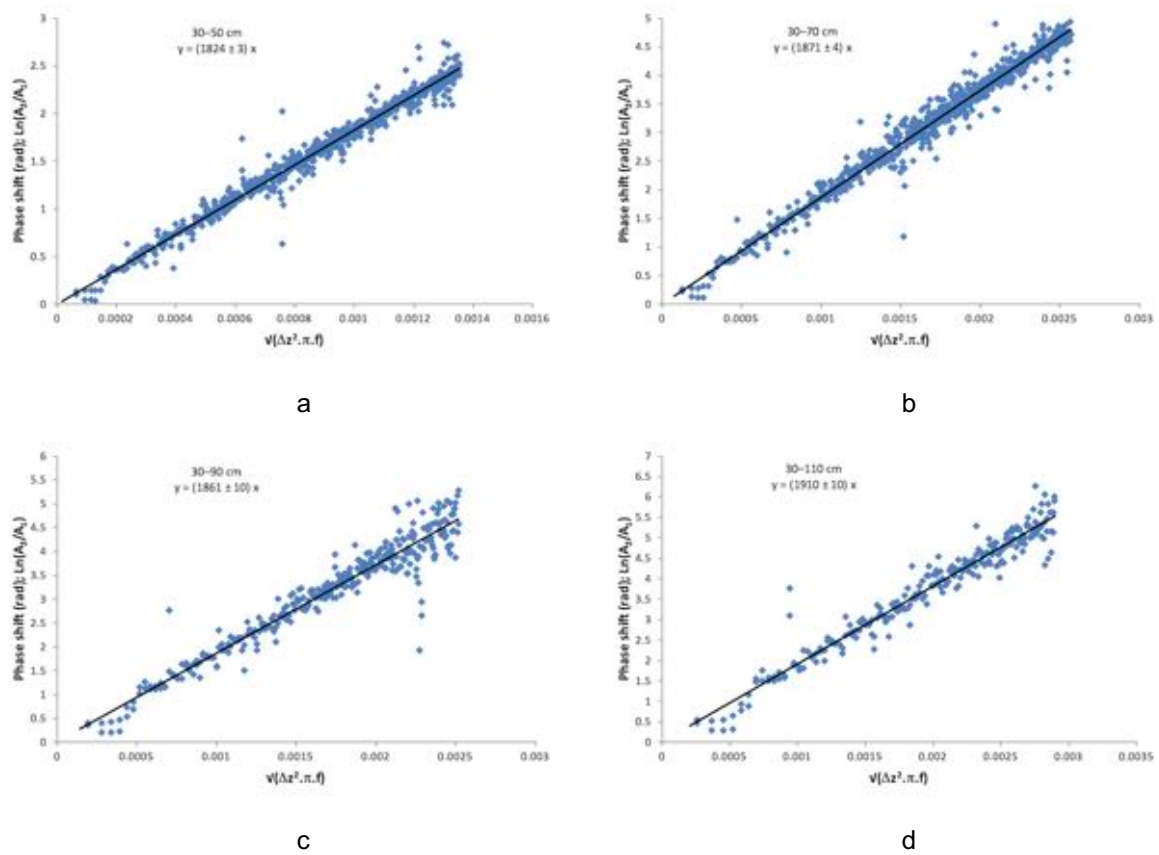


Figure 67. Harmonic spectral determination of thermal diffusivity for depth intervals (a) 30–50 cm, (b) 30–70 cm, (c) 30–90 cm and (d) 30–110 cm at site AZ8. Only relatively noise-free frequencies are plotted. The gradient in each case is theoretically equal to $1/\sqrt{\kappa}$. All values are tightly constrained.

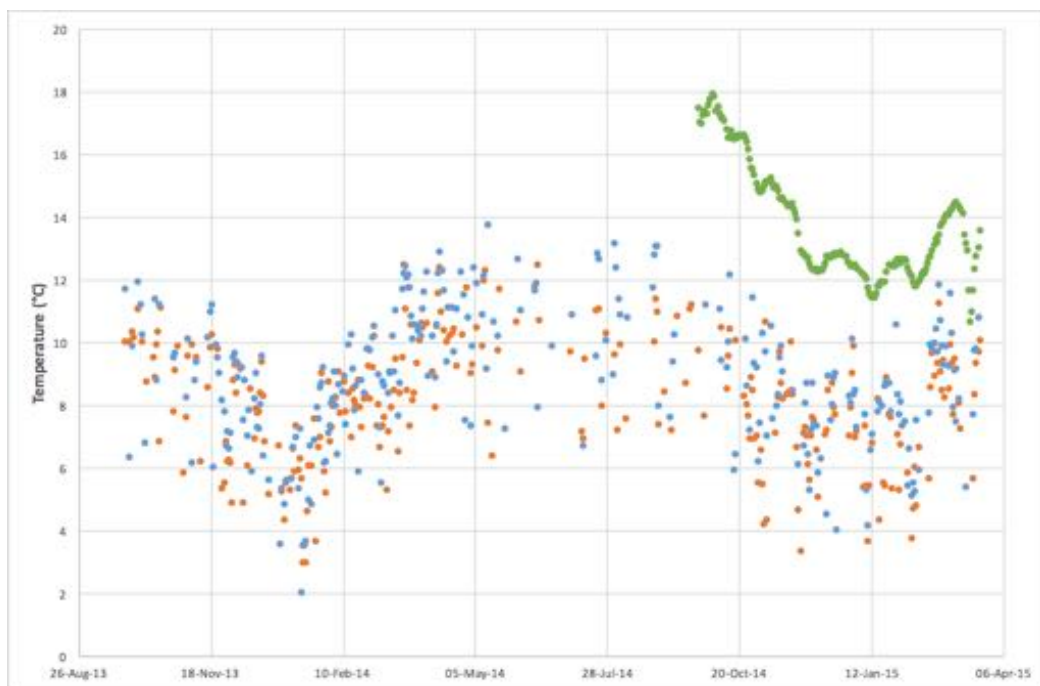


Figure 68. Mean daily temperatures at 30 cm depth measured by a Heat Needle (green dots) at AZ8, and Terra and Aqua night time land surface temperatures (blue and orange dots, respectively).

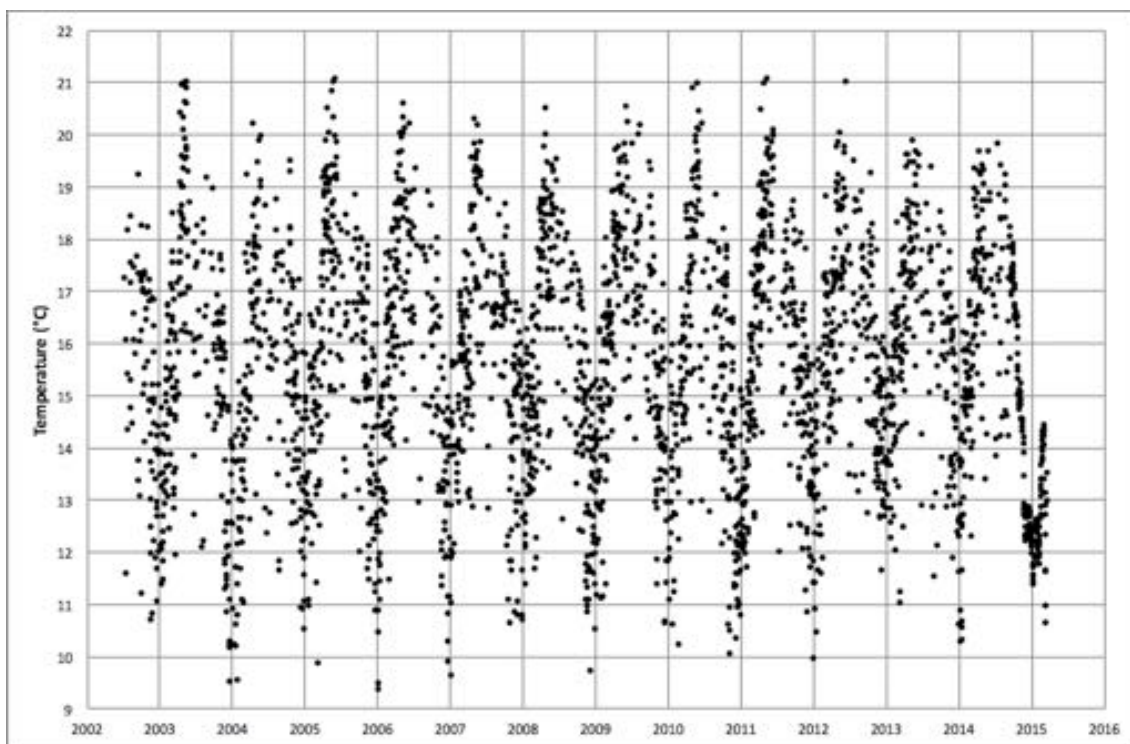


Figure 69. Daily mean temperatures at 30 cm depth at AZ8 since 2002, inferred from Terra and Aqua night time land surface temperatures

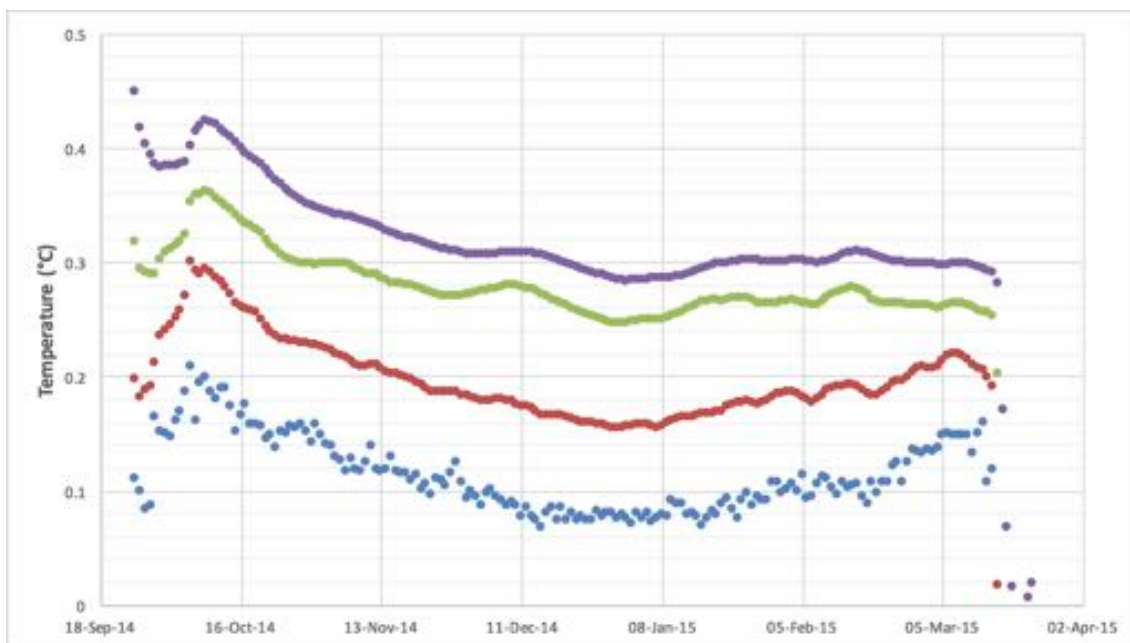


Figure 70. Reduced ground temperatures for 50 cm (blue), 70 cm (red), 90 cm (green) and 110 cm (purple) at AZ8 over the period of the survey

2.6.5 Thermal conductivity and thermal resistance

A successful thermal conductivity measurement was carried out over the time interval (UTC time) 16:01–17:01 on 23 March 2015. Assuming an ‘infinite line source’ of heat at a rate of 14.90 ± 0.04 W/m, the resulting log-linear temperature increases observed at sensor depths (Figure 71) imply thermal conductivities of:

30 cm	0.50 ± 0.05^8 W/mK
50 cm	0.743 ± 0.003 W/mK
70 cm	0.736 ± 0.003 W/mK
90 cm	0.750 ± 0.003 W/mK
110 cm	3.5 ± 1.0^9 W/mK

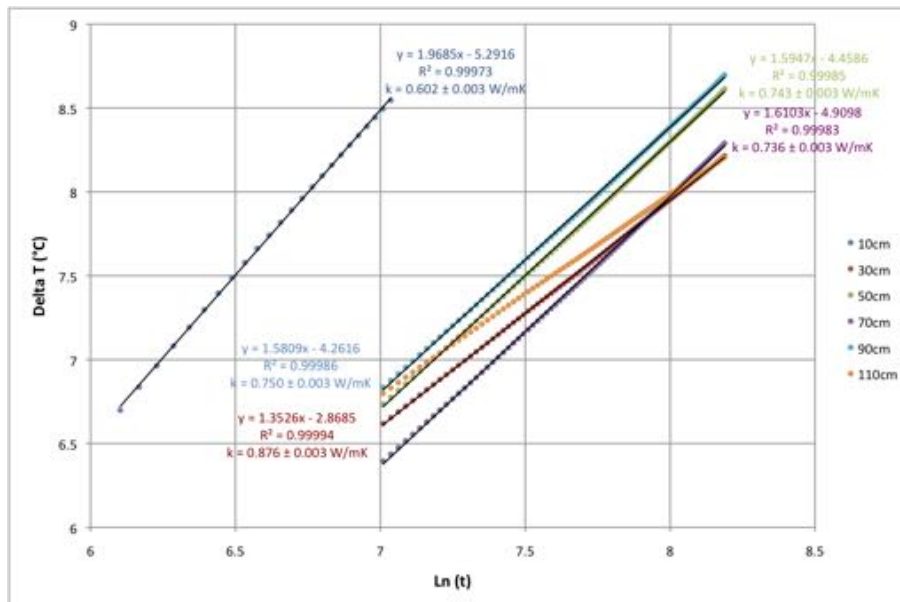


Figure 71. Temperature increase versus the natural log of heating time in March 2015 for site AZ8.

Thermal resistance is the integral of physical depth divided by thermal conductivity. The thermal resistance from 30 cm to each deeper sensor can be estimated from the thermal conductivity values above:

50 cm	$0.100/0.50 + 0.100/0.743 =$	$0.335 \text{ m}^2\text{K/W}$
70 cm	$0.335 + 0.100/0.743 + 0.100/0.736 =$	$0.605 \text{ m}^2\text{K/W}$
90 cm	$0.605 + 0.100/0.736 + 0.100/0.750 =$	$0.874 \text{ m}^2\text{K/W}$
110 cm	$0.874 + 0.100/0.750 + 0.100/3.5 =$	$1.036 \text{ m}^2\text{K/W}$

In a steady state conductive setting, temperature increases linearly with thermal resistance at a gradient equal to the conductive heat flow. A straight line of best fit provides an estimate of the mean conductive heat flow at any given moment. Figure 72 shows a sample of Bullard plots of ‘change in reduced temperature’ versus thermal resistance at one-month intervals during the recording period. The gradient of each plot indicates the ‘reduced surface heat flow’ at that time, while the coefficient of determination (R^2) indicates the degree of linearity.

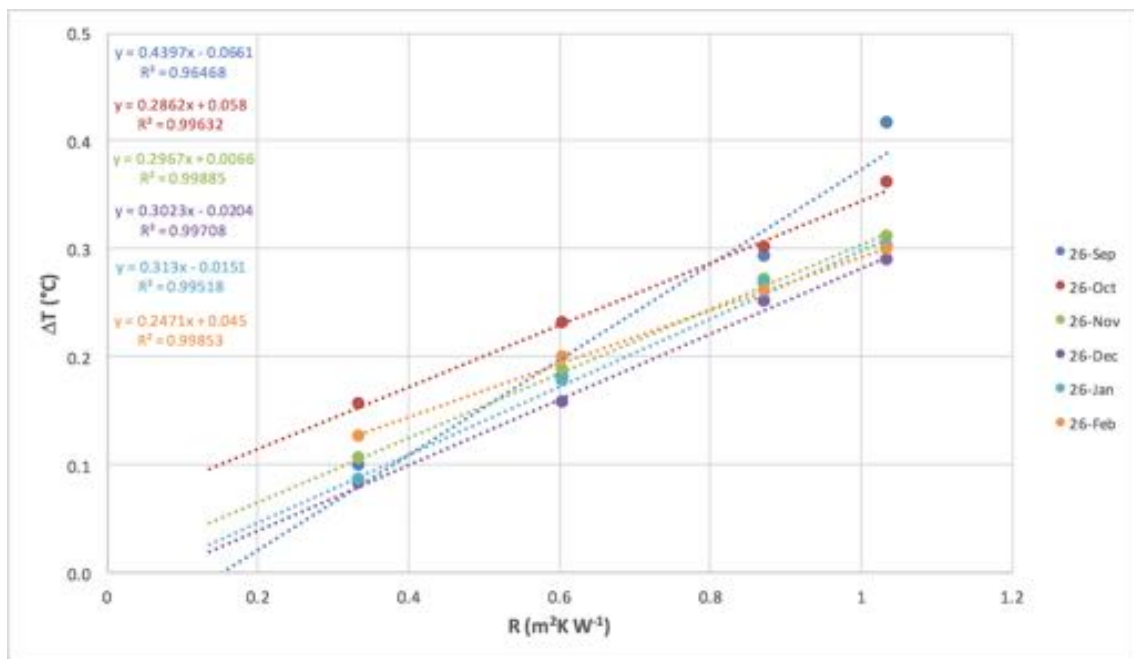


Figure 72. Bullard plots of change in ‘reduced ground temperature’ (ΔT) versus thermal resistance (R) at monthly intervals for site AZ8. The equations of the lines of best fit are given in the top left corner of the plot. The gradients indicate ‘reduced surface heat flow’ in Wm^{-2} . R^2 = coefficient of determination.

2.6.6 Reduced surface heat flow through time

Variation in ‘reduced surface heat flow’ through time is derived from the gradient of the Bullard plot for successive days. The red line on Figure 73 shows ‘reduced surface heat flow’ as a function of time for AZ8. It indicates relatively constant geophysical heat flow at $0.30 \pm 0.02 \text{ Wm}^{-2}$ over the five-month period from 1 October 2014 to 28 February 2015.

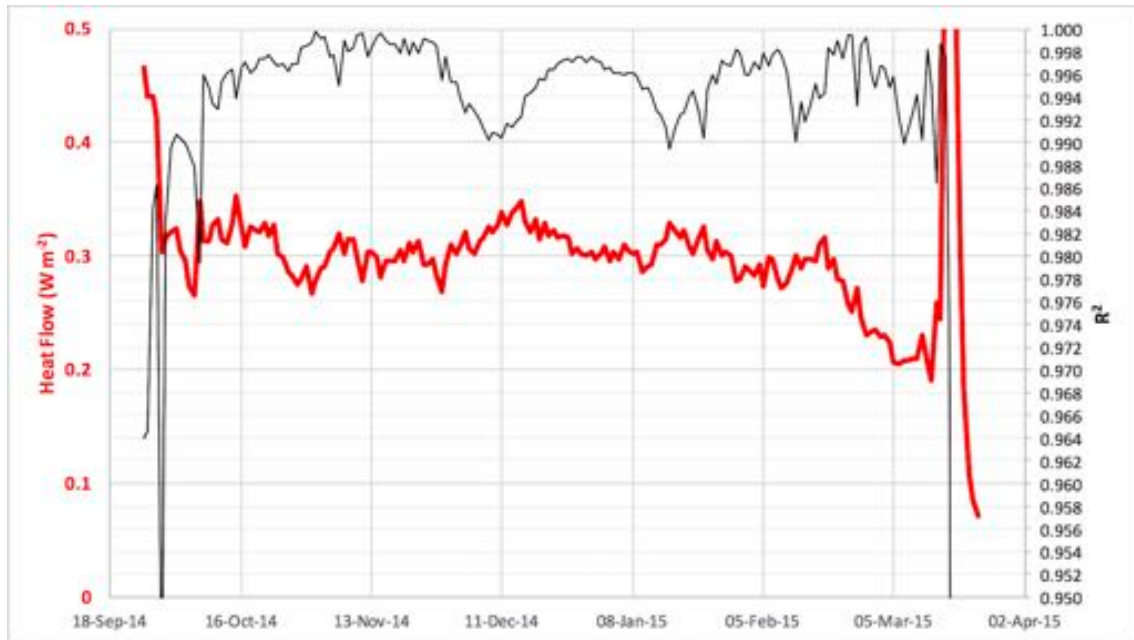


Figure 73. ‘Reduced surface heat flow’ versus time for site AZ8 (red, left axis); Coefficient of determination (black, right axis).

2.6.7 Summary

The reduced surface heat flow at this location is estimated at $0.30 \pm 0.02 \text{ W/m}^2$.

While almost 5 times the mean global continental heat flow (e.g. Beardsmore and Cull, 2001¹⁰), the value is low compared to sites AZ1, AZ2, AZ4 and AZ6 and can be considered a local background value. It suggests, however, the presence of an anomalous heat source somewhere beneath AZ8 relative to ‘normal’ continental crust; perhaps a cooling magmatic intrusion related to the Los Azufres system.

3.0 Conclusions

3.1 Reduced surface heat flow

Figure 74 displays reduced surface heat flow through time at all six sites on the same set of axes. It reveals distinct differences in the magnitude and temporal stability of the geophysical component of surface heat flow between sites. Heat flow was elevated (relative to 'background' site AZ8) at AZ1, AZ2, AZ4 and AZ6. Heat flow at site AZ1 was stable at $1.63 \pm 0.01 \text{ Wm}^{-2}$ for most of the survey period. Heat flow at site AZ2 remained relatively static at $2.15 \pm 0.05 \text{ Wm}^{-2}$ over a three-month period before gradually declining by 25% then rapid recovering to initial levels. This indicates a transient heat sink somewhere beneath the top meter of soil, perhaps related to water movement into or out of the nearby stream. Heat flow at AZ4 was stable at $1.90 \pm 0.05 \text{ Wm}^{-2}$ over most of the survey period. Heat flow values at AZ6 and AZ8 were static at $3.05 \pm 0.05 \text{ Wm}^{-2}$ and $0.30 \pm 0.02 \text{ Wm}^{-2}$, respectively, for most of the survey period. Reduced surface heat flow at AZ7 was $0.10 \pm 0.05 \text{ Wm}^{-2}$ for most of the survey period, suggesting homogenization of shallow sub-surface temperatures at that site by infiltrating meteoric water.

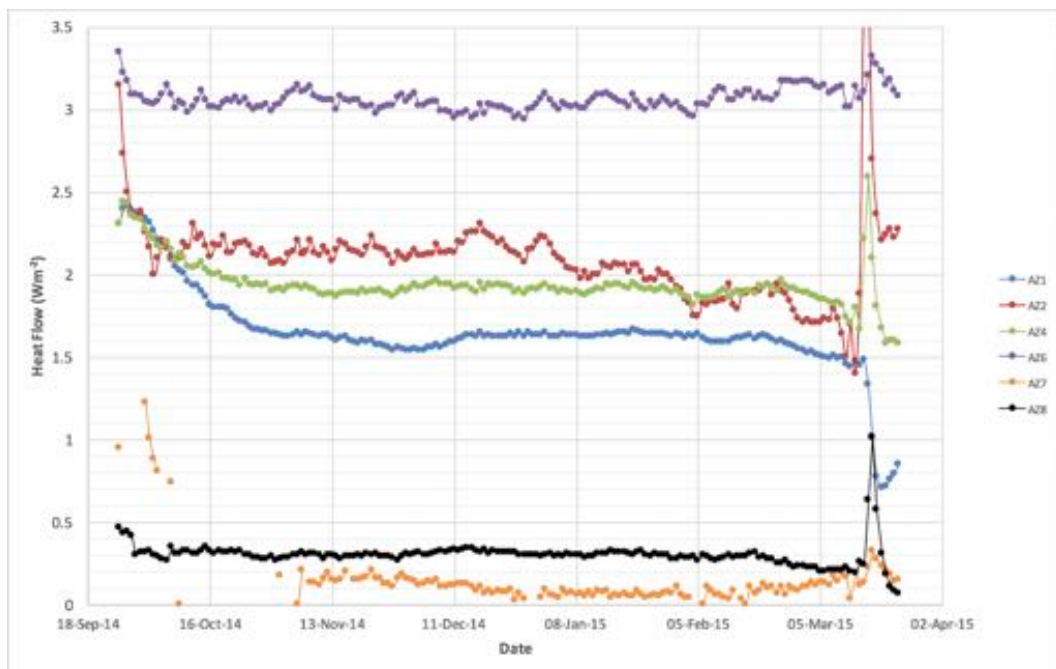


Figure 74. Reduced surface heat flow through time for all sites.

The instabilities in reduced surface heat flow observed at all sites in the final weeks of the survey coincided with short-period, high-magnitude variations in surface

temperature. Under these conditions, small errors in thermal diffusivity estimates can exaggerate errors between the calculated and observed diffusion of the surface temperature signal, which manifest as apparent fluctuations in heat flow.

Figure 75 shows the ‘static’ reduced surface heat flow for all sites at the end of December 2014 (three months after the Heat Needle survey commenced) superimposed on a Google Earth image. It also shows values of conductive heat flow based on borehole thermal gradient measurements (Espinoza-Ojeda et al., 2017¹¹).

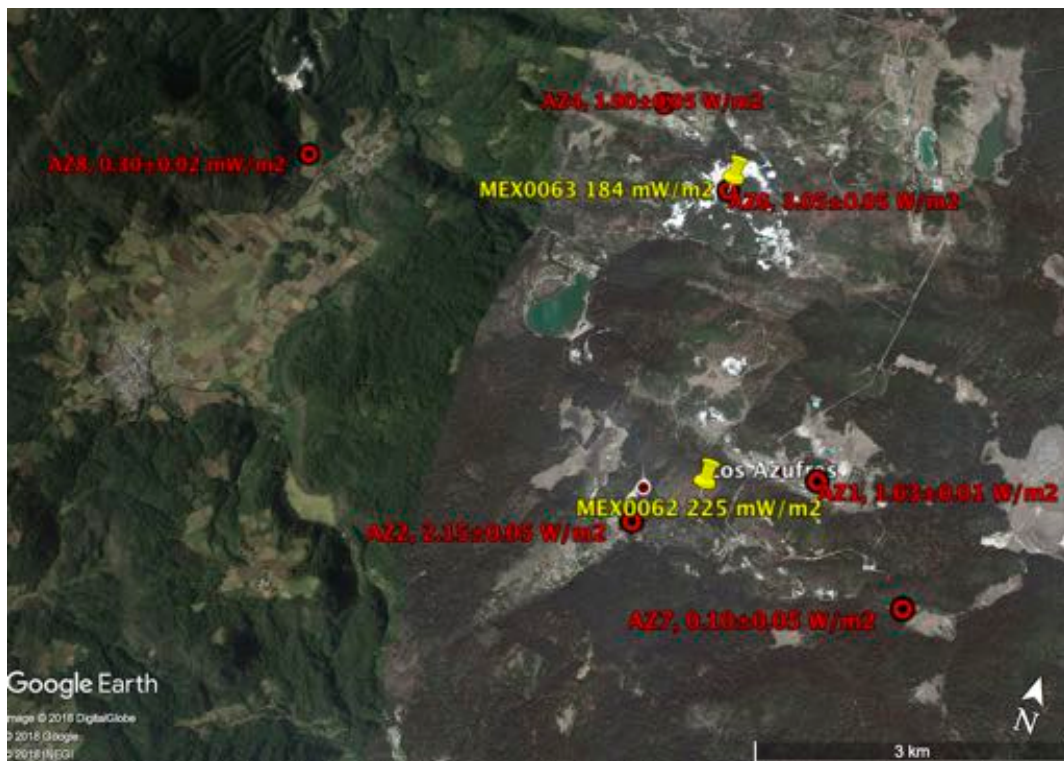


Figure 75. ‘Static’ reduced surface heat flow for all sites at the end of December 2014 (red). Published¹¹ conductive heat flow values based on borehole thermal gradient measurements (yellow pins).

3.2 Implications of results

The results at all sites indicate that, under the right conditions, Heat Needles produce ‘reduced surface heat flow’ values to their design precision of $\pm 0.01 \text{ W/m}^2$. It is very difficult to gauge the absolute accuracy of the current results because there is no means by which to independently validate the measurements of reduced heat flow in the top meter of soil. But the sound physics underpinning the processing algorithm, the tightly constrained and consistent estimates of thermal diffusivity, the highly linear

¹¹ Espinoza-Ojeda, O.M., Prol-Ledesma, R.M., Iglesias, E.R. and Figueroa-Soto, A. (2017). Update and review of heat flow measurements in Mexico. *Energy*, 121, 466–479.

Bullard plots, and the relatively stable values of reduced surface heat flow over several months, all support the reliability of the outcomes.

The discrepancy between ‘reduced surface heat flow’ and borehole conductive heat flow at site AZ6 (heat flow site ‘MEX00063’¹¹) indicates that ‘reduced surface heat flow’ might not be a direct indicator of thermal conditions deep beneath the site. This is not surprising. Three-dimensional (indeed *four-dimensional*) heat transfer in an active hydrothermal system such as exists at Los Azufres is complex. Convection redistributes heat laterally and vertically along fluid flow paths, with conduction dominating heat transfer between these pathways. The conductive heat flow in the top meter at AZ6 ($3.05 \pm 0.05 \text{ Wm}^{-2}$) very likely reflects a shallow conduit of hot fluid feeding the nearby thermal manifestations as evidenced on Figure 76. The depth of the conduit could be estimated from the temperature of the springs (eg 62°C), the ‘reduced surface temperature’ (14°C , from Section 2.4.4) and the ‘reduced thermal gradient’ (4°Cm^{-1} , from Figure 48); a depth of 12 m in this example.

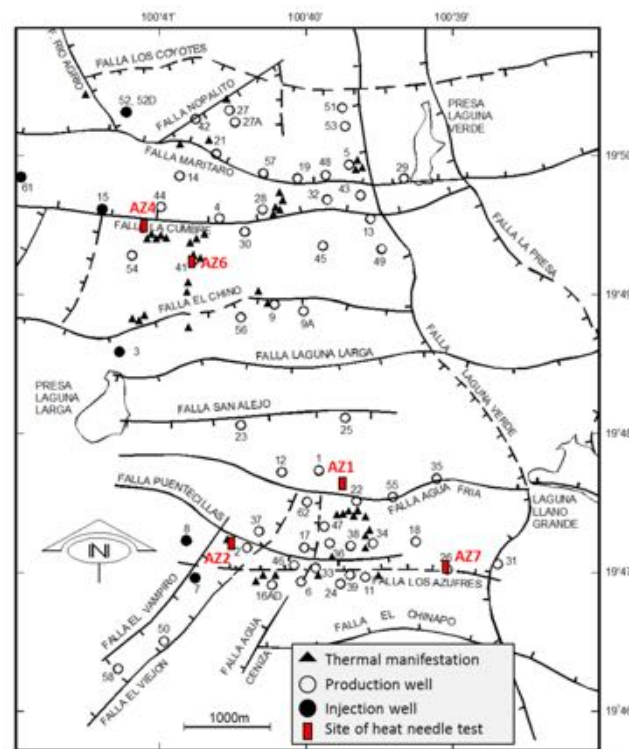


Figure 76. Wells locations, identified structures, thermal manifestations and Heat Needle sites in the Los Azufres geothermal field. Modified after Arellano *et al.* (2015)¹².

¹² Arellano-G., V.M., Ramírez-M., M., Barragán-R., R.M., Paredes-S., A., Aragón-A., A., López-B., S. and Casimiro-E., E. (2015). Condiciones termodinámicas de los fluidos del yacimiento de Los Azufres (México) y su evolución en respuesta a la explotación (1979-2011). *Memorias del XXII Congreso Anual de la Asociación Geotérmica Mexicana*, Cuernavaca, Mor., Mexico, 10-11 de Marzo 2015.

The 'reduced surface heat flow' trends for AZ6, AZ2 and AZ7 highlight the issue of site selection for Heat Needle surveys. A survey to detect deep geothermal reservoirs should avoid sites above suspected pathways of shallow groundwater flow, where meteoric water can percolate and 'flush' heat away before it reaches the surface, or where geothermal fluids can locally elevate the shallow thermal gradient. However, the law of 'conservation of energy' dictates that heat removed from one location must reach the surface at another location, either through advection with surface emissions of hot water and steam, or through conduction. Combining observations of surface manifestations with methodical mapping of reduced surface heat flow would reveal the geometry of subsurface fluid pathways, the total heat budget of a geothermal system, and the likely location of deep reservoirs.

Heat Needle surveys should become a routine, pre-drilling risk mitigation strategy for all convection-dominated geothermal play types. Future 'heat maps' will image the extent, magnitude and geometry of geothermal heat sources (eg Figure 77).

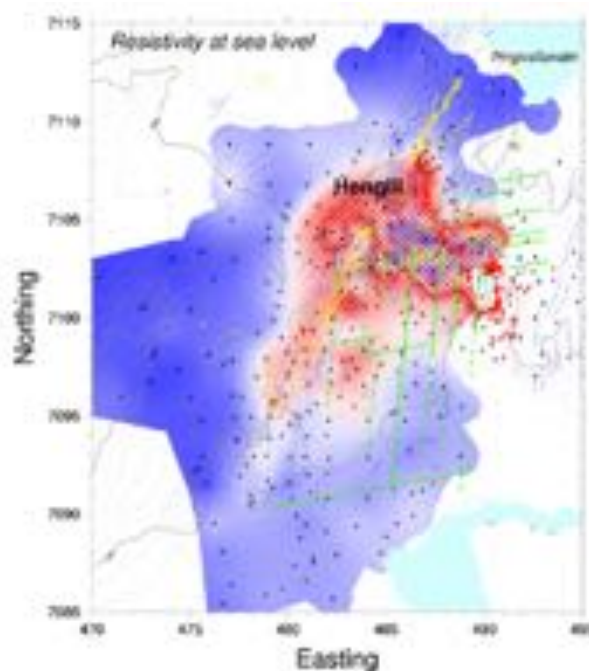


Figure 77. An electrical resistivity depth-slice through a geothermal system in Iceland (After Árnason *et al.*, 2010¹³), representing how a future 'reduced surface heat flow' map might delineate and quantify the thermal signature of a geothermal system.

¹³ Árnason, K., Eysteinnsson, H. and Hersir, G.P. (2010), "Joint 1D inversion of TEM and MT data and 3D inversion of MT data in the Hengillarea, SW Iceland," *Geothermics*, **39**, 13-34.

Copyright

All data, information, text and figures within this commissioned report are protected under the Australian Copyright Act 1968 (Section 193). HDR is to be duly and correctly attributed if a reader reproduces portions of this report in other forms. All concepts, ideas and other IP expressed in this report remain the property of HDR and Heat Needle Company Pty Ltd.